THE COORDINATION CHEMISTRY OF RHENIUM, GROUP 13 AND LANTHANIDE METAL COMPLEXES: TOWARDS NEW RADIOTHERAPEUTIC AGENTS

by

Michael S. Kovacs

B.Sc. (Hons.), McMaster University, 1996

A THESIS SUBMITTED IN PARTIAL FULFILLMENT OF

THE REQUIREMENTS FOR THE DEGREE OF

DOCTOR OF PHILOSOPHY

in

THE FACULTY OF GRADUATE STUDIES

(Department of Chemistry)

We accept this thesis as conforming to the required standard

THE UNIVERSITY OF BRITISH COLUMBIA

May 2001

In presenting this thesis in partial fulfillment of the requirements for an advanced degree at the University of British Columbia, I agree that the Library shall make it freely available for reference and study. I further agree that permission for extensive copying of this thesis for scholarly purposes may be granted by the head of my department or by his or her representatives. It is understood that copying or publication of this thesis for financial gain shall not be allowed without my written permission.

Michael S. Kovacs

Department of Chemistry
The University of British Columbia
Vancouver, Canada

Date: May 16, 2001.

Abstract

Complexes incorporating the $[Re=O]^{3+}$ core have been synthesized with ligands containing the new methyl substituted phosphine/phenolate PO and PO_2 donor sets, (2-hydroxy-5-methylphenyl)diphenylphosphine (H(MePO)) and bis(2-hydroxy-5-methylphenyl)phenylphosphine ($H_2(Me_2PO_2)$). Reaction of either *mer*-$[ReOCl_3(PPh_3)_2]$ or $[NH_4][ReO_4]$ in CH_3OH with H(MePO) led to formation of $[ReOCl(MePO)_2]$ (**2.1**) in good yield. Reaction of $[NH_4][ReO_4]$ with $H_2(Me_2PO_2)$ in CH_3OH afforded $[ReO(Me_2PO_2)(H(Me_2PO_2))]$ (**2.2**), also in good yield. X-ray crystallographic analyses of **2.1** and **2.2** demonstrated that both complexes are neutral and octahedral, and contain the oxo moiety. The two phosphorus donors are *cis* to one another in **2.1** and **2.2** with a phenol donor *trans* to the oxo moiety. **2.2** has a tridentate Me_2PO_2 ligand as well as a bidentate $H(Me_2PO_2)$ ligand wherein one of the phenol donors is protonated and not bound to the metal centre.

Two complexes have been structurally characterized from the reaction of (*o*-hydroxyphenyl)diphenylphosphine (HPO) with $[Re(Hhypy)(hypyH)Cl_3]$: $[Re(Hhypy)(hypy)(PO)(HPO)]Cl$ (**3.1**) and $[ReCl(Hypy)(hypy)(PO)]$ (**3.2**) (hypy = NNC_5H_4N, Hhypy = $HNNC_5H_4N$, hypyH = NNC_5H_4NH). X-ray crystallography demonstrated that both are Re(III) complexes; **3.1** is monocationic with a N_3OP_2 coordination sphere while **3.2** is neutral with a ClN_3OP coordination sphere. Two phosphorus atoms are bound to **3.1** and are orientated *trans* to one another. One PO ligand is bidentate while the second is monodentate with an unbound, protonated phenol. One hypy is bidentate with the α-nitrogen protonated to give a coordinated diazene (Hhypy), the

second hypy is bound as a bent diazenido group. The structure of **3.2** is nearly identical to that of **3.1** except that the monodentate HPO is replaced by a chloride.

The tripodal amine-phosphinate ligands, tris(4-(phenylphosphinato)-3-benzyl-3-azabutyl)amine ($H_3ppba{\cdot}2HCl{\cdot}H_2O$) and tris(4-(phenylphosphinato)-3-azabutyl)amine ($H_3ppa{\cdot}HCl{\cdot}H_2O$) were synthesized and reacted with Al^{3+}, Ga^{3+}, In^{3+} and the lanthanides (Ln^{3+}). At 2:1 H_3ppba to metal ratios, complexes of the type $[M(H_3ppba)_2]^{3+}$ ($M=Al^{3+}$, Ga^{3+}, In^{3+}, Ho^{3+}-Lu^{3+}) were isolated. The bicapped $[Ga(H_3ppba)_2](NO_3)_2Cl{\cdot}3CH_3OH$ was structurally characterized and was shown indirectly by various techniques to be isostructural with the other $[M(H_3ppba)_2]^{3+}$ complexes. Also, at 2:1 H_3ppba to metal ratios, complexes of the type $[M(H_4ppba)_2]^{5+}$ ($M=La^{3+}$-Tb^{3+}) were characterized, and the X-ray structure of $[Gd(H_4ppba)_2](NO_3)_4Cl{\cdot}3CH_3OH$ was determined. At 1:1 H_3ppba to metal ratios, complexes of the type $[M(H_4ppba)]^{4+}$ ($M=La^{3+}$-Er^{3+}) were isolated and characterized. Elemental analysis and spectroscopic evidence supported the formation of a 1:1 monocapped complex. Reaction of 1:1 ratios of H_3ppa with Ga^{3+} results in formation of $[Ga(ppa)]{\cdot}3H_2O$. The formation of an encapsulated 1:1 complex is supported by elemental analysis and spectroscopic evidence.

Table of Contents

Abstract			ii
Table of Contents			iv
Lists of Figures			vii
Lists of Tables			ix
Lists of Abbreviations			xi
Acknowledgments			xv
Dedication			xvi
Chapter One	Introduction		
	1.1.	General Introduction	1
	1.2.	References	15
Chapter Two	Phosphine-Phenolate Complexes Containing the $[Re=O]^{3+}$ Core		
	2.1.	Introduction	17
	2.2.	Experimental	20
	2.3.	Results and Discussion	23
		2.3.1. $[Re=O]^{3+}$ Complex of H(MePO)	23
		2.3.2. $[Re=O]^{3+}$ Complex of $H_2(Me_2PO_2)$	26
		2.3.3. Reaction of 2.1 and 2.2 with Hydrazines	29
	2.4.	Conclusions	31
	2.5.	References	32

Chapter Three Phosphine-Phenolate Complexes Containing Rhenium-Hydrazine Cores

3.1. Introduction 35

3.2. Experimental 40

3.3. Results and Discussion 44

3.3.1. $[Re(Hhypy)(hypyH)Cl_3]$ + HPO 44

3.3.2. $[Re(Hhypy)(hypyH)Cl_3]$ + H_2PO_2 & $H_2(Me_2PO_2)$ 51

3.3.3. $[Re(N_2PhMe)_2(MePO)_2][BPh_4]$ 53

3.4. Conclusions 57

3.5. References 58

Chapter Four Lanthanide(III) and Group 13 Metal Complexes Containing Tripodal Amine Phosphinate Ligands

4.1. Introduction 61

4.2. Experimental 66

4.3. Results and Discussion 72

4.3.1. Synthesis of the Tripodal Amine-Phosphinate Ligands H_3ppba & H_3ppa 72

4.3.2. 2:1 Complexes of H_3ppba with the Group 13 Metals and the Lanthanides 75

4.3.3. 1:1 Complexes of H_3ppba with the Lanthanides 85

4.3.4. 1:1 Complex of Ga^{3+} and H_3ppa 90

Chapter Four (cont.) 4.4. Conclusions 93

4.5. References 95

Chapter Five Conclusions and Further Thoughts

5.1. General Conclusions 97

5.2. Suggestions for Future Work 100

5.3. References 102

Appendix 103

Lists of Figures

Figure	Description	Page
1.1.	Two currently approved radiopharmaceuticals: (left) ^{99m}Tc-sestamibi (Cardiolite®); (right) ^{99m}Tc-D,L-HM-PAO (Ceretec®).	3
1.2.	Two examples of the bifunctional chelate approach: (left) DMP444; (right) RP419.	6
1.3.	(left) Ethylenediaminetetramethylenephosphonate, EDTMP; (right) Ethylenediaminetetraacetate, EDTA.	10
1.4.	1,4,7,10-cyclododecyltetraamine-tetramethylenephosphonate, DOTMP.	11
2.1.	ORTEP diagram of [$ReOCl(MePO)_2$], **2.1** (with the solvent molecules and H-atoms omitted); 50% thermal probability ellipsoids are shown.	24
2.2.	ORTEP diagram of [$ReO(Me_2PO_2)(H(Me_2PO_2))$], **2.2** (with the solvent molecules and H-atoms omitted); 50% thermal probability ellipsoids are shown.	27
3.1.	Selected Rhenium Hydrazine Complexes Containing Halide and Phosphine Ligands.	37
3.2.	ORTEP diagram of the cation $[Re(Hhypy)(hypy)(PO)(HPO)]^+$, **3.1** (with the solvent molecules, H-atoms and the counteranions omitted); 50% thermal probability ellipsoids are shown.	46

Figure	Description	Page
3.3.	ORTEP diagram of [ReCl(Hhypy)(hypy)(PO)], **3.2**; 50% thermal probability ellipsoids are shown.	49
3.4.	Four Possible Diastereomers of **3.5**.	55
4.1.	Examples of amine-phosphinate ligands: (left) DOTA-type ligands; (right) tris(4-(phenylphosphinato)-3-methyl-3-azabutyl)amine, (H_3ppma).	64
4.2.	ORTEP diagram of the $[Ga(H_3ppba)_2]^{3+}$ cation with the solvent molecules and the aromatic rings removed for clarity; 50% thermal probability ellipsoids are shown.	76
4.3.	IR spectra of $[M(H_3ppba)_2](NO_3)_2Cl$, M as indicated.	80
4.4.	Selected IR spectra of $[M(H_4ppba)_2](NO_3)_4Cl$, M as indicated. The IR spectrum of **4.1** (M=Ga) is included for comparison.	82
4.5.	ORTEP diagram of the $[Gd(H_4ppba)_2]^{5+}$ cation with the solvent molecules and the aromatic rings removed for clarity; 50% thermal probability ellipsoids are shown.	83
4.6.	IR spectra of $[Ln(H_4ppba)](NO_3)_3Cl$, Ln as indicated. The IR spectrum of **4.1** (M=Ga) is included for comparison.	88
4.7.	IR spectra of $[Ga(ppa)]\cdot 3H_2O$ (**4.4**) (top) and $H_3ppa\cdot HCl\cdot H_2O$ (bottom).	91
4.8.	^1H NMR spectra (300 MHz) of $[Ga(ppa)]\cdot 3H_2O$ (**4.4**) (top) and $H_3ppa\cdot HCl\cdot H_2O$ (bottom) in d_4-methanol; (* = H_2O and CH_3OH impurities).	92

Lists of Tables

Table	Description	Page
1.1.	Selected β-Emitting Radionuclides Proposed for Therapeutic Use.	7
2.1.	Selected Bond Lengths (Å) and Angles (deg) in $[ReOCl(MePO)_2]$ (**2.1**).	25
2.2.	Selected Bond Lengths (Å) and Angles (deg) in $[ReO(Me_2PO_2)(H(Me_2PO_2))]$ (**2.2**).	28
3.1.	Selected Bond Lengths (Å) and Angles (deg) in [Re(Hhypy)(hypy)(PO)(HPO)]Cl (**3.1**).	47
3.2.	Selected Bond Lengths (Å) and Angles (deg) in [ReCl(Hhypy)(hypy)(PO)] (**3.2**).	50
3.3.	Selected ^1H & ^{31}P NMR spectral data for [Re(Hhypy)(hypy)(PO)(HPO)]Cl (**3.1**), [ReCl(Hhypy)(hypy)(PO)] (**3.2**), $[Re(Hhypy)(hypy)(HPO_2)(H_2PO_2)]Cl$ (**3.3**), and $[Re(Hhypy)(hypy)(H(Me_2PO_2))(H_2(Me_2PO_2))]Cl$ (**3.4**).	52
4.1.	Preparative details for the synthesis of $[M(H_3ppba)_2](NO_3)_2Cl{\cdot}xCH_3OH$.	69
4.2.	Preparative details for the synthesis of $[M(H_4ppba)_2](NO_3)_4Cl{\cdot}xCH_3OH$.	69
4.3.	Preparative details for the synthesis of $[M(H_4ppba)](NO_3)_3Cl{\cdot}xH_2O$.	70

Table	Description	Page
4.4.	Selected bond lengths (Å) and bond angles (deg) in $[Ga(H_3ppba)_2](NO_3)_2Cl{\cdot}3CH_3OH$ (**4.1**).	77
4.5.	+LSIMS data for all 2:1 H_3ppba complexes.	79
4.6.	Elemental analyses for selected 2:1 H_3ppba complexes.	81
4.7.	Selected bond lengths (Å) and bond angles (deg) in $[Gd(H_4ppba)_2](NO_3)_4Cl{\cdot}3CH_3OH$ (**4.2**).	84
4.8.	+LSIMS data for all 1:1 H_3ppba complexes.	86
4.9.	Elemental analyses for all 1:1 H_3ppba complexes.	89
A1.	Selected Crystallographic Data for All Metal Complexes.	108
A2.	Bond Lengths (Å) for $[ReOCl(MePO)_2]$ (**2.1**).	109
A3.	Bond Angles (deg) for $[ReOCl(MePO)_2]$ (**2.1**).	110
A4.	Bond Lengths (Å) for $[ReO(Me_2PO_2)(H(Me_2PO_2))]$ (**2.2**).	112
A5.	Bond Angles (deg) for $[ReO(Me_2PO_2)(H(Me_2PO_2))]$ (**2.2**).	113
A6.	Bond Lengths (Å) for [Re(Hhypy)(hypy)(PO)(HPO)]Cl (**3.1**).	115
A7.	Bond Angles (deg) for [Re(Hhypy)(hypy)(PO)(HPO)]Cl (**3.1**).	117
A8.	Bond Lengths (Å) for [ReCl(Hhypy)(hypy)(PO)] (**3.2**).	121
A9.	Bond Angles (deg) for [ReCl(Hhypy)(hypy)(PO)] (**3.2**).	122
A10.	Bond Lengths (Å) for $[Ga(H_3ppba)_2](NO_3)_2Cl{\cdot}3CH_3OH$ (**4.1**).	124
A11.	Bond Angles (deg) for $[Ga(H_3ppba)_2](NO_3)_2Cl{\cdot}3CH_3OH$ (**4.1**).	126
A12.	Bond Lengths (Å) for $[Gd(H_4ppba)_2](NO_3)_4Cl{\cdot}3CH_3OH$ (**4.2**).	129
A13.	Bond Angles (deg) for $[Gd(H_4ppba)_2](NO_3)_4Cl{\cdot}3CH_3OH$ (**4.2**).	130

List of Abbreviations

Abbreviation	Meaning
Å	angstrom, 1×10^{-10} metre
Anal	analytical
ATPase	adenosine triphosphatase
β	beta particles
BAM	biologically active molecule
°C	degrees Celsius
Calcd	calculated
Ci	Curie (3.7×10^{10} disintegrations per second)
cm^{-1}	wavenumber(s) (reciprical centimetre)
δ	chemical shift in parts per million (ppm) from a standard (NMR)
d	doublet (NMR)
dd	doublet of doublets (NMR)
deg	degree(s)
diphos	1,2-bis-(diphenylphosphino)ethane
DMF	dimethylformamide
DMSO	dimethylsulfoxide
DOTA	1,4,7,10-tetraazacyclododecane-1,4,7,10-tetraacetate
DOTMP	1,4,7,10-cyclododecyltetraaminetetramethylenephosphonate
DTPA	diethylenetriaminepentaacetate
EDTA	ethylenediaminetetraacetate
EDTMP	ethylenediaminetetramethylenephosphonate

eV	electron volt(s)
FDA	food and drug administration
FT	fourier transform
γ	gamma rays
g	gram(s); gas
h	hour(s)
HEDP	hydroxyethylene diphosphonate
H(MePO)	(2-hydroxy-5-methylphenyl)diphenylphosphine
$H_2(Me_2PO)$	bis(2-hydroxy-5-methylphenyl)phenylphosphine
HM-PAO	3,6,6,9-tetramethyl-4,8-diazaundecane-2,10-dione dioxime
HPO	(*o*-Hydroxyphenyl)diphenylphosphine
H_2PO_2	bis(*o*-hydroxyphenyl)phenylphosphine
H_3ppa	tris(4-(phenylphosphinato)-3-azabutyl)amine
H_3ppba	tris(4-(phenylphosphinato)-3-benzyl-3-azabutyl)amine
H_3ppma	tris(4-(phenylphosphinato)-3-methyl-3-azabutyl)amine
HPLC	high performance liquid chromatography
HPS	(*o*-thiophenyl)diphenylphosphine
HYNIC	N-oxysuccinimidylhydrazinonicotinamide
hypy	2-hydrazinopyridine
H_xPO_x	general term for a phenylphosphine-phenol ligand
Hz	hertz (s^{-1})
IR	infrared
J	coupling constant (NMR)
K	Kelvin(s)

L	litre
Ln	lanthanides
LSIMS	liquid secondary ion mass spectrometry
μ	micro (10^{-6})
m	milli (10^{-3})
M	molar (moles/litre for concentration); metal; mega (10^{6})
MAb	monoclonal antibody
min	minute(s)
mom	methoxymethyl
MRI	magnetic resonance imaging
m/z	mass to charge ratio (in mass spectrometry)
ν	stretching frequency
NCA	no carrier added
NMR	nuclear magnetic resonance
ORTEP	Oak Ridge Thermal Ellipsoid Program
pH	negative logarithm of the proton concentration or activity
pK_a	negative logarithm of the acid dissociation constant (K_a)
ppm	parts per million
s	second(s); singlet (NMR)
S	goodness of fit (X-ray crystallography)
T	temperature
$t_{1/2}$	half-life
TMEDA	tetramethylethylenediamine
TMS	tetramethylsilane (NMR)

V	volume
y	year(s)
Z	number of molecules per unit cell (X-ray crystallography)

Acknowledgments

First and foremost, I must acknowledge Professor Chris Orvig for his careful guidance, continuous support and boundless enthusiasm. He allowed me the freedom to explore my scientific interests, and taught me by example how optimism, careful observation and a lot of hard work can turn a perceived failure into an unmitigated success.

I would like to thank Dr. Kathie Thompson, my eternal coffee companion and expert parenting consultant, for sharing in many interesting conversations, both scientific and personal. I would also like to thank Professor Harvey "Uncle" Schugar for his guidance and personal insight while working in our group on sabbatical. Acknowledgment is made to Dr. Brian Patrick and the late Dr. Steve Rettig of UBC, and Dr. Tom Emge at Rutgers, for their help in determining the X-ray crystal structures.

I gratefully acknowledge the assistance of the support staff in the department, particularly Ms. Liane Darge and Ms. Marietta Austria (NMR), Mr. Peter Borda (elemental analysis) and the entire mass spectrometry staff. I am indebted to NSERC, DuPont Pharmaceuticals and the UBC Chemistry Department for financial support.

I acknowledge my Équipe Orvig Team collaborators Mark Lowe, Peter Hein, and Sherwin Sattarzadeh, as well as my colleagues Leon, Marco, Pete, Ashley, "Grandpa" Buglyó, Paul, Ika, Lenny, Jason, Barry, Dave, Alex and other past and present members of the Orvig Group for the good times and happy memories.

Finally, I must acknowledge my wife Ann Marie for providing her never ending caring and support throughout the long course of my academic studies. I would also like to thank my parents, my sister, as well as Ann's parents and sisters for their patience, support and understanding.

I dedicate this thesis to my wife Ann Marie,

and my beautiful baby girl Emily Caroline,

with all my love.

Chapter One

Introduction

1.1. General Introduction

Nuclear medicine is a branch of medicine dealing with the use of radioactive isotopes in the diagnosis and treatment of disease. Celebrating its centennial at the time of this writing, nuclear medicine began in 1901 with the use of naturally occurring radium to treat skin lesions by Henri Danlos, a French physician.[1] However, the concept was largely limited until the 1930's and 1940's because very few radioactive sources of sufficient intensity and variety existed before that time. The problem was solved when Enrico Fermi successfully built the world's first nuclear reactor in 1935 and discovered that radioisotopes could be artificially synthesized by neutron bombardment. The invention of the cyclotron by E.O. Lawrence in 1930 also circumvented this problem; Fermi and Lawrence were awarded Nobel prizes back-to-back in 1938/39 for their efforts. The infrastructure of nuclear reactors and cyclotrons that now exists supplies the world demand for the approximately 35 radioactive isotopes approved for use in the preparation of radiopharmaceuticals.

The vast majority of radiopharmaceuticals approved for clinical use are diagnostic drugs: compounds that are used to measure biological function and diagnose disease. More than 85% of these diagnostic drugs incorporate the workhorse of nuclear medicine, technetium-99m (^{99m}Tc).[2-5] The nuclear properties of ^{99m}Tc are ideal for its widespread use in diagnostic radiopharmaceuticals. ^{99m}Tc emits a γ-ray of 140 keV (89%), which is

perfectly suited for detection by the types of gamma cameras used in most hospitals. Its 6 h half-life is short enough to minimize the radiation dose to the patient, but it also allows sufficient time to synthesize the radiopharmaceutical, assess its purity, administer it to the patient, allow for biodistribution, and perform the actual imaging. The isotope requires no significant infrastructure to be present at the site of administration.

Unlike isotopes that must be prepared in a reactor or cyclotron, ^{99m}Tc can be obtained from the convenient $^{99}Mo/^{99m}Tc$ generator system that was developed in 1961 at the Brookhaven National Laboratory.

$$^{99}Mo \xrightarrow{66\ h} {}^{99m}Tc \xrightarrow{6\ h} {}^{99}Tc \xrightarrow{2 \times 10^5\ y} {}^{99}Ru$$

The parent nuclide ^{99}Mo is synthesized by neutron bombardment and is incorporated in an alumina column as $[^{99}MoO_4]^{2-}$. The long half-life of ^{99}Mo allows it to be synthesized off site with minimal loss of activity. A transient equilibrium exists between ^{99}Mo and its short-lived daughter; this equilibrium allows the isolation of no-carrier-added ^{99m}Tc every 23-24 h. Elution of the column with sterile saline solution obtains $[^{99m}TcO_4]^-$ exclusively, through an ion exchange effect; $[^{99}MoO_4]^{2-}$ is 100% retained under these conditions. It is important to remember that $[TcO_4]^-$ must be the starting material for any proposed Tc-based radiopharmaceutical.

Beginning with the use of $[^{99m}TcO_4]^-$ as a thyroid-imaging agent, technetium-based diagnostic agents have gone through several design cycles in becoming a mature discipline. Initially, $[^{99m}TcO_4]^-$ was used either directly (*e.g.* as an I^- mimic for thyroid imaging), or was used in simple labeling experiments. Examples of the latter include Tc-sulphur colloid and Tc-labeled erythrocytes (red blood cells) for the imaging and measurement of blood flow and associated abnormalities. These, and many such similar

diagnostic agents, are still in use, but in general they are poorly characterized and very little is known of their chemical structure.

The so-called "technetium essential" complexes comprise most of the first generation of technetium-based diagnostic agents. The Tc in these complexes is an integral part of the function and structure; hence the radiopharmaceutical would not remain intact and would not be delivered to the target if the Tc therein were absent. The design of this generation of diagnostic agents was much more methodical and deliberate. This was fueled largely by the pioneers who had a great role in the elucidation of the basic coordination chemistry of Tc. Two highly successful diagnostic agents that were the result of these efforts are shown in Figure 1.1.

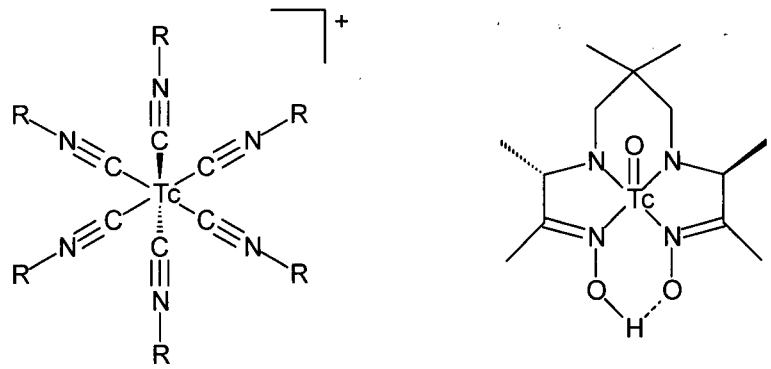

R = $CH_2C(CH_3)_2OCH_3$

Figure 1.1. Two currently approved radiopharmaceuticals: (left) ^{99m}Tc-sestamibi (Cardiolite®); (right) ^{99m}Tc-D,L-HM-PAO (Ceretec®).[5]

^{99m}Tc-sestamibi (Cardiolite®) is approved for myocardial perfusion imaging.[2,4,6,7*] The radiopharmaceutical is an octahedral, monocationic Tc(I) complex containing six neutral isonitrile ligands. The complex was originally believed to be a K^+ mimic that is taken up into actively contracting heart muscle by Na^+/K^+ ATPase, an integral membrane protein involved in the energetics of all cell types.[2] However, competition experiments later demonstrated this to be false, although it is still believed that the mechanism of uptake is related to its mimicry of K^+.[8,9] Under mildly stressful conditions, sufficient uptake of the complex into the heart provides a suitable target to background ratio for imaging (1.5% of the injected dose). In areas of the heart that are not receiving adequate blood flow, uptake of the complex is restricted and "cold" spots in the diagnostic image are observed.

^{99m}Tc-D,L-HM-PAO (Ceretec®) elaborated the use of coordination chemistry in the design of radiopharmaceuticals even further and was the first Tc-based diagnostic agent to be fully characterized prior to FDA approval.[2,10] This neutral $[Tc=O]^{3+}$ complex is approved for cerebral blood flow imaging to evaluate stroke and other cerebral diseases, and is designed to penetrate the blood-brain-barrier by diffusion. Stereochemistry plays a vital role in the pharmacokinetics of this complex. The D,L diastereomer is retained in the brain sufficiently long to obtain a diagnostic image, but the meso diastereomer diffuses back out of the brain too quickly.[11]

Efforts to advance diagnostic agents to the next generation have been focused on the development of "technetium tagged" radiopharmaceuticals.[5] Techniques related to the synthesis of complex biomolecules, as well as knowledge of their biochemical targets, have benefited immensely from advances in molecular biology and genetic engineering.

* ^{99m}Tc-sestamibi is also marketed under the trade name Miraluma® for early stage breast cancer imaging.

Therefore, the ability to label a wide variety of these biomolecules with Tc for diagnostic purposes is highly desirable.

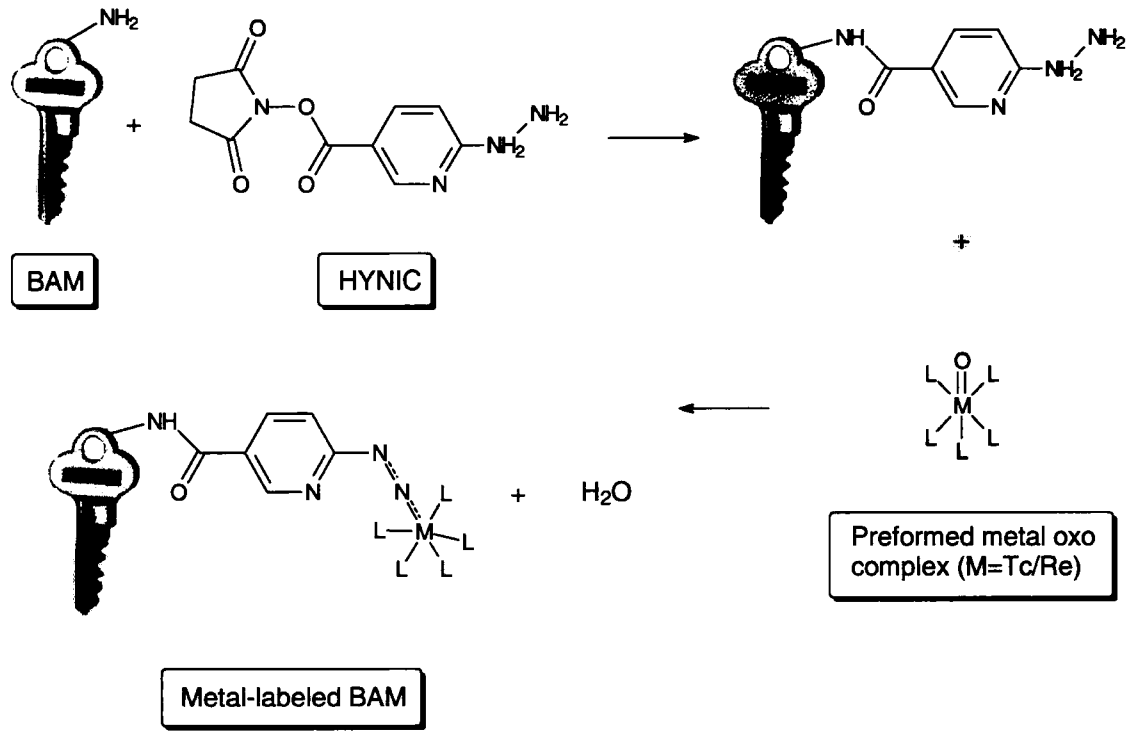

Scheme 1.1

For the general purpose of polypeptide labeling, the bifunctional chelate approach has received extensive attention (NB: The linker does not necessarily need to be a chelate by definition, but rather any ligating group). The functional groups on the chelate are designed to form a bridging spacer between the polypeptide and the metal. The most successful bifunctional ligating group to date is N-oxysuccinimidylhydrazinonicotinamide (HYNIC).[12] The activated ester is first reacted with the amine side chain of the biologically active molecule (BAM) to make a hydrazine-conjugate (Scheme 1.1). The hydrazine functional group is then reacted with

Tc to form a stable metal-labeled BAM. Since HYNIC only forms a monodentate complex with Tc, careful consideration must be given to introduce the coligands L in order to stabilize the resulting conjugate.

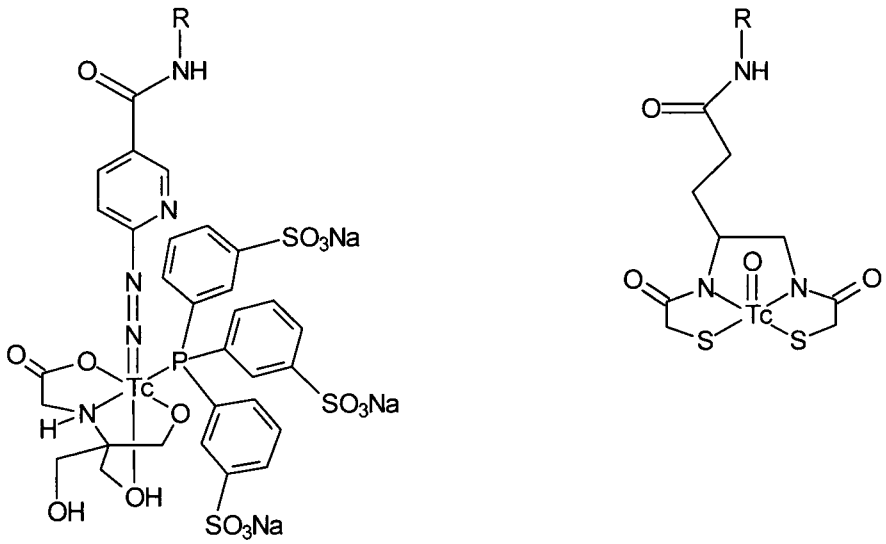

Figure 1.2. Two examples of the bifunctional chelate approach: (left) DMP444; (right) RP419.[12] R represents the GPIIb/IIIa platelet receptor antagonist.

There are several applications of the bifunctional chelate approach, two of which (Figure 1.2) involve the Tc labeling of the GPIIb/IIIa cyclic platelet receptor antagonist.[12-17] The GPIIb/IIIa receptor is involved in blood clotting and recognizes the Arg-Gly-Asp tripeptide sequence. A HYNIC bioconjugate of the antagonist has been used to image thrombi in canine models.[16] DMP444 uses a system of two different coligands to stabilize the complex, namely triglycine and triphenylphosphinetrisulfonate (TPPTS). An example of a non-HYNIC bioconjugate, RP419 uses a N_2S_2 bifunctional chelate to bridge the $[Tc{=}O]^{3+}$ core to the same GPIIb/IIIa antagonist.[17]

Therapeutic radiopharmaceuticals are molecules labeled with isotopes for the express purpose of killing diseased tissue (notably cancerous tumors) with ionizing radiation.[18] The idea was first put to clinical use in 1941 when $^{131}I^-$ was administered to treat thyroid cancer, a practice still in use today.[19] Early treatment of bone cancers used simple inorganic ions such as chromic ^{32}P-phosphate colloid and $^{89}Sr^{2+}$ chloride (a Ca^{2+} analogue).[18] Both minerals are taken up by the main mineral component of bone, hydroxyapatite, particularly in areas of rapid bone growth such as a tumour. $^{89}Sr^{2+}$ chloride was used for over 50 years and was finally approved by the U.S. Food and Drug Administration (FDA) in 1995 for this application.[18]

Table 1.1. Selected β-Emitting Radionuclides Proposed for Therapeutic Use.[18]

Radionuclide	$t_{1/2}$, days	E_β max, MeV	γ energy, MeV
^{32}P	14.3	1.71	
^{89}Sr	50.5	1.46	
^{90}Y	2.7	2.27	
^{131}I	8.0	0.81	0.364 (81%)
^{149}Pm	2.2	1.07	0.286 (3%)
^{153}Sm	1.9	0.8	0.103 (29%)
^{166}Ho	1.1	1.6	0.81 (6.3%)
^{177}Lu	6.7	0.50	0.113 (6.4%) 0.208 (11%)
^{186}Re	3.8	1.07	0.137 (9%)
^{188}Re	0.7	2.11	0.155 (15%)

These three relatively primitive treatments share several features in common with any therapeutic radiopharmaceutical. All three isotopes are β-emitters (Table 1.1). High-energy electrons emitted from the nuclei of these radionuclides provide a homogeneous radiation dose with the power to kill the targeted tissue. The β energy determines the distance over which the radiation dose can be delivered (anywhere from 2 mm for the weakest to 12 mm for the strongest). Other radionuclides that decay by emission of α particles or Auger electrons have also been proposed, but have not received as much attention.

In order for the dose to reach the target, therapeutic radiopharmaceuticals must also have a suitable half-life. There is no "best" half-life; rather, the optimum half-life depends on the *in vivo* localization and clearance times. The goal is to optimize uptake in order to deliver the maximum radiation dose to the target tissue. If the half-life is too short, decay will occur before the radionuclide reaches its intended target, a problem common with monoclonal antibodies (MAbs), which have long residence times. Too long a half-life is also not desirable; most of the radiation dose will be excreted long after the radionuclide has cleared the intended target. A long half-life also requires that a higher dose of radionuclide be given, a practice that inevitably increases the radiation dose to non-target tissues and causes unwanted side effects.

Radionuclides must also be available with high specific activity, *i.e.* at the no-carrier-added (NCA) level (≥ 2-5 Ci/μg). Because of the constraints of decay properties, half-life, specific activity, availability, and cost, the number of radionuclides suitable for use in therapy is relatively limited. Since the elements most commonly used in organic

chemistry do not meet these requirements, the role of inorganic chemistry becomes all the more important in the design of therapeutic radiopharmaceuticals (Table 1.1).

All the requirements stated above relate to the actual radionuclides themselves. The key to a successful radiotherapeutic agent is to design a molecule that has significant uptake in the target *vs.* the background (≥ 10%). With $^{131}I^-$, $^{89}Sr^{2+}$ or ^{32}P, the delivery of the radiation dose to the target is accomplished by using small inorganic ions that are natural substrates for the target (or nearly so in the case of $^{89}Sr^{2+}$). For various reasons, the utility of these three isotopes is largely limited to their current applications. Radioiodine labeling of organic molecules is commonplace, but the physical properties of ^{131}I limit its utility. All of the proposed isotopes in Table 1.1, with the exception of those mentioned above, are not natural substrates and have no known biological roles. Much as Tc-based diagnostics have benefited from sophisticated approaches based on coordination chemistry, it is hoped that the design of radiotherapeutic agents can also be accomplished with the study of relevant metal ions and appropriate ligands.

The final consideration for a radiotherapeutic agent based on a metal complex is stability. There is little point to design and introduce a complex, if it is subsequently demetallated, particularly if the intact complex is required for the therapeutic agent to work. Ligand design becomes crucial in this regard; the resulting complexes must be kinetically inert and thermodynamically stable *in vivo*, yet they must still allow for a mechanism of clearance after the radiation dose is delivered.

In 1997, ^{153}Sm-EDTMP (Quadramet®) was the first coordination complex designed for radiotherapeutic use to be approved by the U.S. FDA. The complex is used for the palliation of skeletal metastases associated with cancer. The EDTMP ligand is the

tetra-substituted methylenephosphonate analogue of EDTA (Figure 1.3). The complex is prepared in a 250-300:1 ligand-to-metal ratio and is administered intravenously. The phosphonate group is believed to act as a phosphate analogue; the complex is taken up into hydroxyapatite wherein the $^{153}Sm^{3+}$ becomes incorporated into the bone matrix. At an administered dose of 1 mCi/kg body weight, significant pain relief was demonstrated in 70-80% of the patients studied during clinical trials.[18] This dose is approximately ¼ of that required using $^{89}Sr^{2+}$ chloride; side effects related to bone marrow suppression are seen in both treatments, but the patients recovered twice as fast.[18] In a recent study, bone uptake of ^{153}Sm-EDTMP was shown to be 29.2% of the total injected dose after 3 hours, and 47.7% after 24 hours.[20]

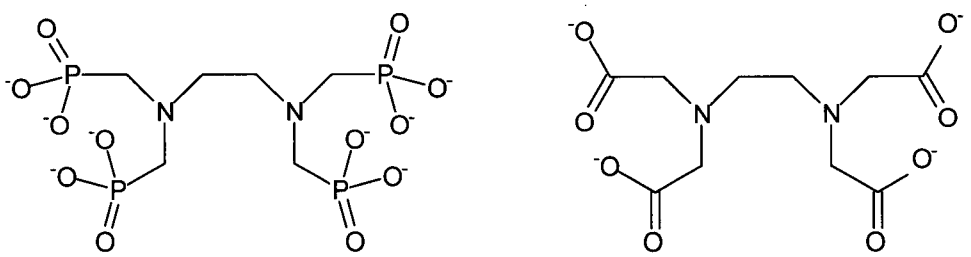

Figure 1.3. (left) Ethylenediaminetetramethylenephosphonate, EDTMP; (right) Ethylenediaminetetraacetate, EDTA.

Referring to Table 1.1, there are two clear groups of isotopes that are most relevant to the field of radiotherapeutic agents, *i.e.* rhenium and the lanthanides. The latter are already implemented in the form of ^{153}Sm-EDTMP, but the potentially useful lanthanides are by no means restricted to Sm. Preliminary work has already been published on ^{166}Ho-DOTMP, a tetra methylene-substituted cyclen complex (Figure

1.4).[18] The ability to adapt proven ligand systems to the lanthanides, all of which exhibit similar chemical properties across the series, is highly desirable. In theory, the nuclear properties of the various lanthanides could be incorporated into similar ligand systems in order to fine-tune the therapeutic properties of the resulting radiopharmaceutical by adjusting both the ligand and the metal ion.

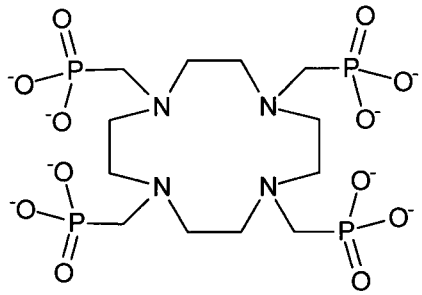

Figure 1.4. 1,4,7,10-cyclododecyltetraaminetetramethylenephosphonate, DOTMP.

The chemistry of the lanthanides has been under extensive recent investigation, particularly because of applications as fluorescent probes and as contrast agents in magnetic resonance imaging (MRI).[21,22] With few exceptions, the entire lanthanide series is trivalent under ambient conditions (Ln^{3+}). The screening of nuclear charge by the f electrons is inefficient, which results in the lanthanide contraction; the ionic radii decrease by 10-15% across the series. The electron density of the f electrons is arranged such that little interaction occurs with coordinated ligands. This results in many of the observed properties, *e.g.* the complete lack of ligand field effects and long fluorescence lifetimes. Ln^{3+} are hard oxophilic metals; ligand donor atom design has been almost exclusively limited to hard nitrogen and oxygen atoms in amines, carboxylates and phosphonates. Uncomplexed Ln^{3+} ions are extensively hydrolyzed at physiological pH; multidentate chelating ligands are necessary to provide thermodynamic stability, prevent

hydrolysis and protect the metal against complexation/reaction with endogenous ligands *in vivo*.

Rhenium, the 3rd row congener of technetium, is an even more attractive proposition to include in a radiotherapeutic agent. The ionic radii of Tc and Re are very similar due to the aforementioned lanthanide contraction and the range of accessible oxidation states is comparable. In principle, one should be able to redesign established Tc-containing diagnostics and subsequently use them as Re-based therapeutics.[4,18,23] There are two proposed isotopes of rhenium, namely ^{186}Re and ^{188}Re (Table 1.1). Rhenium-186 is capable of delivering a sizeable dose of radiation (β_{max} = 1.07 MeV) over an extended period of time due to its relatively long (3.8 day) half-life. The primary disadvantage of ^{186}Re lies in its preparation by neutron bombardment; it is nearly impossible to produce the isotope at the NCA level.[18] Clinical trials have shown that the ^{186}Re complex of hydroxyethylene diphosphonate (HEDP) is an effective agent for the palliation of bone cancer metastases, analogous to the ^{99m}Tc-HEDP complex that images the same metastases.[24,25] In a recent study, ^{186}Re-HEDP was shown to have 13.7% bone uptake after 3 hours, and 21.8% after 24 hours.[20] Although uptake is not as high as ^{153}Sm-EDTMP,[20] the uptake is still adequate for therapy. Rhenium-188 delivers a dose with higher tissue-penetrating power (β_{max} = 2.12 MeV) to a distance of 11 mm. Since ^{188}Re can be obtained from a ^{188}W/^{188}Re generator, it offers a distinct advantage over isotopes such as rhenium-186 that must be synthesized off-site by neutron activation, or many other isotopes requiring sizable infrastructure for their preparation.[18] The primary disadvantage of ^{188}Re is its short half-life of 17 h, a problem largely circumvented by the availability of the generator system.

The challenges that must be overcome to extend this chemistry to rhenium are significant, however. Foremost from the clinical standpoint is the much stricter target to background ratios that must be achieved for therapeutic *vs.* diagnostic use. Rhenium is more kinetically inert than technetium and it is also much more difficult to reduce from $[MO_4]^-$ (M = Tc, Re), the preferred starting material in nuclear medicine. The differences in oxidative strength may also be problematic because oxidation to $[ReO_4]^-$ *in vivo* provides an efficient mechanism of elimination. For these reasons, it may require considerable research to extend working diagnostic technetium systems to potentially therapeutic rhenium systems.

The main purpose of this project was to investigate the fundamental coordination chemistry of Re and the lanthanides. The ligands were chosen with careful consideration given to the intended application of the resulting complexes as radiotherapeutic agents. Chapter 2 describes the preparation of Re complexes with phosphine-phenolate ligands, a proven system that is known to form stable complexes of Re and Tc.[26]

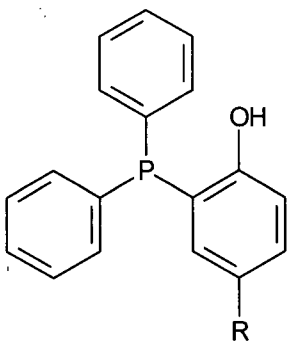

HPO (R=H)
H(MePO) (R=Me)
H(*t*-BuPO) (R=*t*-Bu)

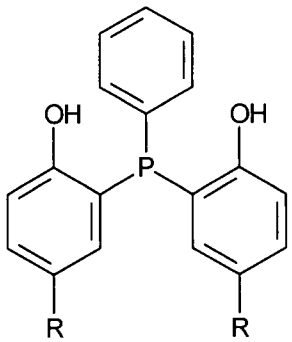

H_2PO_2 (R=H)
$H_2(Me_2PO_2)$ (R=Me)
$H_2(t\text{-}Bu_2PO_2)$ (R=*t*-Bu)

It was hoped that these complexes would provide a simple route to form "rhenium tagged" therapeutics via the HYNIC bifunctional chelate approach. Chapter 3 describes the preparation of ternary complexes of rhenium containing phosphine-phenolate ligands and organohydrazines. These complexes are models that prove the possible utility of phosphine-phenolate ligands in the HYNIC system. Chapter 4 describes the preparation of lanthanide complexes containing tripodal amine phosphinate ligands, and their group 13 (Al^{3+}, Ga^{3+} and In^{3+}) analogues.

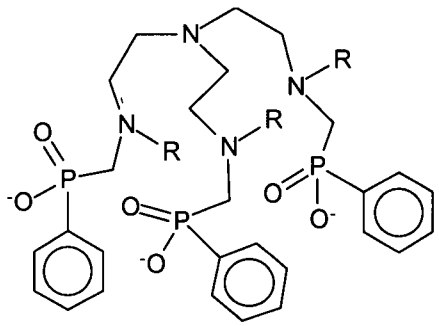

ppba (R=Bz)
ppa (R=H)

The purpose is to design new ligand systems for metal essential radiotherapeutic agents, analogous to ^{153}Sm-EDTMP. As mentioned above, multidentate ligands containing oxygen and nitrogen are ideal for the chelation of lanthanides. The introduction of phosphinate groups as oxygen donors into a tren-based tripod was investigated, and the resulting lanthanide and group 13 complexes are reported.

1.2. References

1) Grigg, E. R. N. *Diagnostic Nuclear Medicine*; Gottschalk, A. and Potchen, E. J., Ed.; Williams & Wilkins: Baltimore, 1976, pp 1.

2) Jurisson, S.; Desilets, C. P.; Jia, W.; Ma, D. *Chem. Rev.* **1993**, *93*, 1137.

3) McCarthy, T. J.; Schwarz, S. W.; Welch, M. J. *J. Chem. Ed.* **1994**, *71*, 830.

4) Dilworth, J. R.; Parrott, S. J. *Chem. Soc. Rev.* **1998**, *27*, 43.

5) Jurisson, S. S.; Lydon, J. D. *Chem. Rev.* **1999**, *99*, 2205.

6) Schwochau, K. *Angew. Chem., Int. Ed. Engl.* **1994**, *33*, 2258.

7) Hom, R. K.; Katzenellenbogen, J. A. *Nucl. Med. Biol.* **1997**, *24*, 485.

8) Deutsch, E.; Bushong, W.; Glavan, K. A.; Elder, R. C.; Sodd, V. J.; Scholz, K. L.; Fortman, D. L.; Lukes, S. J. *Science* **1981**, *214*, 85.

9) Piwnica-Worms, D.; Kronauge, J. F.; Holman, B. L.; al, e. *J. Nucl. Med.* **1988**, *29*, 55.

10) Jurisson, S.; Schlemper, E. O.; Troutner, D. E.; Canning, L. R.; Nowotnik, D. P.; Neirinckx, R. D. *Inorg. Chem.* **1986**, *25*, 543.

11) Sharp, P. F.; Smith, F. W.; Gemmell, H. G.; Lyall, D.; Evans, N. T. S.; Gvozdanovic, D.; Davidson, J.; Tyrrell, D. A.; Pickett, R. D.; Neirinckx, R. D. *J. Nucl. Med.* **1986**, *27*, 171.

12) Liu, S.; Edwards, D. S. *Chem. Rev.* **1999**, *99*, 2235.

13) Liu, S.; Edwards, D. S.; Looby, R. J.; Harris, A. R.; Poirier, M. J.; Barrett, J. A.; Heminway, S. J.; Carroll, T. R. *Bioconjugate Chem.* **1996**, *7*, 63.

14) Edwards, D. S.; Liu, S. *Transition Met. Chem.* **1997**, *22*, 425.

15) Edwards, D. S.; Liu, S.; Barrett, J. A.; Harris, A. R.; Looby, R. J.; Ziegler, M. C.; Heminway, S. J.; Carroll, T. R. *Bioconjugate Chem.* **1997**, *8*, 146.

16) Barrett, J. A.; Crocker, A. C.; Damphousse, D. J.; Heminway, S. J.; Liu, S.; Edwards, D. S.; Lazewatsky, J. L.; Kagan, M.; Mazaika, T. J.; Carroll, T. R. *Bioconjugate Chem.* **1997**, *8*, 155.

17) Liu, S.; Edwards, D. S.; Barrett, J. A. *Bioconjugate Chem.* **1997**, *8*, 621.

18) Volkert, W. A.; Hoffman, T. J. *Chem. Rev.* **1999**, *99*, 2269.

19) Becker, D. V.; Swain, C. T. *Semin. Nucl. Med.* **1996**, *26*, 155.

20) Brenner, W.; Kampen, W. U.; Kampen, A. M.; Henze, E. *J. Nucl. Med.* **2001**, *42*, 230.

21) Lauffer, R. B. *Chem. Rev.* **1987**, *87*, 901.

22) Caravan, P.; Ellison, J. J.; McMurry, T. J.; Lauffer, R. B. *Chem. Rev.* **1999**, *99*, 2293.

23) Heeg, M. J.; Jurisson, S. S. *Acc. Chem. Res.* **1999**, *32*, 1053.

24) Deklerk, J. M. H.; Vanhetschip, A. D.; Zonnenberg, B. A.; Vandijk, A.; Quirijnen, J. M. S. P.; Blijham, G. H.; Vanrijk, P. P. *J. Nucl. Med.* **1996**, *37*, 244.

25) Elder, R. C.; Yuan, J.; Helmer, B.; Pipes, D.; Deutsch, K.; Deutsch, E. *Inorg. Chem.* **1997**, *36*, 3055.

26) Luo, H.; Setyawati, I.; Rettig, S. J.; Orvig, C. *Inorg. Chem.* **1995**, *34*, 2287.

Chapter Two

Phosphine-Phenolate Complexes Containing the $[Re=O]^{3+}$ Core

2.1. Introduction

The $[M=O]^{3+}$ core (M=Tc, Re) is ubiquitous, particularly in the Tc complexes used in diagnostic nuclear medicine (*e.g.* Ceretec®, Figure 1.1).[1-3] The M(V) oxidation state is easily accessible from $[MO_4]^-$ (M(VII)) starting materials by reduction, and most M(V) complexes are stable under ambient conditions. $[M=O]^{3+}$ species exhibit weak, temperature-independent paramagnetism and are diamagnetic.[4] The majority of complexes containing the $[M=O]^{3+}$ core have either 5 coordinate square pyramidal geometry or 6 coordinate octahedral geometry.

A large series of 6 coordinate $[Re=O]^{3+}$ complexes containing phosphines and halides has been known for many years, *e.g.* *mer*-$ReOCl_3(PPh_3)_2$.[4,5] These complexes are most commonly made by reacting a strong hydrohalic acid solution containing $[ReO_4]^-$ ("hydroperrhenic acid") with the appropriate phosphine. Under these conditions, reduction/complexation occurs and the $[Re=O]^{3+}$ complexes are isolated in near quantitative yield. The complexes exhibit excellent hydrolytic stability and are air stable. This class of complexes, although highly useful as starting materials, is not directly suitable for application in nuclear medicine because of the presence of the labile halide groups.

Phosphine-phenolate ligands of the type HPO and H_2PO_2 (H_xPO_x) (Scheme 2.1) and related systems have been reported to form oxo, nitrido and imido M(V) complexes

with rhenium and technetium.[6-13] Similar to the highly successful N_xS_{3-x} and N_xS_{4-x} donor sets which favour the formation of square pyramidal $[Re=O]^{3+}$ complexes,[14-17] the H_xPO_x ligands were originally designed to incorporate a mixed soft/hard donor set in order to stabilize intermediate oxidation states of Tc and Re. In this regard they have been highly successful; all of the complexes reported before this study contain Re(V), and most contain the $[Re=O]^{3+}$ core. The complexes retain many of the properties of compounds such as *mer*-$ReOCl_3(PPh_3)_2$, including octahedral geometry, but reduce the number of, or eliminate completely, the labile halide ligands.

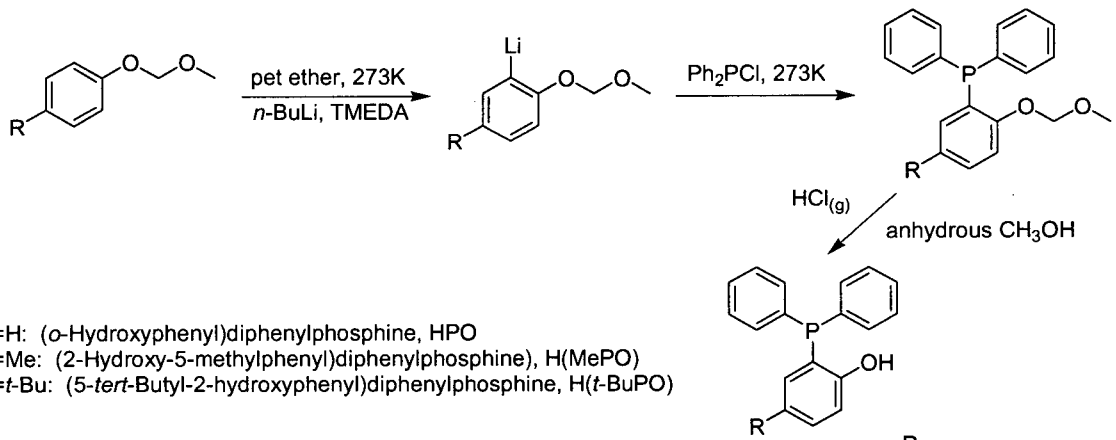

Scheme 2.1

A series of *para*-substituted alkyl HPO and H_2PO_2 derivatives have been synthesized in our group by modifying the published preparations for HPO[18] and H_2PO_2[6] (Scheme 2.1).[19] The synthetic methodology is relatively unchanged except for the use of *para*-substituted phenols in the first step. After mom (methoxymethyl) protection, the *para*-substituted phenols are ortho lithiated and then reacted with the appropriate chlorophenylphosphines, which are subsequently deprotected. The difficulty of isolating pure product increases dramatically both with the size and number of alkyl substituents.

Compared to the unsubstituted compounds, the methyl and *t*-butyl derivatives have enhanced solubility in organic solvents. In particular, the H_2PO_2 system shows remarkably higher solubility on going from the unsubstituted to the *t*-butyl-substituted compound. In addition to enhancing solubility, the alkyl substituents also provide convenient ^1H and ^{13}C NMR handles in the metal complexes. The resulting changes in lipophilicity were undertaken to allow isolation of crystals for X-ray structural analysis, which have been difficult to obtain, particularly in the case of H_2PO_2 complexes.

In this chapter, the synthesis and subsequent characterization of new complexes based on the $[Re{=}O]^{3+}$ core with the alkyl derivatives H(MePO) and $H_2(Me_2PO_2)$ is reported. Preparation of these complexes was achieved from a variety of rhenium starting materials, including $[ReO_4]^-$, a necessary requirement for any radiopharmaceutical agent. The ability of these new $[Re{=}O]^{3+}$ complexes to react with various organohydrazines was also investigated. The resulting HYNIC model could be used to evaluate the feasibility of using PO_x ligands in the HYNIC system.

2.2. Experimental

Materials. (2-Hydroxy-5-methylphenyl)diphenylphosphine (H(MePO))[19], bis(2-hydroxy-5-methylphenyl)phenylphosphine ($H_2(Me_2PO_2)$)[19] and *mer*-[$ReOCl_3(PPh_3)_2$][20] were synthesized by published methods. All solvents were of HPLC grade and were obtained from Fisher. When anhydrous solvents were required, they were dried using conventional procedures.[21] Reactions were carried out under Ar, although all of the product metal complexes were found to be air and moisture stable. Concentrated HCl and NEt_3 were obtained from commercial sources (Fisher) and were used without further purification. 2-Hydrazinopyridine, 2-hydrazino-2-imidazoline, phenylhydrazine, N,N-phenylmethylhydrazine and N,N-dimethylhydrazine were used as obtained from Aldrich. [NH_4][ReO_4] was a gift from Johnson-Matthey and was also used without purification.

Instrumentation. Mass spectra were obtained with either a Kratos MS 50 (electron impact ionization, EIMS) or a Kratos Concept II H32Q instrument (Cs^+-LSIMS with positive ion detection). Infrared (IR) spectra in the range 4000-500 cm^{-1} were recorded as KBr disks with a Mattson Galaxy Series 5000 FTIR spectrophotometer. Microanalyses for C, H, N, and Cl were performed by Mr. P. Borda in this department. ^1H NMR spectra were recorded on a Bruker AC-200E (200 MHz) NMR spectrometer with δ referenced downfield from external TMS. $^{31}P\{^1H\}$ NMR spectra were recorded on Bruker AC-200E (81 MHz) or Bruker AMX-500 (202.5 MHz) spectrometers with δ referenced to external 85% aqueous phosphoric acid.

Preparation of Compounds. [ReOCl(MePO)$_2$], (2.1). Method A: *mer*-[$ReOCl_3(PPh_3)_2$] (84 mg, 0.10 mmol)[20] and H(MePO)·CH_3OH (74 mg, 0.23 mmol) were dissolved in ethanol (10 mL), and refluxed under Ar for 30 minutes. Three drops of triethylamine were added and the subsequent mixture was refluxed for a further 60 minutes. The solvent was removed; the green solid was redissolved into a minimum amount of CH_2Cl_2. Diethyl ether (20 mL) was added and the solution was cooled; the resulting white precipitate of [$NHEt_3$]Cl was removed by filtration and *n*-pentane (200 mL) was added to the green solution to produce a green precipitate, after partial removal of solvent. The green precipitate was filtered, washed liberally with *n*-pentane and dried *in vacuo* to yield 48 mg (59 %). The product was soluble in acetone, acetonitrile, $CHCl_3$ and CH_2Cl_2, but insoluble in Et_2O and *n*-pentane Anal. Calcd (found) for $C_{38}H_{32}ClO_3P_2Re$: C, 55.64 (55.72); H, 3.93 (3.97); Cl 4.32 (4.22). (+)LSIMS: *m/z* = 785 ([M-Cl]$^+$). IR (cm^{-1}): 957 (Re=O). ^1H NMR (CD_2Cl_2) δ: 7.8-6.0 (overlapping, 26 H, aromatic *H*), 2.26 (s, 3H, C*H*$_3$), 2.20 (s, 3H, C*H*$_3$). $^{31}P\{^1H\}$ NMR (CD_2Cl_2, 202.5 MHz) δ: 15.25 (d, $^2J_{PP'}$ = 10 Hz), 2.05 (d, $^2J_{PP'}$ = 10 Hz). Crystals suitable for X-ray structure analysis were grown by slow diffusion of pentane into a CH_2Cl_2 solution of the complex.

Method B: To a 25 mL ethanol solution of [NH_4][ReO_4] (78.8 mg, 0.294 mmol) and H(MePO)•CH_3OH (248 mg, 0.765 mmol) was added one drop of concentrated HCl. This solution was refluxed for two hours under Ar; triethylamine (150 mg, 0.15 mmol) was then added, and the solution was further refluxed overnight. The resulting green solution was filtered, and then purified on a silica gel column using 20:1 $CHCl_3/CH_3OH$ eluent (TLC R_f 0.69, green). After removal of the solvent, the solid was recrystallized

from a saturated solution of $CHCl_3$ and *n*-pentane, and was dried *in vacuo* overnight. The resulting olive green solid was found to be identical to **2.1** synthesized by method A, yield 118 mg (49 %).

[ReO(Me$_2$PO$_2$)(H(Me$_2$PO$_2$))], (2.2). To a 20 mL ethanol solution of $[NH_4][ReO_4]$ (30 mg, 0.11 mmol) and $H_2(Me_2PO_2)\bullet CH_3OH\bullet HCl$ (100 mg, 0.25 mmol) was added one drop of concentrated HCl. This solution was refluxed for several hours under Ar, triethylamine (100 mg, 0.1 mmol) was then added, and the solution was further refluxed overnight. The resulting green solution was filtered and then purified on a silica gel column using 20:1 $CHCl_3/CH_3OH$ eluent (TLC R_f 0.75, green). After removal of the solvent, a green solid was isolated and dried *in vacuo*, yield 40 mg (43%). Anal. Calcd (found) for $C_{40}H_{35}O_5P_2Re\bullet H_2O$: C, 55.74 (55.62); H, 4.33 (4.33). (+)LSIMS: *m/z* = 845 ($[M+H]^+$). IR (cm^{-1}): 965 (Re=O). ^1H NMR (CD_3OD) δ: 7.9-5.7 (overlapping, 22H aromatic *H*), 2.27 (s, 3H, C*H*$_3$), 2.21 (s, 3H, C*H*$_3$), 2.12 (s, 3H, C*H*$_3$), 2.09 (s, 3H, C*H*$_3$). $^{31}P\{^1H\}$ NMR (CD_3OD, 202.5 MHz) δ: 21.14 (d, $^2J_{PP'}$ = 4 Hz), 12.69 (d, $^2J_{PP'}$ = 4 Hz). Crystals suitable for X-ray structure analysis were grown by slow evaporation of an acetonitrile/methanol/acetone solution of the complex.

X-ray crystallographic analyses of 2.1 and 2.2. Please refer to the appendix for experimental details, and for complete tables of bond lengths and bond angles.

2.3. Results and Discussion

2.3.1. $[Re=O]^{3+}$ Complex of H(MePO)

$[ReOCl(MePO)_2]$ **(2.1)** was prepared in good yield by reaction of H(MePO) with *mer*-$[ReOCl_3(PPh_3)_2]$ under basic conditions. The complex was also made from $[NH_4][ReO_4]$ by reduction of the metal in the presence of H(MePO) and HCl, an important result because of the preference for $[^{186/188}ReO_4]^-$ as a starting material in nuclear medicine. After sufficient time for the reduction, the reaction mixture was made basic; the complex was formed and isolated in good yield. The mechanism of the reduction was not investigated in detail, but the reaction does not produce the oxide of H(MePO) as an oxidation product. **2.1** is soluble in organic solvents such as methanol and dichloromethane, but is insoluble in diethyl ether or less polar solvents.

The diagnostic Re=O stretch in the IR spectrum of **2.1** at 957 cm^{-1} is consistent with values for related rhenium oxo complexes.[6,7] The +LSIMS spectrum shows only a small trace of the parent peak at *m/z* 820 and is dominated by the parent minus chloride cation peak at *m/z* 785. The presence of one chloride was verified by elemental analysis. The complex does not precipitate upon addition of sodium tetraphenylborate, indicating that it is neutral and not cationic in solution.

The ^1H NMR spectrum of **2.1** shows two methyl resonances, as expected for a *bis* complex of low symmetry. The 26:6 integration between the aromatic and the methyl groups is consistent with the proposed formulation. The two doublets in the ^{31}P NMR spectrum possess a $^2J_{(P,P)}$ coupling constant of 10 Hz, consistent with two mutually *cis* phosphorus nuclei in dichloromethane solution. The related complex $[ReOCl(PO)_2]$ is also *cis*-(P,P) when synthesized in alcohol solution.[6] The addition of the methyl group

does not create enough steric hindrance for the complex to convert to the *trans*-(P,P) stereoisomer. Only the one stereoisomer reported appears to form in this reaction.

Single crystals for an X-ray structural analysis of **2.1** were obtained by slow diffusion of pentane into a dichloromethane solution of the purified complex (Table 2.1, Figure 2.1). The complex is a neutral, distorted octahedral [$Re{=}O^{3+}$] complex with a P_2O_3Cl coordination sphere. Two pentane molecules are incorporated in the crystal lattice per complex, for a total of 16 in the unit cell. As expected, the MePO ligands act as uninegative, bidentate chelates with the oxo group and the chloride filling the remaining octahedral coordination sites. One Me-PO ligand occupies two equatorial sites and the other occupies both an equatorial site and the axial site *trans* to the oxo group.

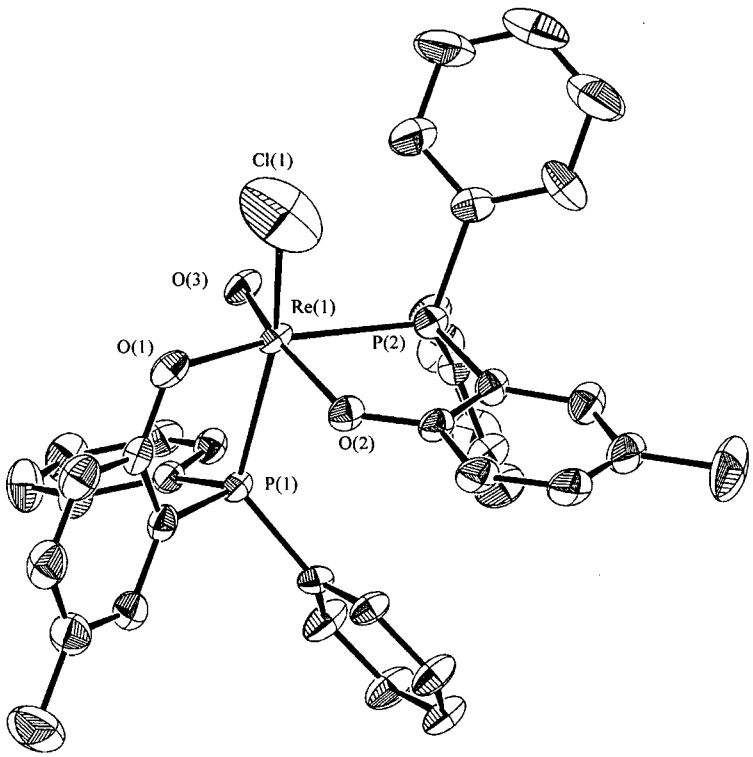

Figure 2.1: ORTEP diagram of [$ReOCl(MePO)_2$], **2.1** (with the solvent molecules and H-atoms omitted); 50% thermal probability ellipsoids are shown.

The Re=O bond length of 1.680 Å is identical to that in the reported structure of $[ReOCl(PO)_2]$.[7] The Re-P bond lengths are comparable, with Re-P *trans* to the chloride slightly elongated compared to Re-P *trans* to the phenolic O donor. This is contrary to the reported $[ReOCl(PO)_2]$ structure wherein both bond lengths are *circa* 0.04 Å longer and the opposite effect was observed. It is possible that the methyl groups on the phenol ring are causing electronic effects. If this is the case, the effects are not centered at the phenolic oxygen because the Re-O bond lengths remain essentially unchanged. The *cis* Re-Cl bond length is 0.14 Å shorter than that reported previously, but the isotropic refinement of the structure revealed that there may be some disorder in the chloro position affecting the reported bond length.

Table 2.1: Selected Bond Lengths (Å) and Angles (deg) in $[ReOCl(MePO)_2]$ (**2.1**).

Re=O(3)	1.680(4)	Cl(1)-Re-O(3)	98.23(16)
Re-Cl(1)	2.264(4)	P(1)-Re-O(1)	100.69(5)
Re-P(1)	2.4457(15)	P(1)-Re-O(2)	83.41(12)
Re-P(2)	2.4206(17)	P(1)-Re-O(3)	91.00(14)
Re-O(1)	2.013(4)	P(2)-Re-O(1)	160.08(10)
Re-O(2)	2.044(3)	P(2)-Re-O(2)	77.96(12)
Cl(1)-Re-P(1)	162.66(10)	P(2)-Re-O(3)	87.18(14)
Cl(1)-Re-P(2)	94.44(12)	O(1)-Re-O(2)	82.57(15)
Cl(1)-Re-O(1)	81.89(15)	O(1)-Re-O(3)	112.70(16)
Cl(1)-Re-O(2)	91.57(14)	O(2)-Re-O(3)	162.80(15)

The bond angles indicate that the coordination in **2.1** is best described as distorted octahedral. Most of the bond angles are similar to those in $[ReOCl(PO)_2]$ with one notable exception: the bidentate phenol ring that is coordinated both through an axial and equatorial position is twisted away from the chloride. The Cl(1)-Re-O(2) angle is compressed 7° as the phenol is brought closer to the chloride and the Cl(1)-Re-O(2) angle is opened by 5°. This, in effect, moves the ring and its methyl group away from the proximity of the chloride. This effect is likely a combination of the increased steric bulk of the methyl group and the shortened Re-Cl bond length.

2.3.2. $[Re=O]^{3+}$ Complex of $H_2(Me_2PO_2)$

$[ReO(Me_2PO_2)(H(Me_2PO_2))]$ (**2.2**) was synthesized from $[NH_4][ReO_4]$ by reducing perrhenate in the presence of the ligand and HCl. As with **2.1**, no phosphine oxide products were detected in the reaction mixture. After reduction, addition of excess base formed a green complex that was soluble in ethanol. This enhanced solubility is presumably due to the methyl groups since the analogue $[ReO(PO_2)(HPO_2)]$ is insoluble in ethanol.[6] Pure **2.2** was isolated in reasonable yield after purification using silica gel chromatography. The formation of a rhenium oxo complex is evident from the 965 cm^{-1} band in the infrared spectrum, and its formulation is supported by the +LSIMS spectrum. As expected for a *bis* complex, the ^1H NMR spectrum shows four methyl resonances which integrate to give the theoretical 22:12 aromatic:methyl ratio. The ^{31}P NMR spectrum shows two doublets with a $^2J_{(P,P)}$ coupling constant of 4 Hz, consistent with two mutually *cis* phosphorus nuclei in solution. At 25°C, there is no indication of any exchange between the free arm of the bidentate ligand with the tridentate Me_2PO_2 ligand.

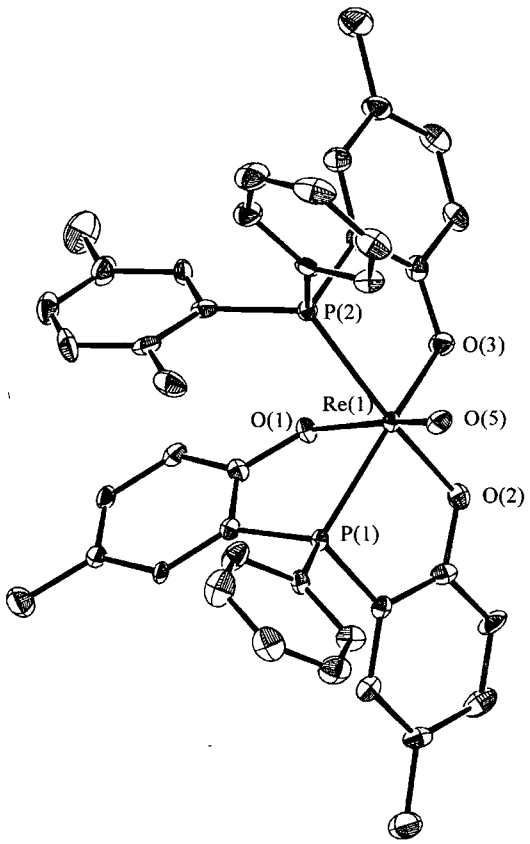

Figure 2.2: ORTEP diagram of [ReO(Me_2PO_2)(H(Me_2PO_2))], **2.2** (with the solvent molecules and H-atoms omitted); 50% thermal probability ellipsoids are shown.

Single crystals were isolated from a slowly evaporated acetonitrile/methanol/acetone solution of the purified complex. The discrete, monometallic compound has a distorted octahedral geometry with a P_2O_4 donor set (Table 2.2, Figure 2.2). One Me_2PO_2 ligand is bound in a facial, tridentate fashion with P and O atoms occupying equatorial positions, and the remaining oxygen occupying the axial position trans to the oxo linkage. The second Me_2PO_2 ligand is bound in an equatorial bidentate fashion with the remaining O protonated and uncoordinated to Re. The addition of acetonitrile to the crystal growing solution was necessary and suitable crystals could not be obtained without it. Indeed, the crystal structure shows two

acetonitrile molecules per complex, one of which is hydrogen bound to the free phenolic OH with a N-O contact of 2.82(1) Å.

Table 2.2: Selected Bond Lengths (Å) and Angles (deg) in $[ReO(Me_2PO_2)(H(Me_2PO_2))]$ (**2.2**).

Re=O(5)	1.666(4)	P(2)-Re-O(1)	79.7(1)
Re-P(1)	2.410(2)	P(2)-Re-O(2)	160.9(1)
Re-P(2)	2.458(2)	P(2)-Re-O(3)	82.3(1)
Re-O(1)	2.035(4)	P(2)-Re-O(5)	93.9(2)
Re-O(2)	2.018(4)	O(1)-Re-O(2)	88.1(2)
Re-O(3)	2.003(4)	O(1)-Re-O(3)	85.1(2)
P(1)-Re-P(2)	108.24(5)	O(1)-Re-O(5)	163.6(2)
P(1)-Re-O(1)	75.0(1)	O(2)-Re-O(3)	82.0(2)
P(1)-Re-O(2)	82.4(1)	O(2)-Re-O(5)	101.5(2)
P(1)-Re-O(3)	155.0(1)	O(3)-Re-O(5)	109.2(2)
P(1)-Re-O(5)	93.0(1)		

A search of the Cambridge Crystallographic Database[22] reveals that **2.2** is the second rhenium PO_2 complex structure to be reported, after $[ReO(PO)(PO_2)]$.[6] The Re=O bond length in **2.2** (1.666(4) Å) is consistent; Re-P bond lengths are typical, but the bidentate Re-P bond is significantly longer than in its tridentate analogue. This may be caused by the additional steric hindrance of the free phenolic OH and its concomitant hydrogen-bonded acetonitrile. The phenol OH on the bidentate ligand is distorted away

from the oxo group by over 10° from the 90° octahedral ideal. This distortion towards the axially coordinated phenol ring may add further steric stress to the bidentate ligand. Similarly, the tridentate ligand is distorted away from the oxo group. This is necessary for the axial phenol group to coordinate *trans* to the oxo group. The resulting 163.6(2)° O(1)-Re-O(5) angle is far from linear and suggests that the tridentate ligand is under strain. In both cases, the phosphine atoms lie within a few degrees of the ideal 90°, relative to the oxo.

2.3.3. Reaction of 2.1 and 2.2 with Hydrazines

There are examples in the literature of the successful bioconjugation of $[Tc{=}O]^{3+}$ complexes with the bifunctional chelate HYNIC.[23-28] Typically, a HYNIC-labeled biomolecule is reacted with pertechnetate in the presence of the ligand and a reducing agent. In some cases, the reducing agent is not necessary due to the reductive capacity of the hydrazine.[29] Reactions of various hydrazines with **2.1** and **2.2** were attempted in order to extend this type of chemistry to rhenium, and to test the feasibility of this approach. Under no conditions would a hydrazine complex form with **2.1** or **2.2**, even at a 20:1 hydrazine:Re ratio. None of 2-hydrazinopyridine, 2-hydrazino-2-imidazoline, phenylhydrazine, N,N-phenylmethylhydrazine or N,N-dimethylhydrazine produced any product. In each case, **2.1** or **2.2** were recovered from the reaction mixture in near quantitative yield. In order to drive the elimination of the Re=O oxygen atom as water (Scheme 1.1) to form a hydrazine complex, temperatures as high as 180°C were used, with and without molecular sieves, but all attempts were unsuccessful. Addition of $NaBH_4$ as a reducing agent did not promote formation of complex by reduction/complexation. Since hydrazine-containing complexes of Re are known to be

accessible from halogen/phosphine complexes containing the $[Re=O]^{3+}$ core (Chapter 3), it is surprising that the reaction with **2.1** and **2.2** was unsuccessful.

An alternative route to HYNIC bioconjugates of PO_x and hydrazines is possible: preformation of PO_x/hydrazine-containing metal complexes, followed by subsequent conjugation to the biomolecule. This idea will be explored further in Chapter 3. Perhaps the ligands are far too kinetically inert and thermodynamically stable to allow coordination of hydrazine and reduction of the metal with the concomitant elimination of the oxo group as water.

2.4. Conclusions

New alkylated derivatives of the H_xPO_x system have been synthesized and isolated in pure form. The presence of the methyl groups increased the solubility of the ligands, and of the final complexes, in organic solvents. The methyl groups also provided a convenient ^1H NMR probe as the number of peaks provided an estimate of the purity and identity of the resulting complexes.

2.1 was obtained by reaction of H(MePO) with *mer*-$[ReOCl_3(PPh_3)_2]$ and in a reduction/complexation reaction from $[NH_4][ReO_4]$. **2.2** was obtained by direct reaction of $H_2(Me_2PO_2)$ with $[NH_4][ReO_4]$. The easy synthesis of each complex from $[ReO_4]^-$ is significant, since this is a strict requirement for any radiopharmaceutical that must incorporate rhenium. The increased solubility was exploited to grow X-ray quality crystals of **2.1** and **2.2**; in the latter case, the second structurally characterized complex of its type. **2.1** and **2.2** have a *cis*-(P,P) arrangement of the ligands, both in solution and the solid state. The complexes appear to be inert and show no evidence of exchange between the ligands at the NMR timescale.

In an attempt to form mixed PO_x / hydrazine complexes, **2.1** and **2.2** were reacted with a variety of hydrazines under a wide range of conditions. The PO_x ligands are clearly not suitable for this type of reaction since no products were isolated from these reactions.

2.5. References

1) Jurisson, S.; Desilets, C. P.; Jia, W.; Ma, D. *Chem. Rev.* **1993**, *93*, 1137.

2) Dilworth, J. R.; Parrott, S. J. *Chem. Soc. Rev.* **1998**, *27*, 43.

3) Jurisson, S. S.; Lydon, J. D. *Chem. Rev.* **1999**, *99*, 2205.

4) Rouschias, G. *Chem. Rev.* **1974**, *74*, 531.

5) Fergusson, J. E. *Coord. Chem. Rev.* **1966**, 459.

6) Luo, H.; Setyawati, I.; Rettig, S. J.; Orvig, C. *Inorg. Chem.* **1995**, *34*, 2287.

7) Bolzati, C.; Tisato, F.; Refosco, F.; Bandoli, G.; Dolmella, A. *Inorg. Chem.* **1996**, *35*, 6221.

8) Loiseau, F.; Connac, F.; Lucchese, Y.; Dartiguenave, M.; Fortin, S.; Beauchamp, A. L.; Coulais, Y. *Inorg. Chim. Acta* **2000**, *306*, 94.

9) Loiseau, F.; Lucchese, Y.; Dartiguenave, M.; Coulais, Y. *Polyhedron* **2000**, *19*, 1111.

10) Connac, F.; Lucchese, Y.; Gressier, M.; Dartiguenave, M.; Beauchamp, A. L. *Inorg. Chim. Acta* **2000**, *304*, 52.

11) Nock, B.; Maina, T.; Tisato, F.; Papadopoulos, M.; Raptopoulou, C. P.; Terzis, A.; Chiotellis, E. *Inorg. Chem.* **1999**, *38*, 4197.

12) Nock, B.; Maina, T.; Tisato, F.; Papadopoulos, M.; Raptopoulou, C. P.; Terzis, A.; Chiotellis, E. *Inorg. Chem.* **2000**, *39*, 2178.

13) Nock, B.; Maina, T.; Tisato, F.; Raptopoulou, C. P.; Terzis, A.; Chiotellis, E. *Inorg. Chem.* **2000**, *39*, 5197.

14) Chi, D. Y.; O'Neil, J. P.; Anderson, C. J.; Welch, M. J.; Katzenellenbogen, J. A. *J. Med. Chem.* **1994**, *37*, 928.

15) Meegalla, S.; Plössl, K.; Kung, M.-P.; Stevenson, D. A.; Liable-Sands, L. M.; Rheingold, A. I.; Kung, H. F. *J. Am. Chem. Soc.* **1995**, *117*, 1137.

16) Papadopoulos, M. S.; Pirmettis, I. C.; Pelecanou, M.; Raptopoulou, C. P.; Terzis, A.; Stassinopoulou, C. I.; Chiotellis, E. *Inorg. Chem.* **1996**, *35*, 7377, and references therein.

17) Hansen, L.; Lipowska, M.; Melendez, E.; Xu, X.; Hirota, S.; Taylor, A. T.; Marzilli, L. G. *Inorg. Chem.* **1999**, *38*, 5351 and references therein.

18) Rauchfuss, T. B. *Inorg. Chem.* **1977**, *16*, 2966.

19) Kovacs, M. S.; Hein, P.; Sattarzadeh, S.; Patrick, B. O.; Emge, T. J.; Orvig, C. , Submitted for publication.

20) Chatt, J.; Rowe, G. A. *J. Chem. Soc.* **1962**, 4019.

21)Perrin, D. D.; Armarego, W. L. F.; Perrin, D. R. *Purification of Laboratory Chemicals*; 2nd ed.; Pergamon Press: Toronto, 1980.

22) Allen, F. H.; Kennard, O. *Chemical Design Automation News* **1993**, *8*, 31.

23) Liu, S.; Edwards, D. S.; Looby, R. J.; Harris, A. R.; Poirier, M. J.; Barrett, J. A.; Heminway, S. J.; Carroll, T. R. *Bioconjugate Chem.* **1996**, *7*, 63.

24) Liu, S.; Edwards, D. S.; Harris, A. R.; Singh, P. R. *Appl. Radiat. Isot.* **1997**, *48*, 1103-1111.

25) Edwards, D. S.; Liu, S.; Barrett, J. A.; Harris, A. R.; Looby, R. J.; Ziegler, M. C.; Heminway, S. J.; Carroll, T. R. *Bioconjugate Chem.* **1997**, *8*, 146.

26) Barrett, J. A.; Crocker, A. C.; Damphousse, D. J.; Heminway, S. J.; Liu, S.; Edwards, D. S.; Lazewatsky, J. L.; Kagan, M.; Mazaika, T. J.; Carroll, T. R. *Bioconjugate Chem.* **1997**, *8*, 155.

27) Larsen, S. K.; Solomon, H. F.; Caldwell, G.; Abrams, M. J. *Bioconjugate Chem.* **1995**, *6*, 635.

28) Rajopadhye, M.; Harris, T. D.; Yu, K.; Glowacka, D.; Damphousse, P. R.; Barret, J. A.; Heminway, S. J.; Edwards, D. S.; Carroll, T. R. *Bioorg. Med. Chem. Lett.* **1997**, *7*, 955.

29) Abrams, M. J.; Juweid, M.; tenKate, C. I.; Schwartz, D. A.; Hauser, M. M.; Gaul, F. E.; Fuccello, A. J.; Rubin, R. H.; Strauss, H. W.; Fischman, A. J. *J. Nucl. Med.* **1990**, *31*, 2022.

Chapter Three

Phosphine-Phenolate Complexes

Containing Rhenium-Hydrazine Cores

3.1. Introduction

As previously noted in Chapter 2, the synthesis of hydrazine-containing ternary complexes failed when $[ReOCl(MePO)_2]$ **(2.1)** and $[ReO(Me_2PO_2)(H(Me_2PO_2))]$ **(2.2)** were reacted directly with various organohydrazines. Therefore, it is not possible to use the synthetic route shown pictorially in Scheme 1.1. A possible alternative route to HYNIC complexes is through the preformed chelate approach (Scheme 3.1).[1]

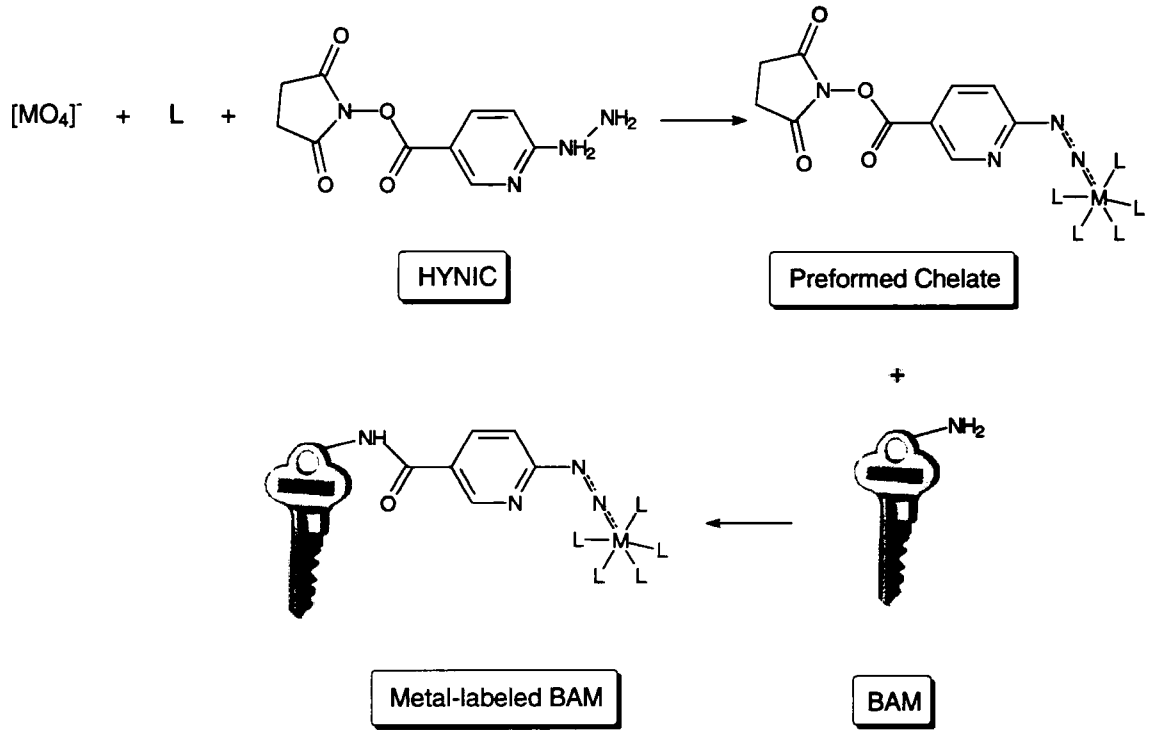

Scheme 3.1

The preformation of hydrazine-containing metal complexes, followed by reaction with H_xPO_x and subsequent conjugation to the biomolecules offers many advantages over indirect labeling approach (Scheme 1.1), wherein the hydrazine and biomolecules are incorporated into the complex last. To compensate for the increased kinetic inertness of rhenium relative to technetium, conditions may be required that are too harsh for the biomolecule to tolerate. This synthetic route is advantageous because the complex can be formed under relatively harsh conditions before the biomolecule is introduced.[2]

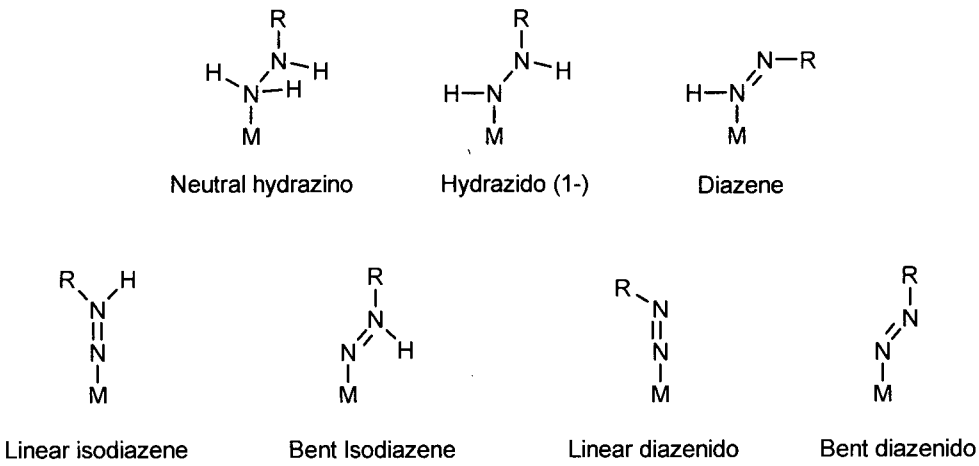

Scheme 3.2

The coordination chemistry of rhenium with hydrazines is rich and varied.[3-22] There are at least 7 known coordination modes known with various oxidation states of metal and hydrazine (Scheme 3.2).[17] Most of these compounds are mixed complexes of a hydrazine with phosphines and halogens, and most have been made by convenient reduction of *mer*-$[ReOCl_3(P)_2]$ (P = PPh_3 or PMe_2Ph) to form five or six coordinate *bis*hydrazine complexes, with the hydrazine ligands *cis* to each other (Figure 3.1).[6-9,11,12,16] It is curious that many hydrazines are reactive with *mer*-$[ReOCl_3(P)_2]$ (P = PPh_3

or PMe_2Ph), but not with the PO_x-containing complexes **2.1** and **2.2**, since both contain the $[Re=O]^{3+}$ core with mixed phosphines and halogens.

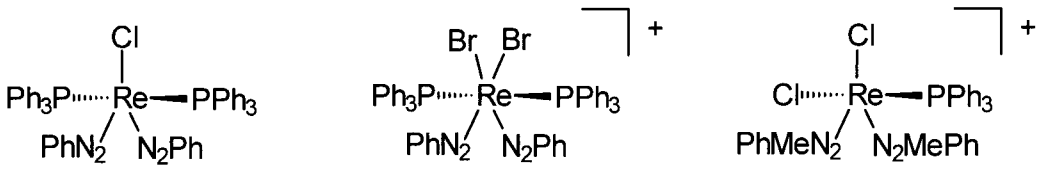

Figure 3.1: Selected Rhenium Hydrazine Complexes Containing Halide and Phosphine Ligands.

As alluded to above, $[ReCl(N_2Ph)_2(PPh_3)_2]$ (Figure 3.1, left) is formed by direct reaction of $[ReOCl_3(PPh_3)_2]$ with phenylhydrazine.[18] The *para*-bromophenylhydrazine analogue has been structurally characterized as a five coordinate complex with the two diazenido ligands *cis* to each other.[11] There is extensive evidence that $[ReCl(N_2Ph)_2(PPh_3)_2]$ reacts in halogenated solvents to form a six coordinate μ-chloro bridged dimer.[9] If HCl is added to a solution of the complex, the protonated six coordinate complex $[ReCl_2(N_2Ph)(HN_2Ph)(PPh_3)_2]$ is isolated; the analogous bromo complex can be isolated by substituting HBr.[9] Interestingly, the oxidation of $[ReCl(N_2Ph)_2(PPh_3)_2]$ with Br_2 affords the six coordinate Re complex, $[ReBr_2(N_2Ph)_2(PPh_3)_2][Br]$ (Figure 3.1, centre).[18] Linear isodiazene complexes containg rhenium, phosphines and halides are also known. The reaction of $[ReOCl_3(PPh_3)_2]$ with N,N-phenylmethylhydrazine in methanol yields five coordinate $[ReCl_2(N_2PhMe)_2(PPh_3)][BPh_4]$ (Figure 3.1, right) after the addition of $NaBPh_4$.[12]

There has been a burgeoning interest in synthesizing complexes with the $[Re(Hhypy)(hypy)]^{2+}$ core (hypy = $N_2C_5H_4N$) as models for the HYNIC bioconjugation of metal complexes (Scheme 3.3).[23,24] The $[Re(Hhypy)(hypyH)Cl_3]$ parent complex can

be synthesized by reaction of $[ReO_4]^-$ with 2-hydrazinopyridine hydrochloride in methanol.[23,25] The ligand reduced Re(VII) to Re(III) after which the oxidized organodiazenes (hypy) coordinated to the metal in a unique bidentate bent diazene (Hhypy) and in a monodentate linear diazenido fashion with the pyridine nitrogen protonated in the latter case (hypyH). The chloro complex is not expected to be stable *in vivo*. Since the initiation of our studies, others have tried to stabilize the core through the formation of ternary complexes, demonstrating that thiols, including HPS (the thiol equivalent of HPO), could be used to form complexes with the $[Re(Hhypy)(hypy)]^{2+}$ core.[24]

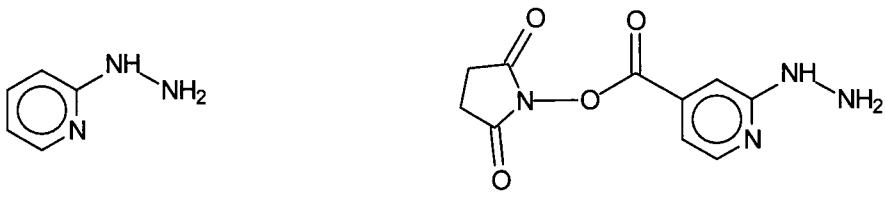

2-hydrazinopyridine (H_3hypy) HYNIC

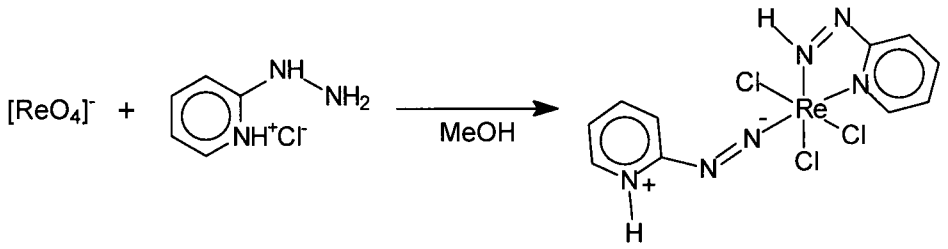

$[Re(Hhypy)(hypyH)Cl_3]$

Scheme 3.3

In order to stabilize this core towards hydrolysis *in vivo*, we thought that the H_xPO_x ligands could be bound to the metal as ancillary ligands. Recently, a variety of tethered "3+2" rhenium oxo complexes with mixed N_xS_{3-x} and PO have been

elaborated.[26-28] These compounds appear to be very stable - some were able to withstand a glutathione challenge experiment for 24 h.[26] No known ternary complexes of hydrazine/diazo ligands and H_xPO_x have been included in the literature prior to this report. The ability of H_xPO_x to stabilize intermediate oxidation states and to form hydrolytically stable complexes indicates that the ligand may well be an excellent choice for use in the HYNIC system. To this end, we decided to investigate the reactivity of these ligands with the $[Re(Hhypy)(hypy)]^{2+}$ core.

To further explore the reactivity of H_xPO_x, attempts were made to synthesize mixed hydrazine-PO_x complexes starting from the known complexes in Figure 3.1. It was hoped that the PO_x ligands would displace PPh_3 and halide ligands to form more hydrolytically stable complexes. The discovery of new hydrazine-based cores is attractive for a number of reasons. Besides the obvious patent implications, the elimination of the potentially interfering pyridyl donor in HYNIC may result in a more simplified scheme to functionalize biomolecules. The N,N-phenylmethylhydrazine complexes are particularly attractive; only four of the possible seven hydrazine coordination modes (Scheme 3.2) are possible due to the methyl group (two are possible if only the N=N modes are considered).

3.2. Experimental

Materials. (*o*-Hydroxyphenyl)diphenylphosphine (HPO)[29], bis(*o*-hydroxyphenyl)phenylphosphine (H_2PO_2)[30], (2-hydroxy-5-methylphenyl)diphenylphosphine (H(MePO))[31], bis(2-hydroxy-5-methylphenyl)phenylphosphine ($H_2(Me_2PO_2)$)[31], $[ReCl(N_2Ph)_2(PPh_3)_2]$[18], $[ReBr_2(N_2Ph)_2(PPh_3)_2][Br]$[18], $[ReCl_2(N_2PhMe)_2(PPh_3)][BPh_4]$[12] and [Re(hypy)(hypyH)Cl_3][23,25] were synthesized by published methods. All solvents were of HPLC grade and were obtained from Fisher. When anhydrous solvents were required, they were dried using conventional procedures.[32] Reactions were carried out under Ar, although all of the product metal complexes were found to be air and moisture stable. NEt_3 (Fisher), Br_2, 2-hydrazinopyridine, phenylhydrazine and N,N-phenylmethylhydrazine were obtained from commercial sources (Aldrich) and were used without further purification. $[NH_4][ReO_4]$ was a gift from Johnson-Matthey and was also used without purification.

Instrumentation. Experimental details are identical to those outlined in Section 2.2 with the following exceptions: ^1H NMR spectra were recorded on Bruker AC-200E (200 MHz) or Bruker AV-300 (300 MHz) NMR spectrometers with δ referenced downfield from external TMS. $^{31}P\{^1H\}$ were recorded on Bruker AC-200E (81 MHz) or Bruker AV-300 (121.5 MHz) NMR spectrometers with δ referenced to external 85% aqueous phosphoric acid.

Preparation of Compounds. [Re(Hhypy)(hypy)(PO)(HPO)]Cl, (3.1). Method A: [Re(Hhypy)(hypyH)Cl_3] (62 mg, 0.118 mmol) and HPO (93 mg, 0.294 mmol) were dissolved in 15 mL methanol. The reaction flask was flushed with Ar for 20 minutes,

after which time triethylamine (32 mg, 0.317 mmol) was added. The solution began to turn red immediately and was refluxed overnight. The resulting red solution was purified on a silica gel column using 10:1 $CHCl_3$/MeOH eluent (TLC R_f = 0.12, red). After removal of the solvent, the red product was recrystallized from CH_2Cl_2/CH_3OH, and dried *in vacuo*, yield 80 mg (64 %). Anal. Calcd. (found) for $C_{46}H_{36}ClN_6O_2P_2Re{\cdot}CH_2Cl_2$: C, 52.64 (53.11); H, 3.57 (4.03); N, 7.84 (8.13). (+)LSIMS: *m/z* = 955 ($[M]^+$). ^{1}H NMR (CD_2Cl_2) δ: 8.66 (dd, 1H, α-nitrogen *H*, $^3J_{(H\text{-}P)}$ = 5.1 Hz, $^3J_{(H\text{-}P')}$ = 1.2 Hz), 7.9-6.4 (overlapping multiplets, 36H). ^{31}P NMR (CD_2Cl_2, 81 MHz) δ: 32.9 (d, $^2J_{(P,P)}$ = 202 Hz), 14.1 (d, $^2J_{(P,P)}$ = 202 Hz). Crystals suitable for X-ray structure analysis were grown by slow diffusion of cyclohexane into a chlorobenzene/toluene solution of the isolated complex.

Method B: $[NH_4][ReO_4]$ (100 mg, 0.373 mmol) and 2-hydrazinopyridine·2HCl (270 mg, 1.492 mmol) were combined and stirred into 40 mL methanol. The solution color quickly changed to purple; the reaction solution was refluxed for 30 minutes. After allowing the solution to cool, HPO·HCl (500 mg 1.59 mmol) in 10 mL methanol was added, followed by NEt_3 (300 mg, 2.97 mmol). The mixture was refluxed overnight, and afforded a red mixture of products. The products were separated on silica gel and isolated: **3.1** (190 mg, 48%), **3.2** (26 mg, 10%).

[ReCl(Hhypy)(hypy)(PO)], (3.2). [ReCl(Hhypy)(hypy)(PO)] (20 mg, 24 %) was isolated, on a silica gel column using 10:1 $CHCl_3/CH_3OH$ eluent, as a byproduct of the reaction of **3.1** (TLC R_f = 0.54). IR (cm^{-1}): 1579 ($\nu_{N=N}$), 1551 ($\nu_{N=N}$). (+)LSIMS: *m/z* = 677 ($[M\text{-}Cl]^+$). ^{1}H NMR (CD_2Cl_2) δ: 8.02 (d, 1H, α-nitrogen *H*, $^3J_{(H,P)}$ = 6.1 Hz), 7.7–6.5 (overlapped multiplets, 22H). ^{31}P NMR (CD_2Cl_2, 81 MHz) δ: 25.5 (s). Crystals

suitable for X-ray structure analysis were obtained by slowly evaporating a solution of the complex in CH_2Cl_2/MeOH.

[Re(Hhypy)(hypy)(HPO_2)(H_2PO_2)]Cl (3.3). This complex was synthesized using method A for **3.1** with the substitution of H_2PO_2 for HPO. (+)LSIMS: *m/z* = 987 ($[M]^+$). ^{1}H NMR (CD_3OD) δ: 8.50 (dd, 1H, α-nitrogen *H*, $^3J_{(H-P)}$ = 1.0 Hz, $^3J_{(H-P')}$ = 4.9 Hz), 7.9-6.0 (overlapping multiplets, 34H). ^{31}P NMR (CD_3OD, 81 MHz) δ: 31.8 (d, $^2J_{(P,P)}$ = 207 Hz), 13.5 (d, $^2J_{(P,P)}$ = 202 Hz).

[Re(Hhypy)(hypy)(H(Me_2PO_2))(H_2(Me_2PO_2)]Cl (3.4). This complex was synthesized using method A of the synthesis for **3.1** with the substitution of $H_2(Me_2PO_2)$ for HPO. Only the major product was isolated and characterized. Recrystallization from CH_2Cl_2/CH_3OH afforded pure product, yield 60 mg (45%). Anal. Calcd (found) for $C_{50}H_{46}N_6O_4P_2Re{\cdot}CH_2Cl_2$: C, 54.30 (54.70); H, 4.29 (4.51); N, 7.45 (7.51). (+)LSIMS: *m/z* = 1043 ($[M]^+$). ^{1}H NMR (CD_2Cl_2) δ: 8.45 (dd, 1H, α-nitrogen *H*, $^3J_{(H-P)}$ = 1.1 Hz, $^3J_{(H-P')}$ = 5.0 Hz), 7.9-6.4 (overlapping multiplets, 30H), 2.17 (s, 3H, C*H*$_3$), 2.07 (s, 3H, C*H*$_3$), 1.99 (s, 3H, C*H*$_3$), 1.80 (s, 3H, C*H*$_3$). ^{31}P NMR (CD_2Cl_2, 81 MHz) δ: 32.8 (d, $^2J_{(P,P)}$ = 205 Hz), 12.8 (d, $^2J_{(P,P)}$ = 202 Hz).

[Re(N_2PhMe)$_2$(MePO)$_2$][BPh_4] (3.5). [$ReCl_2(N_2PhMe)_2(PPh_3)$][BPh_4] (300 mg, 0.278 mmol) was dissolved in 50 mL methanol. H(MePO) (204 mg, 0.707 mmol) was added as a 10 mL methanol solution, followed by the dropwise addition of NEt_3 (120 mg, 1.18 mmol). The mixture was stirred overnight at 25°C. After the removal of approximately half of the solvent, a brown precipitate formed, which was isolated by filtration, and purified on a silica gel column (TLC R_f = 0.68) using 9:1 $CHCl_3$:CH_3OH as the eluent (110 mg, 30%). Anal. Calcd (found) for $C_{76}H_{68}BN_4O_2P_2Re{\cdot}0.5CHCl_3$: C, 66.20 (66.80); H, 4.97 (5.04); N, 4.04 (3.95). (+)LSIMS: *m/z* = 1009 ($[M]^+$),

889 ([M-N_2PhMe]$^+$). IR (cm^{-1}): 1593 (N=N). ^{1}H NMR (CD_2Cl_2, 300 MHz) δ: 7.8-6.5 (overlapping, 56 H, aromatic *H*), 3.46 (s, 6H, C*H*$_3$), 2.31 (s, 6H, C*H*$_3$). ^{31}P NMR (CD_2Cl_2, 121.5 MHz) δ: 29.4 (s).

X-Ray Crystallographic Analyses of 3.1 and 3.2. Please refer to the appendix for experimental details, and complete tables of bond lengths and bond angles.

3.3. Results and Discussion

3.3.1. [Re(Hhypy)(hypyH)Cl_3] + HPO

[Re(Hhypy)(hypyH)Cl_3] reacts with HPO directly in methanolic solution in the presence of base to form a mixture of products. Two products in the mixture were isolated and characterized after purification on a silica gel column. The salt [Re(Hhypy)(hypy)(PO)(HPO)]Cl (**3.1**) was the major component (64%); all three chlorine atoms were replaced to give a N_3OP_2 coordination sphere. Neutral [ReCl(Hhypy)(hypy)(PO)] (**3.2**) was isolated as a minor component (24%). A 20:1 molar ratio of HPO:Re improved the yield of **3.1** only slightly and impurities, notably **3.2**, were still present. There is evidence for the presence of other species in the mixture, but they were present in amounts too small to purify and characterize properly.

Complexes **3.1** and **3.2** can also be formed directly from [NH_4][ReO_4] in a "one pot" reaction; reduction/complexation of the perrhenate with 2-hydrazinopyridine in HCl proceeds rapidly in methanol. Addition of excess HPO and sufficient base to neutralize the acid rapidly causes the solution to change color from purple to red. Purification on silica gel affords the same two complexes isolated by the direct route in only slightly diminished yields. The ability to synthesize complexes in a "one pot" reaction is highly desirable for preparative nuclear medicine, because the required starting material therein is perrhenate.

Strong IR absorptions at 1580 cm^{-1} and 1550 cm^{-1} are indicative of doubly bonded N=N organodiazo coordination in both complexes. The presence of these two identical bands in **3.1** and **3.2** suggests that both hydrazine ligands remain coordinated and retain

significant double bond character in both cases. Clearly the complexes do not contain the Re(V) oxo core; there are no bands in the range 850 – 1050 cm^{-1}. The majority of the spectral features in the infrared spectra are due to the bands arising from the supporting framework of the organic ligands.

The ^{1}H NMR spectrum of **3.1** consists of a very complex aromatic region (not assigned), the α-nitrogen proton, and the phenolic proton. In CH_2Cl_2 one of the hydrazines retains the doubly bent, α-protonated, diazo mode of the starting material [Re(Hhypy)(hypyH)Cl_3]. The α-nitrogen proton appears as an exchangeable, sharp doublet of doublets at 8.79 ppm. This peak is shifted considerably downfield from that in the starting material, where the protonated pyridyl and α-nitrogen proton appear to be under exchange as a broad peak at 4.22 ppm.[23] There is possibly a weak hydrogen bonding interaction with the free pyridine of the monodentate hypy. This interaction is seen in the crystal structure of the complex (*vide infra*) and is apparently retained in solution. The coupling pattern is consistent with two chemically inequivalent ^{31}P nuclei. The exchangeable phenolic proton appears as a broad resonance centered at 2.25 ppm in CH_2Cl_2 solution. The ^{1}H NMR spectrum strongly supports a diamagnetic, monocationic Re(III) metal center.

The ^{31}P NMR spectrum of **3.1** is consistent with the presence of two chemically inequivalent, coordinated phosphines. In sharp contrast to the oxo complexes **2.1** and **2.2**, the 202 Hz coupling constant of the two AB doublets is a strong indication that the phosphorus nuclei are coordinated *trans* to each other in **3.1** in CH_2Cl_2. At 25°C, there is no indication of any fluxional process that exchanges the bidentate and monodentate PO ligands.

Single crystals of **3.1** for an X-ray structural analysis were obtained by the slow diffusion of cyclohexane into a chlorobenzene/toluene solution of the purified complex (Table 3.1, Figure 3.2). The coordination is best described as distorted octahedral with a N_3OP_2 coordination sphere about Re. Using the formalism of the Re(III) starting material [Re(Hhypy)(hypyH)Cl_3], the complex is a Re(III) cation with a chloride counteranion.

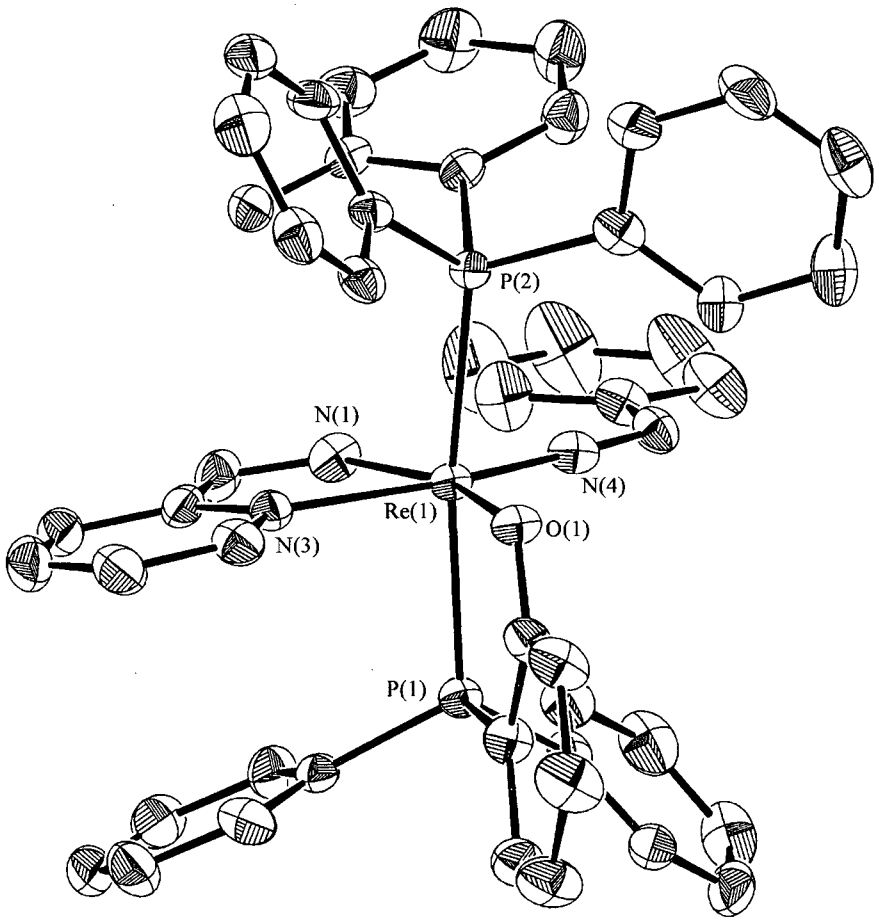

Figure 3.2: ORTEP diagram of the cation $[Re(Hhypy)(hypy)(PO)(HPO)]^+$, **3.1** (with the solvent molecules, H-atoms and the counteranions omitted); 50% thermal probability ellipsoids are shown.

Table 3.1: Selected Bond Lengths (Å) and Angles (deg) in [Re(Hhypy)(hypy)(PO)(HPO)]Cl (**3.1**).

Re-N(1)	1.980(4)	P(1)-Re-N(1)	94.91(14)
Re-N(3)	2.158(5)	P(1)-Re-N(3)	86.03(13)
Re-N(4)	1.780(5)	P(1)-Re-N(4)	94.83(15)
Re-O(1)	2.032(3)	P(2)-Re-O(1)	86.18(9)
Re-P(1)	2.4137(14)	P(2)-Re-N(1)	98.19(14)
Re-P(2)	2.4666(14)	P(2)-Re-N(3)	96.52(13)
N(1)-N(2)	1.299(7)	P(2)-Re-N(4)	86.66(15)
N(4)-N(5)	1.240(7)	O(1)-Re-N(1)	160.03(16)
O(1)-Re-N(4)	109.65(15)	O(1)-Re-N(3)	87.92(13)
N(1)-Re-N(3)	72.26(17)	Re-N(1)-N(2)	126.3(4)
N(1)-Re-N(4)	90.11(18)	N(1)-N(2)-C(19)	110.7(5)
N(3)-Re-N(4)	162.35(16)	Re-N(4)-N(5)	177.0(4)
P(1)-Re-P(2)	166.82(4)	N(4)-N(5)-C(24)	118.5(5)
P(1)-Re-O(1)	80.98(9)		

The two diazo groups are *cis* to one another and both bond lengths therein are well within the range for N=N double bonds. One hypy is bidentate; the protonated diazo and pyridyl nitrogens form a 5-membered ring with a bite angle of 72.26(17)°. The other hypy is monodentate and is bound through the diazo group only. The diazo group on the bidentate hypy is best described as a "doubly bent" diazene ligand since the Re-N(1)-N(2) and the N(1)-N(2)-C(19) bond angles are both within 10° of 120°. The monodentate

diazo group has a nearly linear Re-N(4)-N(5) bond angle, a bent N(4)-N(5)-C(24) bond angle 120°, and should be regarded as a "singly bent" diazenido ligand. The Re-N(1) bond length of 1.980(4) Å is significantly longer than the Re-N(4) bond length of 1.780(5) because of the α-nitrogen proton on N(1). There is a weak 2.870(8) Å hydrogen bond contact between N(1) and the monodentate pyridyl nitrogen N(6), which is deprotonated. The α-nitrogen proton H(95) was included in the refinement of the structure. The N(2)-N(1)-N(6) angle of 134.8(3)° and the N(1)-H(95)-N(6) angle of 149(5)° indicate some strain associated with this interaction. The interaction of N(1) and N(6) through H(95) may contribute to the large ^{1}H NMR chemical shift of the α-nitrogen proton that is retained in solution.

As indicated in the ^{31}P NMR spectrum, the two phosphorus nuclei are *trans*, with a P(1)-Re-P(2) bond angle of 166.82(4) Å. One of the PO ligands is bidentate, forming a 5-membered ring with a bite angle of 80.98(9)°. The second PO ligand is bound only through the phosphorus, with the protonated phenolic oxygen pointing away from the metal center. The bidentate Re-P(1) bond is approximately 0.05 Å shorter than the monodentate Re-P(2) bond. The two hypy groups are slightly distorted away from P(1) and cause some steric crowding, hence the longer bond to P(2), and the displacement of P(2) towards O(1).

The ^{1}H NMR spectrum of the minor product [ReCl(Hhypy)(hypy)(PO)] (**3.2**) shows roughly the same spectral features, with the omission of the free phenolic proton. The α-nitrogen proton appears as a doublet at 8.02 ppm, indicating coupling to only one ^{31}P nucleus in solution. If insufficient base is added to completely deprotonate the pyridine in the starting material, the ^{1}H NMR resonance of the doublet appears at 3.96 ppm. As in the starting material, the protonated pyridyl proton is under exchange with

the α-nitrogen proton; however, the peak remains a distinct doublet and does not broaden to a singlet. The ^{31}P NMR spectrum of **3.2** has the expected singlet at 25.5 ppm. Again, the NMR evidence supports the presence of a diamagnetic Re(III) metal center.

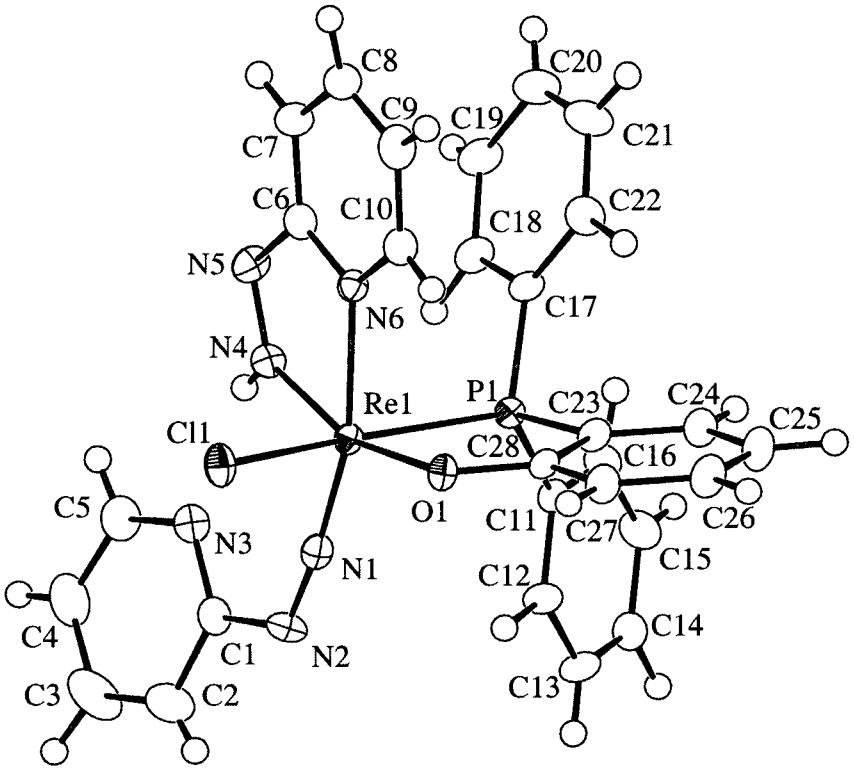

Figure 3.3: ORTEP diagram of [ReCl(Hhypy)(hypy)(PO)], **3.2**; 50% thermal probability ellipsoids are shown.

In most regards, the structure of **3.2** is very similar to that of **3.1** (Table 3.2, Figure 3.3). Crystals were obtained by slow evaporation of a CH_2Cl_2 / CH_3OH solution of the complex. A distorted octahedral N_3POCl donor set surrounds the formally Re(III) metal center, resulting in a neutral complex. The arrangement of the two hypy ligands is identical to that in **3.1**, including the weak pyridine - α-nitrogen contact. The chloride is *trans* to the phosphorus donor of the bidentate PO ligand. The Re-Cl bond is

approximately 0.15 Å longer than the *cis* Re-Cl bond measured in the structure of $[ReOCl(MePO)_2]$. The two hypy ligands are pushed away from the bidentate phosphorus donor and distort the Cl sharply towards the oxygen donor resulting in a P(1)-Re-Cl bond angle of 161.77(5)°.

Table 3.2: Selected Bond Lengths (Å) and Angles (deg) in [ReCl(Hhypy)(hypy)(PO)] (**3.2**).

Re-Cl(1)	2.414(2)	N(4)-Re-O(1)	160.1(2)
Re-N(1)	1.779(5)	N(4)-Re-P(1)	96.14(14)
Re-N(4)	1.942(5)	N(4)-Re-Cl(1)	99.13(14)
Re-N(6)	2.137(5)	N(6)-Re-O(1)	88.3(2)
Re-O(1)	2.035(4)	N(6)-Re-P(1)	88.12(13)
Re-P(1)	2.400(2)	N(6)-Re-Cl(1)	87.20(13)
N(1)-N(2)	1.237(7)	O(1)-Re-P(1)	80.74(11)
N(4)-N(5)	1.312(7)	O(1)-Re-Cl(1)	81.51(11)
N(1)-Re-N(4)	90.7(2)	P(1)-Re-Cl(1)	161.77(5)
N(1)-Re-N(6)	162.4(2)	Re-N(1)-N(2)	174.7(4)
N(1)-Re-O(1)	109.15(18)	N(1)-N(2)-C(1)	118.9(5)
N(1)-Re-P(1)	96.30(15)	Re-N(4)-N(5)	128.7(4)
N(1)-Re-Cl(1)	93.44(15)	N(4)-N(5)-C(6)	108.4(5)
N(4)-Re-N(6)	71.9(2)		

3.3.2. [Re(Hhypy)(hypyH)Cl_3] + H_2PO_2 & $H_2(Me_2PO_2)$

Originally it was hoped that a six coordinate Re(III) complex resembling [Re(hypy)$(PO)_2$] could be synthesized and isolated from the reaction. Since the initiation of our work, a complex of this type has been isolated and characterized from the analogous PS system, [Re(hypy)$(PS)_2$].[24] There appears to be no evidence for the formation of its PO analog, although in the mixture there are small amounts of other species that cannot be fully characterized. The presence of the H-bonded meridional "belt" of hypy ligands appears to be a stable structural motif in this system. Attempts to displace the second hypy ligand by using a 20:1 HPO:Re ratio were unsuccessful. If base is omitted from the synthesis, the starting material remains largely unreacted and is recovered in near quantitative yield.

The phenolic oxygen donor also appears to play a key role in the behavior of the complexes; the relatively soft Re(III) center may be unable to accommodate two such hard phenolic donors. In addition to the "belt" effect, the second hypy may also be regarded as a softer donor that is able to stabilize the Re(III) centre better than the hard phenolate oxygen donors. The remaining coordination site *trans* to the bidentate phosphine displays a distinct preference for soft donors such as Cl^-, the phosphine of PO, or in the case of the analogous PS complex, the thiophenolate donor.[24]

This preference of the metal center for a relatively soft donor set may explain the inability of **2.1** and **2.2** to accept a hydrazine donor and/or reduce the metal center. Coordination to the sterically-crowded octahedral Re center would likely have to occur through a dissociative mechanism. The kinetic inertness and thermodynamic stability of the bidentate and tridentate donors in **2.1** and **2.2** may be too great for the incoming hydrazine to overcome. Remembering that many diazenido complexes have been

synthesized from $[ReOCl_3(PPh_3)]$, the chelate effect of the PO_x ligands in **2.1** and **2.2** is likely responsible for raising the energy barrier too high for diazenido complex formation to occur.

Table 3.3: Selected ^1H & ^{31}P NMR spectral data for [Re(Hhypy)(hypy)(PO)(HPO)]Cl (**3.1**), [ReCl(Hhypy)(hypy)(PO)] (**3.2**), $[Re(Hhypy)(hypy)(HPO_2)(H_2PO_2)]Cl$ (**3.3**), and $[Re(Hhypy)(hypy)(H(Me_2PO_2))(H_2(Me_2PO_2))]Cl$ (**3.4**).

Complex	Alkyl ^1H NMR Signals (ppm)	α-nitrogen ^1H NMR Signals (ppm) and $^3J_{(H-P)}$ / $^3J_{(H-P')}$	^{31}P NMR Signals (ppm) and $^2J_{(P,P)}$
3.1		8.66 (dd)	14.1 (d), 32.0 (d)
		1.2 / 5.1 Hz	202 Hz
3.2		8.02 (d)	25.5 (s)
		6.1 Hz	
3.3		8.50 (dd)	13.5 (d) , 31.8 (d)
		1.0 / 4.9 Hz	207 Hz
3.4	2.17 (s), 2.07 (s), 1.99 (s),	8.45 (dd)	12.8 (d), 32.8 (d)
	1.80 (s)	1.1 / 5.0 Hz	205 Hz

Complexes of this system have also been made with PO_2 and Me_2PO_2; in both cases, octahedral Re(III) complexes with the donor set N_3OP_2 were isolated as the major products. It was hoped that the chelate effect of three free phenolic donors would drive the formation of a $N_2O_2P_2$ coordination sphere, but this was clearly not the case. Crystal

structures were not obtained but the NMR data (Table 3.3) are consistent with the structures presented above. The methyl groups *para* to the phenol provide a convenient ^{1}H NMR "handle".

[Re(Hhypy)(hypy)(HPO_2)(H_2PO_2)]Cl (**3.3**) showed a clear *trans*-(P,P) coupling present in the ^{31}P NMR spectrum. This complex was extremely difficult to separate from the mixture so only the ^{1}H and ^{31}P NMR spectral data are reported. On the basis of these data, the complex is completely analogous to the structurally characterized PO complex, with three protonated phenols not coordinated to the metal centre. [Re(Hhypy)(hypy)($H(Me_2PO_2)$)($H_2(Me_2PO_2)$)]Cl (**3.4**) also appears to have the same structure as the PO complex. There are four methyl resonances in the ^{1}H NMR spectrum with a 1:1:1:1 integration. This information, combined with a *trans*-(P,P) coupling in the ^{31}P NMR spectrum, strongly suggests that the structural motif remains unchanged. The bidentate $H(Me_2PO_2)$ ligand has one free phenol, and the monodentate P-bound $H_2(Me_2PO_2)$ ligand must have two. Hindered rotation about the Re-P bond results in the two singlets of equal integration for the magnetically equivalent methyl groups of the monodentate $H_2(Me_2PO_2)$ ligand. The retention of both hypy ligands is still clearly favored over the three phenolic O donors. Clearly, PO_2 ligands are not very suitable to act as ancillary ligands in this system.

3.3.3. $[Re(N_2PhMe)_2(MePO)_2][BPh_4]$

To explore the possibility of discovering new potentially useful rhenium hydrazine cores, the preparation of new ternary complexes containing PO_x ligands was attempted. $[ReCl(N_2Ph)_2(PPh_3)_2]$, $[ReBr_2(N_2Ph)_2(PPh_3)_2][Br]$ and $[ReCl_2(N_2PhMe)_2(PPh_3)][BPh_4]$ were each reacted with 3 equivalents of H(MePO) in

methanol. It was hoped that the PPh_3 and halide ligands would be displaced by two MePO ligands to form hydrolytically stable ternary complexes containing MePO and hydrazines. In the case of the five coordinate complexes, it was expected that the corresponding six coordinate MePO complex would be isolated.

Under similar reaction conditions, it was found that all three reactions had one distinct disadvantage; the formation of mixtures often precluded the isolation of pure complex. In the case of $[ReCl(N_2Ph)_2(PPh_3)_2]$ and $[ReBr_2(N_2Ph)_2(PPh_3)_2][Br]$, numerous spots were visible on the TLC plate. Attempts to isolate the major products of these reactions by silica gel chromatography were unsuccessful because multiple products were identified by ^1H and ^{31}P NMR spectroscopy in the major bands that were isolated. Attempts to crystallize pure products were equally unsuccessful.

Reaction of H(MePO) with $[ReCl_2(N_2PhMe)_2(PPh_3)][BPh_4]$ was more of a success. Although it also formed a mixture, a product with the composition $[Re(N_2PhMe)_2(MePO)_2][BPh_4]$ (**3.5**) was isolated from the mixture by crystallization. The +LSIMS mass spectrum clearly shows a large cationic peak at *m/z* 1009 that corresponds to the $[Re(N_2PhMe)_2(MePO)_2]^+$ parent. There is no indication of the peak corresponding to the starting material at *m/z* 759.[12] The IR spectrum of the complex has one ν(N=N) absorption at 1593 cm^{-1}, compared to the two ν(N=N) absorptions seen in the starting material at 1560 and 1580 cm^{-1}.[12] This observation supports the formation of a six coordinate complex with higher symmetry than the five coordinate starting material. Elemental analyses were somewhat poor on complex **3.5** and are not reported. It is clear that the isolated complex is contaminated with some unreacted H(MePO) and efforts to remove this impurity were unsuccessful. Attempts to isolate crystals suitable for a X-ray structural characterization were also unsuccessful.

^{1}H and ^{31}P NMR spectroscopies also support the formation of a six coordinate complex. Two singlets that integrate as 6 H each are seen at 3.46 and 2.31 ppm in the ^{1}H NMR spectrum. These signals correspond to the methyl groups on the hydrazines, and the methyl groups on the MePO ligands. The ^{31}P NMR spectrum has one singlet at 29.4 ppm, shifted upfield 7 ppm from the starting material which was reported at 36 ppm.[12] Given the composition of **3.5**, there are 4 possible diastereomers that could be formed (Figure 3.4).

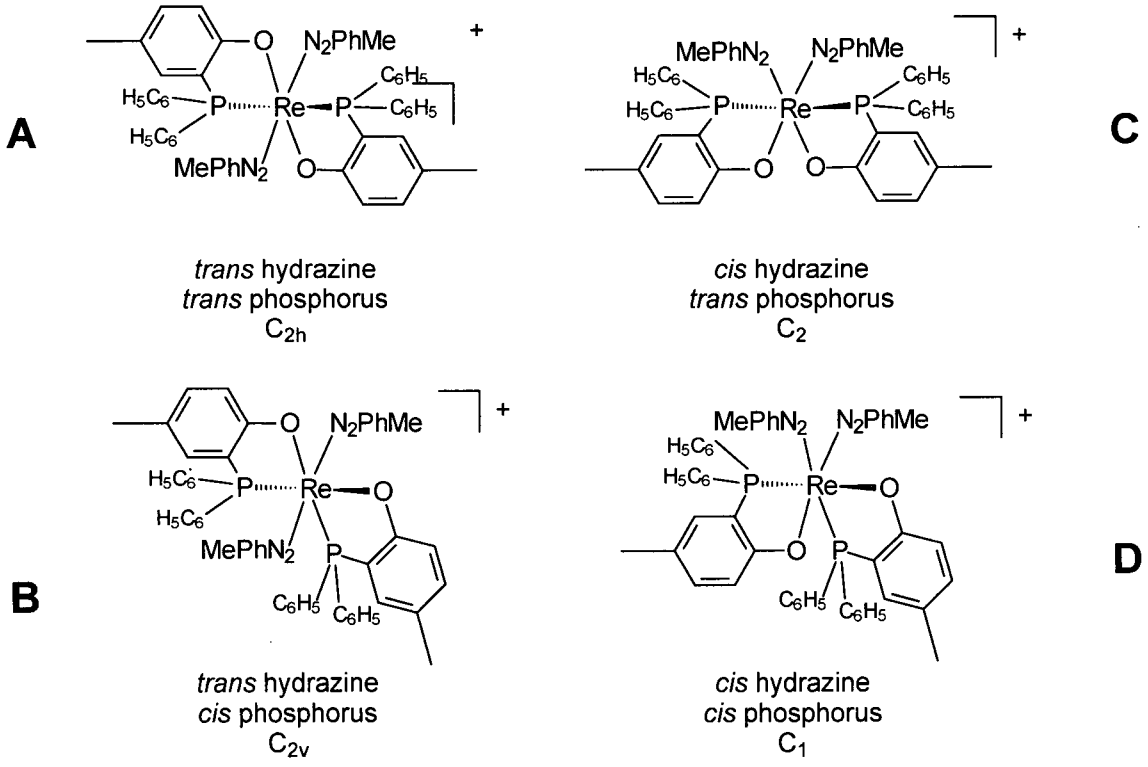

Figure 3.4. Four Possible Diastereomers of **3.5**.

Of the 4 possible diastereomers, only **D** can be discounted on the basis of NMR evidence. **A**, **B** and **C** are all predicted to have 2 magnetically equivalent pairs of methyl groups in the ^{1}H NMR spectrum, and one ^{31}P NMR resonance. However, the formation

of the C_2 symmetric diastereomer **C** is most probable because the *cis*-configuration of the N_2PhMe groups minimizes π-bonding competition for the rhenium d-orbitals.[12] This simple explanation may hold some merit; there appears to be no literature precedent for a complex containing two hydrazine ligands coordinated *trans* to each other. The only possible exception may be complexes of the type *trans*-$[W(N_2)_2(diphos)_2]$, where the terminal dinitrogen ligands are coordinated *trans* to each other.[33] There is a possible explanation to this exception; π-bonding in these complexes is known to be practically non-existent since there is little elongation of the N≡N bond.

3.4. Conclusions

The reaction of [Re(Hhypy)(hypyH)Cl_3] with the PO ligand in the presence of base afforded **3.1** and **3.2** as a mixture. The major product of the reaction was the cationic **3.1**. The neutral minor product **3.2** was easily separated from the cationic **3.1** on silica gel. Crystal structures were obtained for both complexes. **3.1**, a cationic Re(III) complex, was found to have a N_3OP_2 coordination sphere. **3.2**, a neutral Re(III) complex, had a N_3OPCl donor set. Both exhibited the same $[Re(Hhypy)(hypy)]^{2+}$ core with the two P atoms (or P and Cl atoms in the case of **3.2**) *trans* to each other. The +LSIMS, IR and NMR data are consistent with the crystal structures of each. The same reaction was extended to the H_2PO_2 and $H_2(Me_2PO_2)$ ligands to obtain **3.3** and **3.4** respectively as the major products. ^1H and ^{31}P NMR spectral evidence shows these products to have the same structure in solution as the structurally characterized **3.1**. The methyl groups were a useful ^1H NMR probe for **3.4,** where the 1:1:1:1 pattern indicated one bidentate and one tridentate Me_2PO_2 ligand on Re(III). Three of the four phenolic arms remain protonated and uncoordinated in **3.4**. Clearly, the mismatched donor sets of PO_2 and Me_2PO_2 would be unfavorable from a clinical standpoint. **3.5** was synthesized by reaction of $[ReCl_2(N_2PhMe)_2(PPh_3)][BPh_4]$ with H(MePO) in methanol. The +LSIMS, IR and NMR data are consistent with the formation of a six coordinate cation, wherein the two hydrazine ligands are *cis* to each other, and the two phosphorus nuclei are *trans* to each other. No X-ray structural data was obtained for **3.5**.

3.5. References

1) Liu, S.; Edwards, D. S.; Barrett, J. A. *Bioconjugate Chem.* **1997**, *8*, 621.

2) Dilworth, J. R.; Parrott, S. J. *Chem. Soc. Rev.* **1998**, *27*, 43.

3) Nicholson, T.; Mahmood, A.; Morgan, G.; Jones, A. G.; Davison, A. *Inorg. Chim. Acta* **1991**, *179*, 53.

4) Nicholson, T.; Zubieta, J. *Polyhedron* **1988**, *7*, 171.

5) Chatt, J.; Dilworth, J. R.; Leigh, G. L.; Gupta, V. D. *J. Chem. Soc (A)* **1971**, 2631.

6) Duckworth, V. F.; Douglas, P. G.; Mason, R.; Shaw, B. L. *J. Chem. Soc., Chem. Comm.* **1970**, 1083.

7) Mason, R.; Thomas, K. M.; Zubieta, J. A.; Douglas, P. G.; Galbraith, A. R.; Shaw, B. L. *J. Am. Chem. Soc.* **1974**, *96*, 260.

8) Douglas, P. G.; Galbraith, A. R.; Shaw, B. L. *Transition Met. Chem.* **1975/76**, *1*, 17.

9) Dilworth, J. R.; Harrison, S. A.; Walton, D. R. M.; Schweda, E. *Inorg. Chem* **1985**, *24*, 2594.

10) Mohd, H.; Leigh, G. J. *J. Chem. Soc., Dalton Trans.* **1986**, 213.

11) Nicholson, T.; Lombardi, P.; Zubieta, J. *Polyhedron* **1987**, *6*, 1577.

12) Dilworth, J. R.; Jobanputra, P.; Parrott, S. J.; Thompson, R. M.; Povey, D. C.; Zubieta, J. A. *Polyhedron* **1992**, *11*, 147.

13) Dilworth, J. R.; Jobanputra, P.; Miller, J. R.; Parrott, S. J.; Chen, Q.; Zubieta, J. *Polyhedron* **1993**, *12*, 513.

14) Ribeiro, M. T. A.; Pombeiro, A. J. L.; Dilworth, J. R.; Zheng, Y.; Miller, J. R. *Inorg. Chim. Acta* **1993**, *211*, 131.

15) Coutinho, B.; Dilworth, J. R.; Jobanputra, P.; Thompson, R. M.; Schmid, S.; Strähle, J.; Archer, C. M. *J. Chem. Soc., Dalton Trans.* **1995**, 1663.

16) Hirsch-Kuchma, M.; Nicholson, T.; Davison, A.; Davis, W. M.; Jones, A. G. *J. Chem. Soc., Dalton Trans.* **1997**, 3185.

17) Hirsch-Kuchma, M.; Nicholson, T.; Davison, A.; Jones, A. G. *J. Chem. Soc., Dalton Trans.* **1997**, 3189.

18) da Costa, M. T. A. R. S., Dilworth, J.R., Duarte, M.T., Fraústo da Silva, J.J.R., Galvão, A.M., Pombeiro, A.J.L. *J. Chem. Soc. Dalton Trans.* **1998**, 2405.

19) Chakraborty, I.; Bhattacharyya, S.; Banerjee, S.; B.K., D.; Chakravorty, A. *J. Chem. Soc., Dalton Trans.* **1999**, 3747.

20) Albertin, G.; Antoniutti, S.; Bacchi, A.; Ballico, G. B.; Bordignon, E.; Pelizzi, G.; Ranieri, M.; Ugo, P. *Inorg. Chem.* **2000**, *39*, 3265.

21) Albertin, G.; Antoniutti, S.; Bacchi, A.; Bordignon, E.; Miani, F.; Pelizzi, G. *Inorg. Chem.* **2000**, *39*, 3283.

22) Banerjee, S.; Bhattacharyya, S.; B.K., D.; Menon, M.; Chakravorty, A. *Inorg. Chem.* **2000**, *39*, 6.

23) Rose, D. J.; Maresca, K. P.; Nicholson, T.; Davison, A.; Jones, A. G.; Babich, J.; Fischman, A.; Graham, W.; DeBord, J. R. D.; Zubieta, J. *Inorg. Chem.* **1998**, *37*, 2701.

24) Pérez-Lourido, P.; Romero, J.; García-Vázquez, J. A.; Sousa, A.; Maresca, K. P.; Zubieta, J. *Inorg. Chem.* **1999**, *38*, 1511.

25) Nicholson, T.; Cook, J.; Davison, A.; Rose, D. J.; Maresca, K. P.; Zubieta, J. A.; Jones, A. G. *Inorg. Chim. Acta* **1996**, *252*, 421.

26) Nock, B.; Maina, T.; Tisato, F.; Papadopoulos, M.; Raptopoulou, C. P.; Terzis, A.; Chiotellis, E. *Inorg. Chem.* **1999**, *38*, 4197.

27) Nock, B.; Maina, T.; Tisato, F.; Papadopoulos, M.; Raptopoulou, C. P.; Terzis, A.; Chiotellis, E. *Inorg. Chem.* **2000**, *39*, 2178.

28) Nock, B.; Maina, T.; Tisato, F.; Raptopoulou, C. P.; Terzis, A.; Chiotellis, E. *Inorg. Chem.* **2000**, *39*, 5197.

29) Rauchfuss, T. B. *Inorg. Chem.* **1977**, *16*, 2966.

30) Luo, H.; Setyawati, I.; Rettig, S. J.; Orvig, C. *Inorg. Chem.* **1995**, *34*, 2287.

31) Kovacs, M. S.; Hein, P.; Sattarzadeh, S.; Patrick, B. O.; Emge, T. J.; Orvig, C. , Submitted for publication.

32) Perrin, D. D.; Armarego, W. L. F.; Perrin, D. R. *Purification of Laboratory Chemicals*; 2nd ed.; Pergamon Press: Toronto, **1980**.

33) Dori, Z. *Comprehensive Coordination Chemistry*; Wilkinson, G., Gillard, R. D. and McCleverty, J. A., Ed.; Pergamon Press: New York, 1987; Vol. 3, pp 1011.

Chapter Four

Lanthanide(III) and Group 13 Metal Complexes Containing Tripodal Amine Phosphinate Ligands

4.1. Introduction

For many years, the group 13 metals (Al^{3+}, Ga^{3+}, In^{3+}, Tl^{+}) and the lanthanides (Ln^{3+}) have either been employed, or have been investigated for potential use in nuclear medicine. ^{67}Ga(III) and ^{111}In(III) have been used in diagnostic agents, the former for imaging certain types of cancer, and the latter as pretargeting agents for cancer imaging and therapy.[1] The use of $^{201}Tl^{+}$ as a myocardial imaging agent predates the use of ^{99m}Tc for this application, although $^{201}Tl^{+}$ imaging has been largely supplanted by Tc-based diagnostic agents such as Cardiolite® (Figure 1.1). The use of the lanthanides as therapeutic agents has received extensive attention since the US Food and Drug Administration approval of ^{153}Sm(EDTMP) (Figure 1.3) for bone pain palliation in terminal cancer patients. Gd(III) has received extensive attention due to its use in MRI contrast agents.[2]

The lanthanides have the ability to form complexes with a variety of coordination numbers and geometries. Work has been published by our group on the coordination chemistry of the group 13 metals and lanthanides with a variety of amine phenolates, Schiff bases, amine phosphinates and amine pyridyl carboxylates.[3-10] This work has yielded a number of interesting mononuclear, dinuclear and trinuclear complexes with coordination numbers from six to nine (Scheme 4.1). Given that most of the lanthanides

are paramagnetic (which negates the use of NMR spectroscopy in most cases), and that the coordination chemistry of the lanthanides is quite complex, great care must be exercised to characterize structurally the resulting complexes. X-ray crystallography is an indispensable tool, provided that proper precautions are taken to ensure that the crystal is representative of the bulk sample, either in solution or in the solid state.

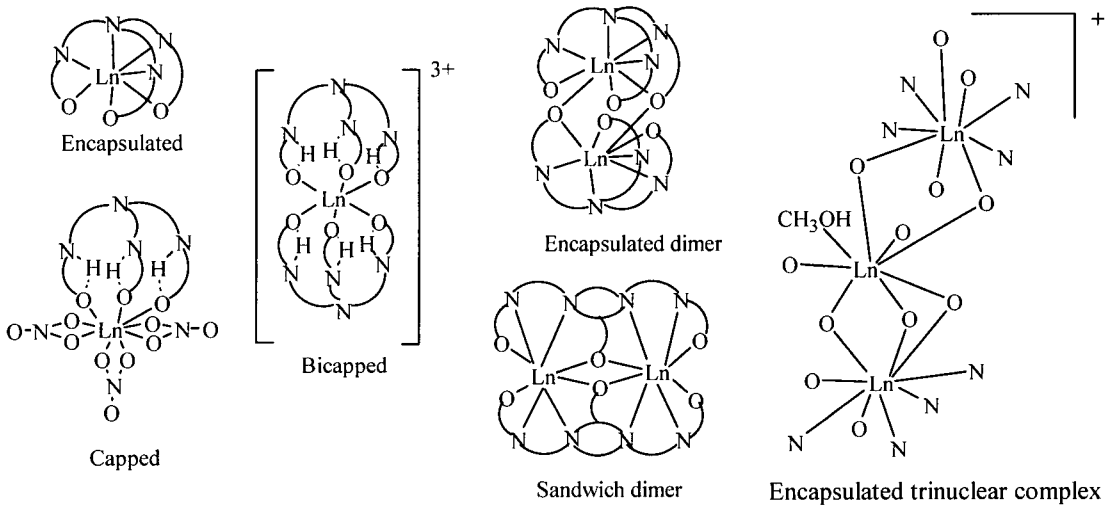

Scheme 4.1[10]

The lanthanide coordination chemistry of a huge variety of chelating ligands containing N and O donor atoms has been investigated.[2] The large majority of these ligands contain between 2-10 amine and carboxylate donors, typically with 2-3 carbon spacers between the amines. Examples using linear and cyclic amines exist, DTPA and DOTA being two of the most successful.[2] The poor hydrolytic stability of amine-carboxylate complexes at low pH is one problem that has been difficult to solve with these systems. The problem arises due to the relatively high pK_a values of the carboxylate groups. Phosphinate donors offer a potential solution to this problem with

their much lower pK_a values. Unlike the dianionic phosphonate group (RPO_3^{2-}) they carry the same charge as a carboxylate group.

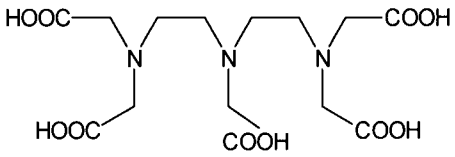

DTPA

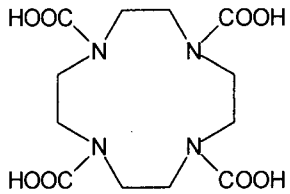

DOTA

Efforts to explore amine-phosphinate ligands with the group 13 metals and the lanthanides have focused on DOTA-type ligands and tren-based tripodal ligands (Figure 4.1). The former have been more thoroughly investigated, and a variety of work has been published on their synthesis, structures of their lanthanide complexes, solution behavior and luminescence properties.[11-16] 1:1 complexes with the lanthanides have been obtained with this type of ligand system and the resulting stereochemistry has been extensively investigated.[15,17-20] In addition to the clockwise and counterclockwise wrapping isomers, six diastereomers have been characterized using a variety of NMR techniques.[15,17-20] The DOTA phosphinate ligands have also been modified to act as bifunctional chelates.[21] The tripodal ligand H_3ppma was found to form 2:1 bicapped complexes with group 13 metals and the lanthanides.[8,9,22] The S_6 symmetry of these bicapped complexes made unique ^{27}Al, ^{71}Ga, and ^{115}In NMR spectroscopic studies amenable that allowed the determination of stability constants below the pH limit of traditional potentiometric techniques.[8]

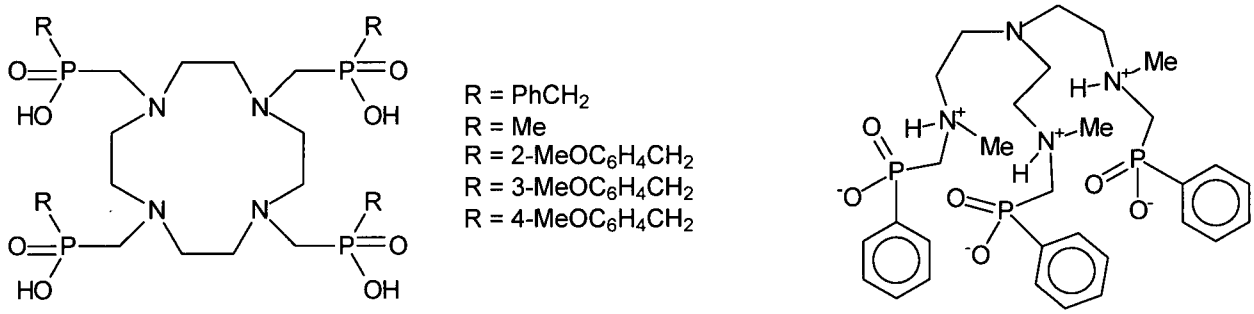

Figure 4.1. Examples of amine-phosphinate ligands: (left) DOTA-type ligands; (right) tris(4-(phenylphosphinato)-3-methyl-3-azabutyl)amine, (H_3ppma).

Encapsulated 1:1 complexes were not obtained in the tripodal amine-phosphinate system. For application in nuclear medicine, this result is a significant setback because 1:1 encapsulated complexes are ideal. Such a complex should have higher thermodynamic stability than a 2:1 bicapped complex; the coordination sphere would contain only donors from the ligand, unlike in the monocapped case, where kinetically labile water molecules or counterions are coordinated. Encapsulated 1:1 complexes are also much less sensitive to entropic effects that occur at extreme dilution. Kinetically inert complexes with high thermodynamic stability are required to prevent demetallation of the complex *in vivo*.

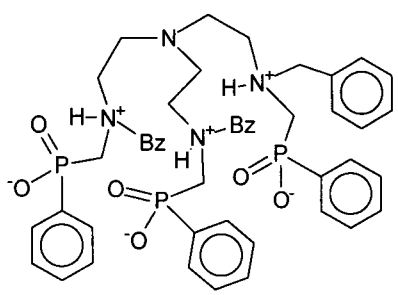

H_3ppba

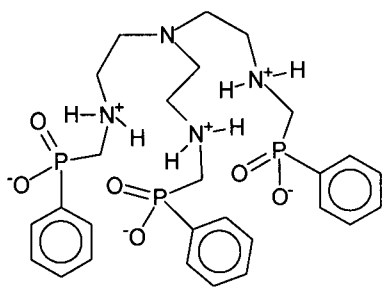

H_3ppa

To investigate the possibility of isolating 1:1 encapsulated complexes containing group 13 metals or the lanthanides, modifications were made to the tripodal amine phosphinate ligands. Attempts were made to prepare new ligands with modifications occurring at the phosphinate R group and/or the amine R group. Although modification at the phosphinate R group was unsuccessful, synthesis of the benzylated amine-phosphinate ligand tris(4-(phenylphosphinato)-3-benzyl-3-azabutyl)amine (H_3ppba) was successful. Two distinct classes of 2:1 complexes, and one class of 1:1 complex were prepared and characterized with the group 13 metals (Al^{3+}, Ga^{3+}, In^{3+}) and the lanthanides. H_3ppba was also used as a synthetic precursor to obtain the unique amine-phosphinate ligand tris(4-(phenylphosphinato)-3-azabutyl)amine (H_3ppa) by N-debenzylation. H_3ppa contains the ammonium salt of a secondary amine. The secondary amine functionality has been elusive in amine phosphinate systems until this report.

4.2. Experimental

Materials. All solvents were of HPLC grade and were obtained from Fisher. When anhydrous solvents were required they were dried using conventional procedures.[23] Ligand synthesis was carried out under Ar; metal complexes were prepared in air and were found to be completely air and moisture stable. HPLC grade methanol (Fisher), tris(2-aminoethyl)amine (W.R. Grace & Co.), benzaldehyde (Aldrich), $NaBH_4$ (Fisher), 37% aqueous formaldehyde (Fisher), concentrated HCl (Fisher), phenylphosphinic acid (Aldrich), 10% Pd on C (Aldrich), and prepurified $H_{2(g)}$ (Praxair) were all obtained from commercial sources and were used without further purification. All hydrated metal salts were used as received and were obtained from Johnson Matthey.

Instrumentation. Experimental details are identical to those outlined in Section 2.2 with the following exceptions: ^1H NMR spectra were recorded on Bruker AC-200E (200 MHz) or Bruker AV-300 (300 MHz) NMR spectrometers with δ referenced downfield from external TMS. $^{13}C\{^1H\}$ NMR spectra were recorded on a Bruker AC-200E (50 MHz) spectrometer with δ referenced downfield from external TMS. $^{31}P\{^1H\}$ NMR spectra were recorded on a Bruker AV-300 (121.5 MHz) NMR spectrometer with δ referenced to external 85% aqueous phosphoric acid. A Parr model 4753 pressure vessel and a model 4316 gauge block assembly equipped with a 140 bar burst plate were used for the hydrogenation reaction.

Preparation of Compounds. Tris(2-benzylaminoethyl)amine.[24] Benzaldehylde (17.5 g, 165 mmol) was added dropwise to a solution of tris(2-aminoethyl)amine (7.3 g, 50 mmol) in ethanol (150 mL). The mixture was stirred for 3

hours, during which it changed to a dark yellow colour. The mixture was cooled in an ice bath, $NaBH_4$ (7.2 g, 190 mmol) was added, and the reaction was allowed to warm to room temperature over 3 hours. The reaction mixture was extracted with 3 x 50 mL portions of diethyl ether and the combined organic layers were subsequently extracted with 200 mL 1M HCl. The HCl layer was then made basic (pH 11) by addition of K_2CO_3 and subsequently extracted with another 3 x 50 mL portions of diethyl ether. The final organic layers were combined, dried over anhydrous $MgSO_4$ and then filtered; the solvent was removed and the pale yellow oil was dried *in vacuo* for 20 hours (yield 9.4 g, 79%). ^1H NMR ($CDCl_3$, 200 MHz) δ: 7.38-7.12 (overlapped multiplets, 15H), 3.71 (s, 6H, benzyl *H*), 2.65 (s, 3H), 2.62 (s, 3H), 2.58 (s, 3H), 2.56 (s, 3H). ^{13}C {^1H} NMR ($CDCl_3$, 50 MHz) δ: 134.2 (s, 3C), 123.2 (s, 6C), 123.1 (s, 6C), 121.9 (s, 3C), 48.7 (s, 3C), 48.3 (s, 3C), 41.6 (s, 3C).

Tris(4-(phenylphosphinato)-3-benzyl-3-azabutyl)amine, H_3ppba·2HCl·H_2O. Tris(2-benzylaminoethyl)amine (2.0 g, 4.8 mmol) was dissolved in 10 mL methanol. Concentrated HCl (20 mL) was added dropwise, followed by phenylphosphinic acid (2.1 g, 15 mmol). The temperature was raised to reflux; 37% aqueous formaldehyde was added dropwise over a 30 min period, and the reaction was refluxed for a further 5 h. After cooling, acetone was added to the creamy yellow-coloured suspension to precipitate the product completely. The product was recovered by filtration and was recrystallized from boiling ethanol to afford the pure white product (yield = 3.8 g, 81%). Anal. Calcd. (found) for $C_{48}H_{57}N_4O_6P_3$·2HCl·H_2O: C, 59.44 (59.44); H, 6.34 (6.18); N, 5.78 (5.95). (+)LSIMS: *m/z* = 879 ($[M+H]^+$). ^1H NMR (CD_3OD, 300 MHz) δ: 7.75-7.15

(overlapped multiplets, 30H), 4.45 (s, 6H), 3.63 (s, 6H), 3.39 (s, 12H). ^{31}P NMR (CD_3OD) δ: 23.2 (s).

Tris(4-(phenylphosphinato)-3-azabutyl)amine, H_3ppa·HCl·H_2O. H_3ppba·2HCl·H_2O (500 mg, 0.510 mmol) was dissolved in 50 mL methanol, to which 10% Pd on C (300 mg, 0.282 mmol) was added as an ethanol suspension (*NB: dry 10% Pd on C will burn if added directly to methanol*). The mixture was stirred at room temperature and reacted with $H_{2(g)}$ (70 bars, 48 hours). The catalyst was removed by filtration on a fine frit, the solvent was removed, and the hygroscopic white product was recrystallized from a hot ethanol/acetone mixture (yield 150 mg, 44%). Anal. Calcd. (found) for $C_{27}H_{39}N_4O_6P_3$·HCl·H_2O: C, 48.91 (49.18); H, 6.38 (6.38); N, 8.45 (7.95). (+)LSIMS: *m/z* = 609 ($[M+H]^+$). ^{1}H NMR (CD_3OD, 300 MHz) δ: 7.87 (s, 6H), 7.50 (s, 9H), 3.16 (s, 12H), 2.95 (s, 6H). ^{31}P NMR (CD_3OD, 121.5 MHz) δ: 21.1 (s).

Synthesis of metal complexes. Detailed procedures are given for representative examples of $[M(H_3ppba)_2]^{3+}$ ($M=Al^{3+}$, Ga^{3+}, In^{3+}, Ho^{3+}-Lu^{3+}), $[M(H_4ppba)_2]^{5+}$ ($M=Ln^{3+}$-Tb^{3+}) and $[M(H_4ppba)]^{4+}$ ($M=La^{3+}$-Tm^{3+}) complexes. Characterization data for all compounds prepared are listed in Tables 4.1, 4.2, 4.3, 4.5, 4.6, 4.8, 4.9 and Figures 4.3, 4.4, 4.6.

General preparative method for the synthesis of $[M(H_3ppba)_2](NO_3)_2Cl·3CH_3OH$ ($M=Ga^{3+}$), (4.1). To a solution of H_3ppba·2HCl·H_2O (100 mg, 0.103 mmol) in 5 mL CH_3OH was added a solution of $Ga(NO_3)_3·6H_2O$ (18.7 mg, 0.052 mmol) in 0.5 mL CH_3OH. Upon standing for 48 hours at room temperature, colourless prismatic crystals formed, of which one was extracted for X-ray structural analysis. The remaining crystals were recovered by filtration (yield 90 mg, 84%).

Table 4.1. Preparative details for the synthesis of $[M(H_3ppba)_2](NO_3)_2Cl{\cdot}xCH_3OH$.

M^{3+}-salt starting material	Product	Yield
$Al(NO_3)_3{\cdot}9H_2O$	$[Al(H_3ppba)_2](NO_3)_2Cl{\cdot}3CH_3OH$	84%
$Ga(NO_3)_3{\cdot}6H_2O$	$[Ga(H_3ppba)_2](NO_3)_2Cl{\cdot}3CH_3OH$ (**4.1**)	84%
$In(NO_3)_3{\cdot}H_2O$	$[In(H_3ppba)_2](NO_3)_2Cl{\cdot}3CH_3OH$	73%
$Ho(NO_3)_3{\cdot}5H_2O$	$[Ho(H_3ppba)_2](NO_3)_2Cl{\cdot}3CH_3OH$	45%
$Er(NO_3)_3{\cdot}5H_2O$	$[Er(H_3ppba)_2](NO_3)_2Cl{\cdot}3CH_3OH$	28%
$Tm(NO_3)_3{\cdot}5H_2O$	$[Tm(H_3ppba)_2](NO_3)_2Cl{\cdot}3CH_3OH$	52%
$Yb(NO_3)_3{\cdot}5H_2O$	$[Yb(H_3ppba)_2](NO_3)_2Cl{\cdot}3CH_3OH$	46%
$Lu(NO_3)_3{\cdot}5H_2O$	$[Lu(H_3ppba)_2](NO_3)_2Cl{\cdot}2CH_3OH$	31%

Table 4.2. Preparative details for the synthesis of $[M(H_4ppba)_2](NO_3)_4Cl{\cdot}xCH_3OH$.

M^{3+}-salt starting material	Product	Yield*
$La(NO_3)_3{\cdot}6H_2O$	$[La(H_4ppba)_2](NO_3)_4Cl{\cdot}xCH_3OH$	
$Ce(NO_3)_3{\cdot}6H_2O$	$[Ce(H_4ppba)_2](NO_3)_4Cl{\cdot}xCH_3OH$	
$Pr(NO_3)_3{\cdot}6H_2O$	$[Pr(H_4ppba)_2](NO_3)_4Cl{\cdot}xCH_3OH$	
$Nd(NO_3)_3{\cdot}5H_2O$	$[Nd(H_4ppba)_2](NO_3)_4Cl{\cdot}xCH_3OH$	
$Sm(NO_3)_3{\cdot}6H_2O$	$[Sm(H_4ppba)_2](NO_3)_4Cl{\cdot}xCH_3OH$	
$Eu(NO_3)_3{\cdot}6H_2O$	$[Eu(H_4ppba)_2](NO_3)_4Cl{\cdot}5CH_3OH$	8%
$Gd(NO_3)_3{\cdot}6H_2O$	$[Gd(H_4ppba)_2](NO_3)_4Cl{\cdot}3CH_3OH$ (**4.2**)	13%
$Tb(NO_3)_3{\cdot}5H_2O$	$[Tb(H_4ppba)_2](NO_3)_4Cl{\cdot}10CH_3OH$	11%
$Dy(NO_3)_3{\cdot}5H_2O$	$[Dy(H_4ppba)_2](NO_3)_4Cl{\cdot}xCH_3OH$	

*Yields are not reported for complexes that were not isolated in pure form (*vide infra*).

Table 4.3. Preparative details for the synthesis of $[M(H_4ppba)](NO_3)_3Cl{\cdot}xH_2O$.

M^{3+}-salt starting material	Product	Yield
$La(NO_3)_3{\cdot}6H_2O$	$[La(ppba)](NO_3)_3Cl{\cdot}3H_2O$	15%
$Ce(NO_3)_3{\cdot}6H_2O$	$[Ce(ppba)](NO_3)_3Cl{\cdot}5H_2O$	16%
$Pr(NO_3)_3{\cdot}6H_2O$	$[Pr(ppba)](NO_3)_3Cl{\cdot}4H_2O$	18%
$Nd(NO_3)_3{\cdot}5H_2O$	$[Nd(ppba)](NO_3)_3Cl{\cdot}4H_2O$	16%
$Sm(NO_3)_3{\cdot}6H_2O$	$[Sm(ppba)](NO_3)_3Cl{\cdot}3H_2O$	24%
$Eu(NO_3)_3{\cdot}6H_2O$	$[Eu(ppba)](NO_3)_3Cl{\cdot}3H_2O$	34%
$Gd(NO_3)_3{\cdot}6H_2O$	$[Gd(ppba)](NO_3)_3Cl{\cdot}3H_2O$ (**4.3**)	33%
$Tb(NO_3)_3{\cdot}5H_2O$	$[Tb(ppba)](NO_3)_3Cl{\cdot}3H_2O$	30%
$Dy(NO_3)_3{\cdot}5H_2O$	$[Dy(ppba)](NO_3)_3Cl{\cdot}3H_2O$	30%
$Ho(NO_3)_3{\cdot}5H_2O$	$[Ho(ppba)](NO_3)_3Cl{\cdot}3H_2O$	22%
$Er(NO_3)_3{\cdot}5H_2O$	$[Er(ppba)](NO_3)_3Cl{\cdot}3H_2O$	14%

General preparative method for the synthesis of $[M(H_4ppba)_2](NO_3)_4Cl{\cdot}3CH_3OH$. ($M=Gd^{3+}$), (4.2). To a solution of $H_3ppba{\cdot}2HCl{\cdot}H_2O$ (100 mg, 0.103 mmol) in 5 mL CH_3OH was added a solution of $Gd(NO_3)_3{\cdot}6H_2O$ (23.2 mg, 0.0515 mmol) in 0.5 mL CH_3OH. During one week of standing at room temperature, colourless hexagonal plates formed, one of which was extracted for X-ray structural analysis. The remaining crystals were recovered by filtration (yield 15 mg, 13%.).

General preparative method for the synthesis of $[M(H_4ppba)](NO_3)_3Cl{\cdot}3H_2O$. ($M=Gd^{3+}$), (4.3). To a solution of $H_3ppba{\cdot}2HCl{\cdot}H_2O$ (100 mg, 0.103 mmol) in 5 mL CH_3OH was added a solution of $Gd(NO_3)_3{\cdot}6H_2O$ (46.4 mg, 0.103 mmol) in 0.5 mL CH_3OH. A precipitate immediately formed out of the mixture and a finely-divided white powder was isolated by filtration (yield 45 mg, 33%). The insolubility of the white powder made it impossible to obtain crystals for X-ray structural analysis.

$[Ga(ppa)]{\cdot}3H_2O$, (4.4). To a solution of $H_3ppa{\cdot}HCl{\cdot}H_2O$ (50 mg, 0.071 mmol) in 5 mL CH_3OH was added a solution of $Ga(NO_3)_3{\cdot}6H_2O$ (25.8 mg, 0.071 mmol) in 0.5 mL CH_3OH. A fine white powder formed over 48 h at room temperature and was isolated by filtration (yield 29 mg, 56%). Anal. Calcd. (found) for $C_{27}H_{36}N_4O_6P_3Ga{\cdot}3H_2O$: C, 44.47 (44.89); H, 5.80 (5.83); N, 7.68 (7.81). (+)LSIMS: m/z = 675 ($[M+H]^+$). IR spectrum: refer to Figure 4.7. ^1H and ^{31}P NMR spectra: refer to Figure 4.8.

X-Ray Crystallographic Analyses of 4.1 and 4.2. Please refer to the appendix for experimental details, and for complete tables of bond lengths and bond angles.

4.3. Results and Discussion

4.3.1. Synthesis of the Tripodal Amine-Phosphinate Ligands H_3ppba & H_3ppa

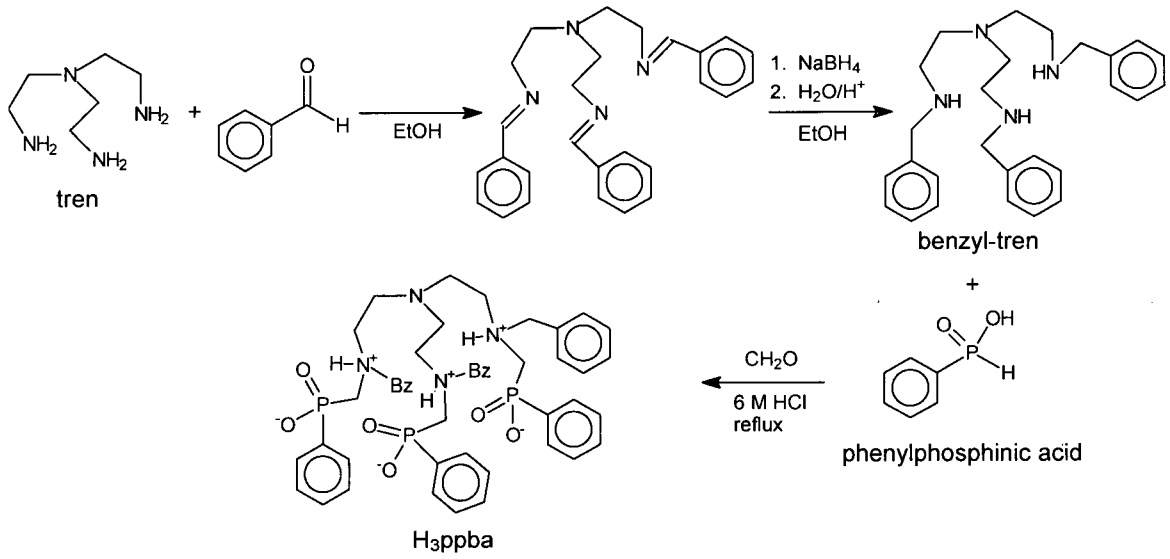

Scheme 4.2

The synthesis of new amine-phosphinate ligands was accomplished by adapting the Moedritzer-Irani reaction[25] to react phenylphosphinic acid with a benzylated derivative of tren in the presence of formaldehyde (Scheme 4.2). The synthesis of tris(2-benzylaminoethyl)amine (the benzylated derivative of tren) was accomplished by standard methods. The Moedritzer-Irani reaction requires that secondary amines be used to prevent the addition of two methylene-phosphinic acid groups to each amine. The product of the reaction is a tertiary amine; the mechanism proceeds similarly to the well-known Mannich reaction.[26] The formaldehyde condenses with the hydrogen on the secondary amine and the hydrogen on the phosphinic acid; the two are joined together via a methylene bridge. The reaction proceeds cleanly under these conditions, but the

presence of HCl and a zwitterionic product severely limits its utility to compounds that can be isolated from the reaction mixture. Recrystallization of the product from the reaction of benzylated tren and phenylphosphinic acid affords pure tris(4-(phenylphosphinato)-3-benzyl-3-azabutyl)amine ($H_3ppba \cdot 2HCl \cdot H_2O$) in good yield. Unfortunately, this ligand is only soluble in methanol, hot ethanol, hot isopropanol, DMSO and DMF. Therefore, the coordination chemistry of this ligand is limited to these solvents only.

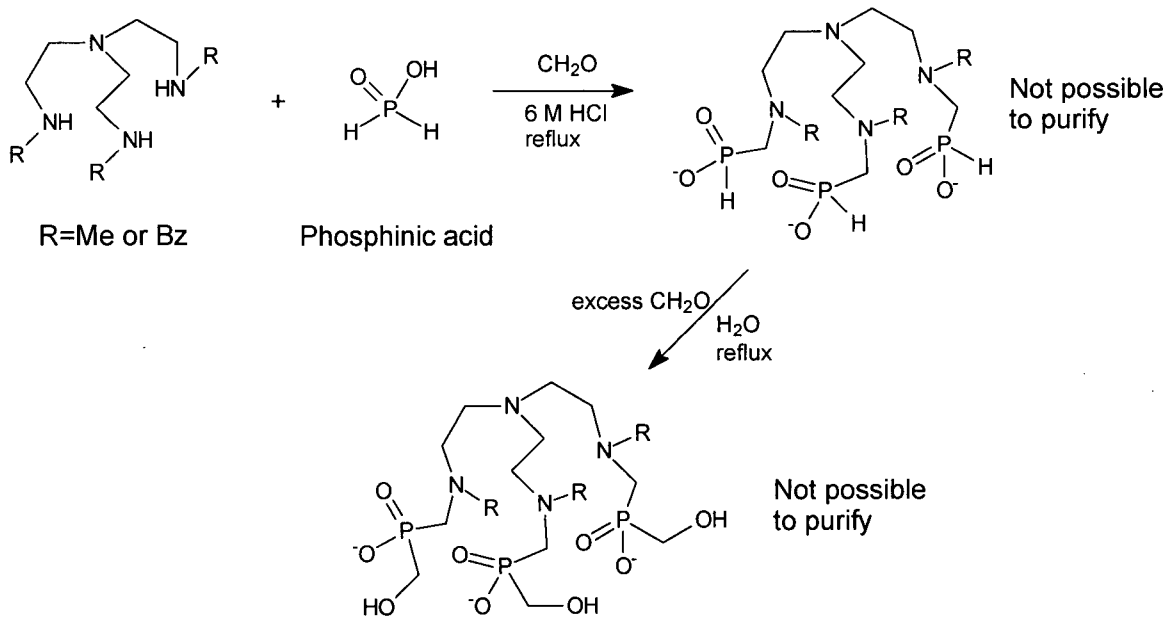

Scheme 4.3

Reaction of methylated or benzylated tren with phosphinic acids other than phenylphosphinic acid did not afford pure product (Scheme 4.3). The original goal was to synthesize tripodal amine-phosphinate ligands with R groups other than phenyl at the phosphinic acid to encourage formation of 1:1 encapsulated complexes with group 13 metals and the lanthanides. The addition of formaldehyde in the first step (Scheme 4.3)

must be made slowly to prevent formation of the unwanted side product $(CH_2OH)_2P(O)OH$.[27] The Moedritzer-Irani reaction appeared to proceed and was monitored by ^1H and ^{31}P NMR spectroscopy, but we were unable to isolate the zwitterionic product. Reaction of the amine-phosphinic acid tripod with excess formaldehyde appeared to form the amine-hydroxymethylenephosphinic acid tripod, but the product was also not possible to isolate (Scheme 4.3).

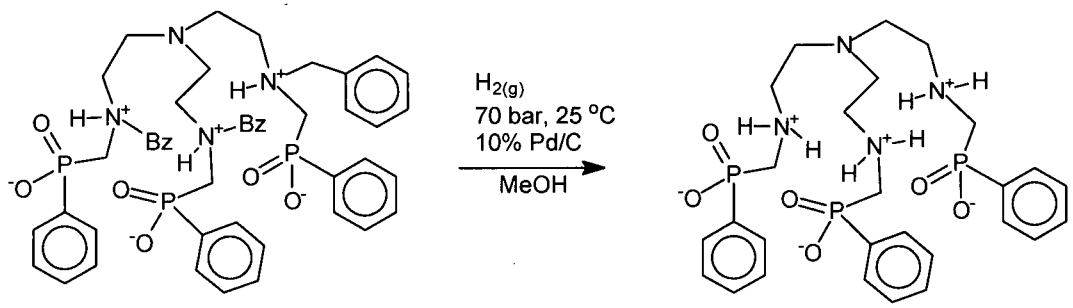

H_3ppba H_3ppa

Scheme 4.4

The possibility of modification at the amine was also investigated. As mentioned above, the benzyl-substituted amine-phosphinate tripod H_3ppba was successfully synthesized. It was not expected that the presence of the three bulky benzyl groups would encourage 1:1 encapsulated complex formation. Removal of these groups by catalytic hydrogenation, however, afforded the novel secondary amine tripod tris(4-(phenylphosphinato)-3-azabutyl)amine (H_3ppa·HCl·H_2O) (Scheme 4.4). The reaction is easily monitored by the loss of the methylene resonance of the benzyl group in the ^1H NMR spectrum at 4.45 ppm. Catalytic hydrogenation of N-benzyl groups is known to be difficult because of the propensity of free amines to poison the Pd catalyst.[28] High

pressure and a large excess of Pd catalyst were required for this reaction to proceed. Hydrogenation reactions are known to produce pure products in high yield; the products of the reaction are H_3ppa and toluene, and the problem of purifying the zwitterionic product from the Moedritzer-Irani reaction is avoided. H_3ppa is highly water-soluble; the ligand is also soluble in alcohols such as methanol and ethanol.

4.3.2. 2:1 Complexes of H_3ppba with the Group 13 Metals and the Lanthanides

Complexes of the ligand H_3ppma (Figure 4.1) were clearly shown to be 2:1 bicapped complexes of the type $[M(H_3ppma)_2](NO_3)_3$, where $M=Al^{3+}$, Ga^{3+}, In^{3+} and Ln^{3+}.[8,9,22] Therefore, the first step of this study was to prepare 2:1 ligand:metal complexes for comparison. All complexes were prepared under similar conditions, and two distinct classes of 2:1 bicapped complexes were identified.

Reaction of one equivalent of $Ga(NO_3)_3 \cdot 6H_2O$ with two equivalents of $H_3ppba \cdot 2HCl \cdot H_2O$ in methanol results in the formation of the 2:1 bicapped complex $[Ga(H_3ppba)_2](NO_3)_2Cl \cdot 3CH_3OH$ (**4.1**). Indicating that complex formation occurs in methanol solution, the ^{31}P NMR singlet of H_3ppba shifted upfield from 23.2 ppm to 14.4 ppm for the complex, but little other information is obtained from NMR spectroscopy. A number of metal salts were tried, including chloride, triflate and perchlorate, but only the mixed nitrate/chloride product formed crystals that were amenable to X-ray structural analysis and had consistent composition. Reactions with Al^{3+}, In^{3+}, and the lanthanides Ho^{3+} through Lu^{3+} formed the same type of tricationic complex. Isolated yields ranged from 31-84%. In the case of the lanthanides, the complexes appeared to have somewhat higher solubility, and yields were difficult to improve. Any attempt to improve the yields

by removing the solvent resulted in the formation of glassy solids with inconsistent compositions according to their elemental analyses.

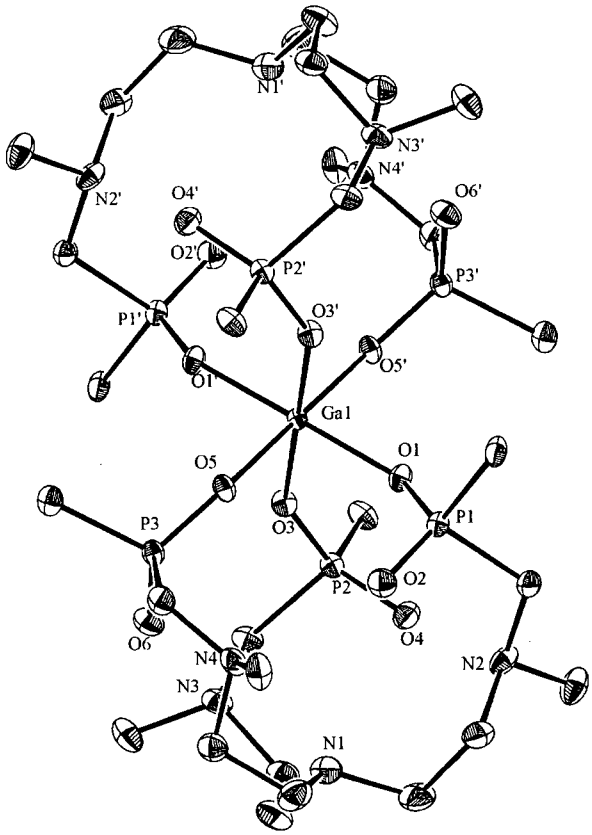

Figure 4.2. ORTEP diagram of the $[Ga(H_3ppba)_2]^{3+}$ cation with the solvent molecules and the aromatic rings removed for clarity; 50% thermal probability ellipsoids are shown.

An X-ray structural analysis was performed on a crystal of **4.1** isolated from the reaction of H_3ppba with Ga^{3+} (Figure 4.2, Table 4.4). The Ga^{3+} ion is clearly bicapped by two H_3ppba ligands; examination of the bond lengths and a difference map indicate that all three of the pendant N atoms are protonated on each H_3ppba ligand. The ligands are best regarded as neutral zwitterions, thus, the complex has an overall +3 charge. The

Ga^{3+} ion is coordinated only by the phosphinato O atom donors with an average Ga-O bond length of 1.95 Å. The two H_3ppba ligands are related to each other through a crystallographic inversion center at the Ga^{3+} ion. Although the portion of the unit cell containing $[Ga(H_3ppba)_2]^{3+}$ is well established, large void spaces exist where satisfactory modeling of mixed NO_3^-, Cl^- and CH_3OH was not possible. Correction of the disordered data in the void spaces resulted in R1 = 0.048. The elemental analyses for the Ga^{3+} and other H_3ppba complexes strongly support the proposed composition.

Table 4.4. Selected bond lengths (Å) and bond angles (deg) in $[Ga(H_3ppba)_2](NO_3)_2Cl{\cdot}3CH_3OH$ (**4.1**).

Ga-O(1)	1.9498(14)	O(1)-Ga-O(3')	88.88(6)
Ga-O(3)	1.9512(15)	O(1)-Ga-O(5')	88.93(6)
Ga-O(5)	1.9515(15)	O(3)-Ga-O(5)	91.10(6)
P(1)-O(1)	1.5052(15)	O(3)-Ga-O(5')	88.90(6)
P(1)-O(2)	1.4927(18)	O(1)-P(1)-O(2)	120.10(9)
P(1)-C(3)	1.833(2)	O(1)-P(1)-C(3)	104.05(9)
P(1)-C(4)	1.796(2)	O(1)-P(1)-C(4)	110.50(10)
Ga-O(1)-P(1)	143.84(9)	O(2)-P(1)-C(3)	110.76(10)
O(1)-Ga-O(3)	91.12(6)	O(2)-P(1)-C(4)	109.84(10)
O(1)-Ga-O(5)	91.07(6)	C(3)-P(1)-C(4)	99.50(10)
O(1)-Ga-O(1')	180.00		

Analogous to the structurally characterized $[In(H_3ppma)_2]^{3+}$ or $[Lu(H_3ppma)_2]^{3+}$ complexes,[8,9] there is nearly S_6 symmetry around the Ga^{3+} ion. In the case of

$[In(H_3ppma)_2]^{3+}$, the crystallographic symmetry imposed perfect 90° and 180° angles between the O atoms of the phosphinato ligands.[8] The 180° angles in $[Lu(H_3ppma)_2]^{3+}$ are crystallographically imposed, and the 88.72(6)° and 91.28(6)° angles are close to 90°.[9] The unique bond angles in **4.1** are 180.00°, 91.12(6)° and 88.88(6)°, therefore, the structure is also an octahedral complex with nearly perfect S_6 symmetry. The bond lengths in each of the three complexes are comparable when the ionic radii are corrected for the three different metals.

Also analogous to the two known H_3ppma complexes, the coordination of each phosphinato O atom introduces a chiral center at each P atom.[8,9] In the **4.1** crystal structure, only the *RRRSSS* diastereomer is observed. In order to accommodate the bulk of the phenyl rings on the phosphinate group, the only other diastereomer that is chemically possible is the *RRSSSR*.[8] There is no evidence for the presence of this diastereomer in the solid state in any of the studies to date.

+LSIMS data for the entire series of complexes demonstrate clearly that 2:1 complexes are formed (Table 4.5). Peaks are seen in each case corresponding to the monocationic 2:1 and 1:1 complexes. Since the ligand peak at 879 is also observed in every case, it is reasonable to conclude that the 1:1 complex is formed by fragmentation in the mass spectrometer and may be regarded as an experimental artifact.

IR spectroscopy shows that Al^{3+}, Ga^{3+}, In^{3+} and the lanthanides Ho^{3+} through Lu^{3+} are completely isostructural (Figure 4.3). The IR spectra have several notable features in the region shown. The peak around 1450 cm^{-1} is attributed to ν(P-Ph); the sharp peak at 1383 cm^{-1} arises from $\nu(NO_3)$; the three large peaks at *ca.* 1190, 1130, 1070 cm^{-1} are attributed to ν(P-O); and the peaks around 700 cm^{-1} are due to ν(P-C) and ν(P-Ph). The intensity and position of all of these peaks remains relatively unchanged in all of the

spectra, except in that of Dy^{3+} and Ho^{3+}, which appear to show some additional spectral features (*vide infra*).

Table 4.5. +LSIMS data for all 2:1 H_3ppba complexes.

Complex	$[M(Hppba)]^+$ *m/z*	$[MH_4(ppba)_2]^+$ *m/z*
$[Al(H_3ppba)_2](NO_3)_2Cl{\cdot}3CH_3OH$	903	1782
$[Ga(H_3ppba)_2](NO_3)_2Cl{\cdot}3CH_3OH$	945	1825
$[In(H_3ppba)_2](NO_3)_2Cl{\cdot}3CH_3OH$	991	1869
$[La(H_4ppba)_2](NO_3)_4Cl{\cdot}xCH_3OH$	1015	1895
$[Ce(H_4ppba)_2](NO_3)_4Cl{\cdot}xCH_3OH$	1016	1896
$[Pr(H_4ppba)_2](NO_3)_4Cl{\cdot}xCH_3OH$	1017	1897
$[Nd(H_4ppba)_2](NO_3)_4Cl{\cdot}xCH_3OH$	1020	1899
$[Sm(H_4ppba)_2](NO_3)_4Cl{\cdot}xCH_3OH$	1028	1906
$[Eu(H_4ppba)_2](NO_3)_4Cl{\cdot}5CH_3OH$	1029	1908
$[Gd(H_4ppba)_2](NO_3)_4Cl{\cdot}3CH_3OH$	1034	1912
$[Tb(H_4ppba)_2](NO_3)_4Cl{\cdot}10CH_3OH$	1035	1913
$[Dy(H_4ppba)_2](NO_3)_4Cl{\cdot}xCH_3OH$	1040	1918
$[Ho(H_3ppba)_2](NO_3)_2Cl{\cdot}3CH_3OH$	1041	1919
$[Er(H_3ppba)_2](NO_3)_2Cl{\cdot}3CH_3OH$	1044	1922
$[Tm(H_3ppba)_2](NO_3)_2Cl{\cdot}3CH_3OH$	1045	1924
$[Yb(H_3ppba)_2](NO_3)_2Cl{\cdot}3CH_3OH$	1050	1928
$[Lu(H_3ppba)_2](NO_3)_2Cl{\cdot}2CH_3OH$	1051	1930

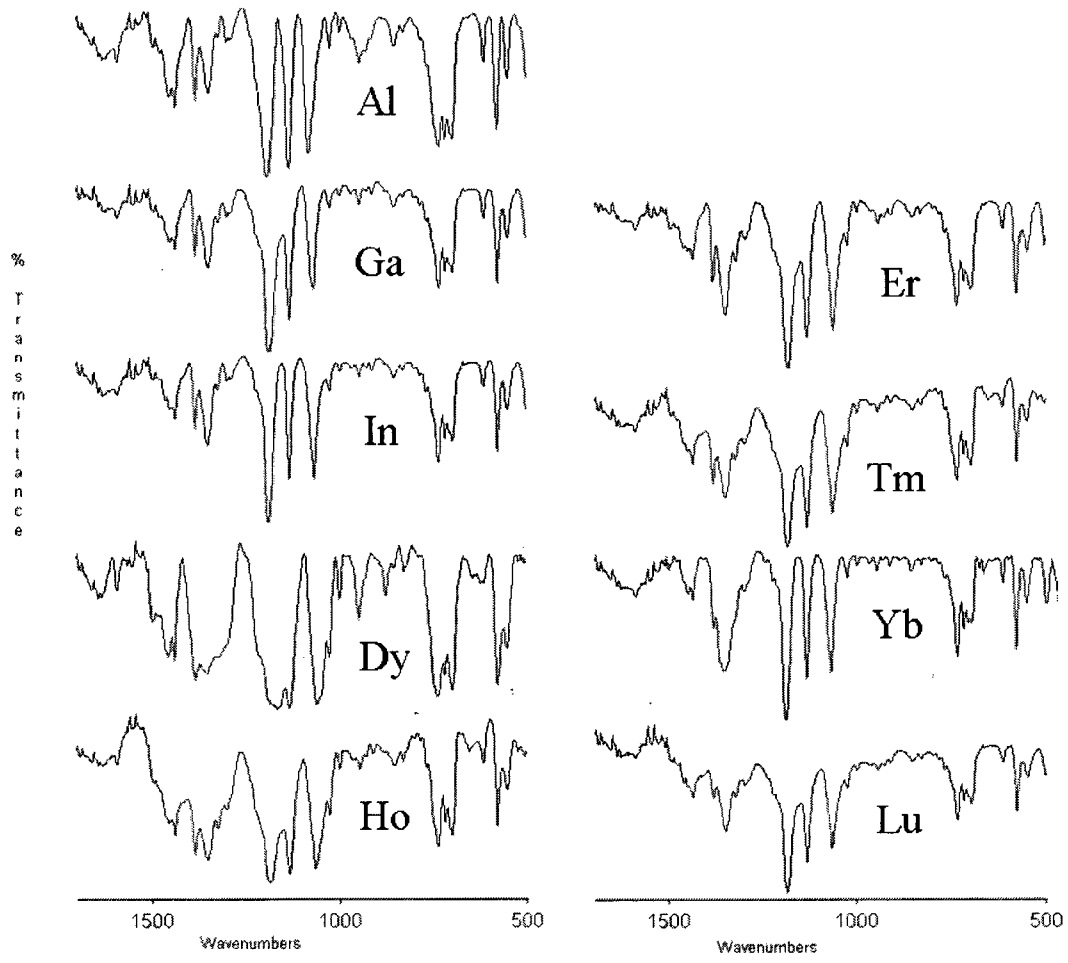

Figure 4.3. IR spectra of $[M(H_3ppba)_2](NO_3)_2Cl$, M as indicated.

For the series of lanthanides La^{3+} through Dy^{3+}, however, the IR spectra were found to differ greatly from the "Ga^{3+} type" structures. The elemental analyses (Table 4.6) of the Eu^{3+}, Gd^{3+} and Tb^{3+} complexes indicate that complexes of the type $[Ln(H_4ppba)_2]^{5+}$ are formed wherein the apical nitrogen of each ligand is protonated to afford a +5 complex. Obtaining good elemental data for this class of complex was difficult. Isolated yields were quite low (10-15%), and only Eu^{3+}, Gd^{3+} and Tb^{3+} complexes were isolated in pure form. Satisfactory elemental analyses for the La-Sm^{3+}

and Dy^{3+} complexes were never obtained. Lying on the border between the +5 and +3 complexes, it is possible that Dy^{3+} formed a mixture of both complex types. The appearance of new features in the IR spectrum of the Dy^{3+} complex supports this hypothesis.

Table 4.6. Elemental analyses for selected 2:1 H_3ppba complexes.

Complex	C	H	N
	Calcd. (found)	Calcd. (found)	Calcd. (found)
$[Al(H_3ppba)_2](NO_3)_2Cl{\cdot}3CH_3OH$	58.28 (58.59)	6.22 (6.35)	6.86 (6.69)
$[Ga(H_3ppba)_2](NO_3)_2Cl{\cdot}3CH_3OH$	57.08 (57.39)	6.10 (6.13)	6.72 (6.37)
$[In(H_3ppba)_2](NO_3)_2Cl{\cdot}3CH_3OH$	55.87 (56.21)	5.97 (5.83)	6.58 (6.50)
$[Eu(H_4ppba)_2](NO_3)_4Cl{\cdot}5CH_3OH$	51.46 (51.45)	5.90 (5.66)	7.13 (7.34)
$[Gd(H_4ppba)_2](NO_3)_4Cl{\cdot}3CH_3OH$	51.77 (52.81)	5.62 (5.68)	7.32 (6.79)
$[Tb(H_4ppba)_2](NO_3)_4Cl{\cdot}10CH_3OH$	50.47 (50.00)	6.23 (5.84)	6.66 (6.61)
$[Ho(H_3ppba)_2](NO_3)_2Cl{\cdot}3CH_3OH$	54.59 (54.75)	5.83 (5.59)	6.43 (6.81)
$[Er(H_3ppba)_2](NO_3)_2Cl{\cdot}3CH_3OH$	54.53 (54.83)	5.82 (5.57)	6.42 (6.71)
$[Tm(H_3ppba)_2](NO_3)_2Cl{\cdot}3CH_3OH$	54.49 (54.91)	5.82 (5.61)	6.42 (6.65)
$[Yb(H_3ppba)_2](NO_3)_2Cl{\cdot}3CH_3OH$	54.33 (54.75)	5.89 (5.59)	6.40 (6.67)
$[Lu(H_3ppba)_2](NO_3)_2Cl{\cdot}2CH_3OH$	54.59 (54.88)	5.70 (5.68)	6.50 (6.37)

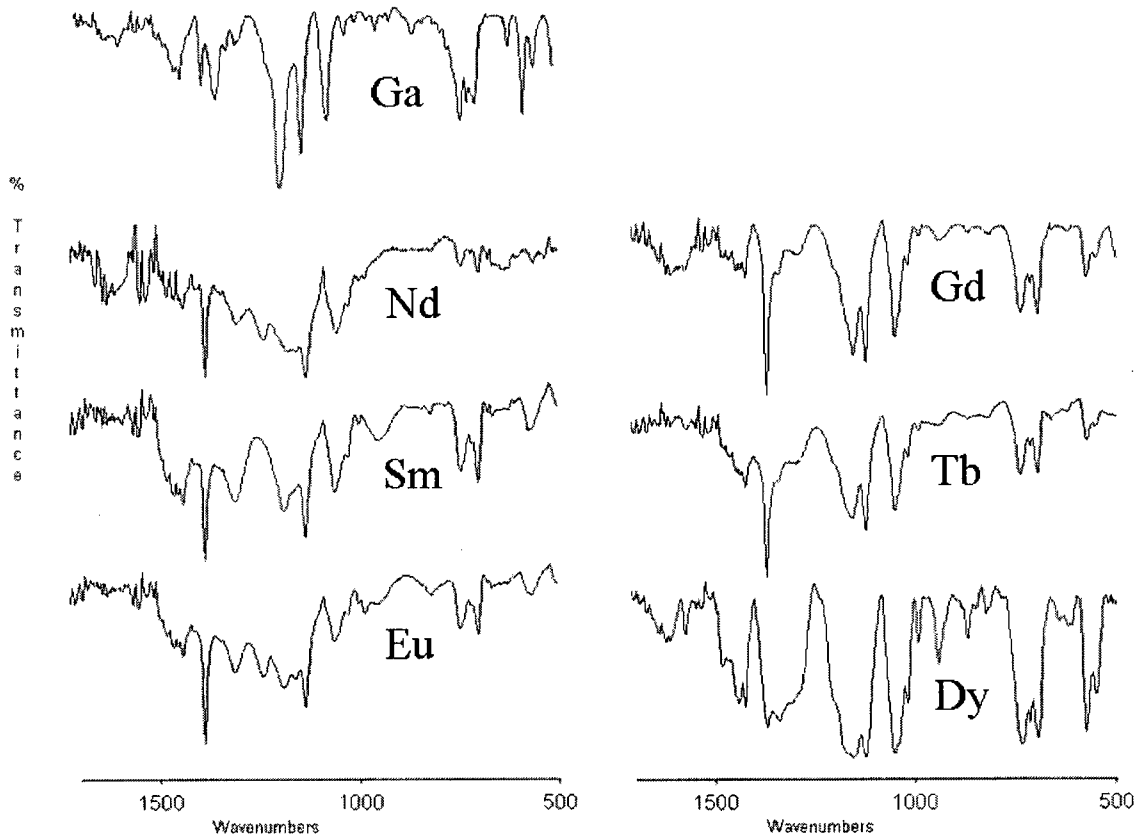

Figure 4.4. Selected IR spectra of $[M(H_4ppba)_2](NO_3)_4Cl$, M as indicated. The IR spectrum of **4.1** (M=Ga) is included for comparison.

Despite the fact that pure complexes could not be obtained for all of the early Ln^{3+} series, the +LSIMS data and IR spectroscopy (Figure 4.4) indicates that these complexes have similarities to the Eu^{3+}, Gd^{3+} and Tb^{3+} complexes. The large shift in frequency of the IR bands associated with P and O bonding may be attributed to a change in the intramolecular H-bonding involving the protonated N atoms. If this is the case, the positions of the transitions in the IR spectra are a remarkably sensitive probe of the intramolecular H-bonding. Although the Sm^{3+} complex has an identical IR spectrum to those of the Gd^{3+} and Tb^{3+} complexes, strangely the Eu^{3+} complex does not, even though

its elemental analysis supports its formulation as $[Eu(H_4ppba)_2]^{5+}$. The Nd^{3+} spectrum is identical to the Eu^{3+} spectrum. The early Ln^{3+} may have a propensity to form a mixture of 2:1 and 1:1 complexes (*vide infra*). This may explain why satisfactory elemental analyses could not be obtained for La^{3+}-Sm^{3+}, and may also explain the presence of the 2:1 peaks in the +LSIMS spectra.

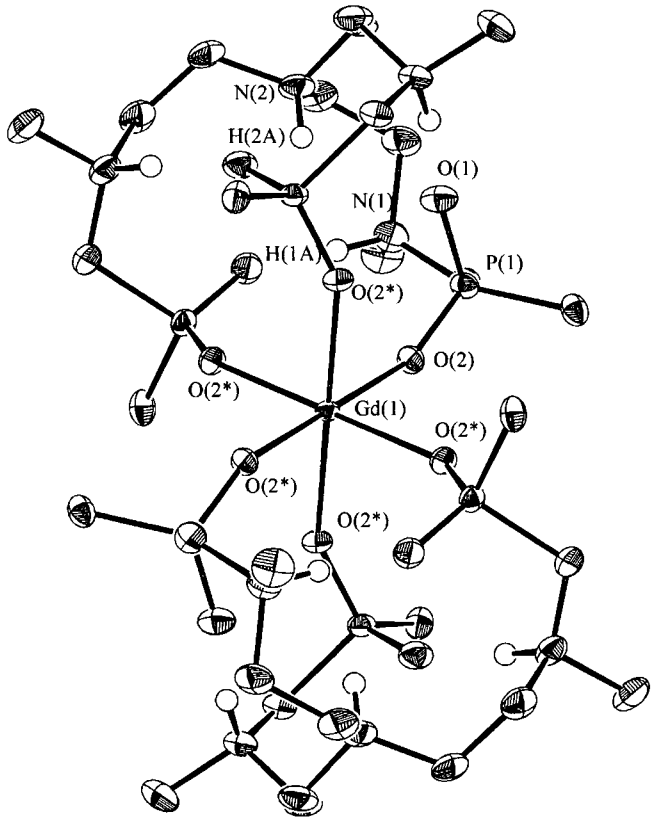

Figure 4.5. ORTEP diagram of the $[Gd(H_4ppba)_2]^{5+}$ cation with the solvent molecules and the aromatic rings removed for clarity; 50% thermal probability ellipsoids are shown.

From the reaction mixture of Gd^{3+} and H_3ppba, a single crystal was obtained and was used in an X-ray structural analysis (Figure 4.5, Table 4.7). The complex has a

bicapped structure similar to that found in **4.1**. Each arm of the tripod is related to the other arms by six-fold crystallographic symmetry. Both the pendant amines and the apical amines are protonated to afford the product complex as $[Gd(H_4ppba)_2](NO_3)_4Cl{\cdot}3H_2O$ (**4.2**). The geometry around Gd^{3+} is nearly octahedral, with unique bond angles of 180.00°, 87.52(6)° and 92.48(6)° between the O phosphinato donor atoms. As in **4.1**, the P atoms in **4.2** have a *RRRSSS* configuration and this is the only diastereomer seen in the solid state. The presence of the $[M(H_4ppba)_2]^{5+}$ complex in the unit cell is very clear, but the six-fold symmetry of the $R\bar{3}$ unit cell complicated the identification of the five counterions and the CH_3OH in the large void spaces of the unit cell. This disorder was modeled with help from the analytical data and was refined to R1 = 0.034.

Table 4.7. Selected bond lengths (Å) and bond angles (deg) in $[Gd(H_4ppba)_2](NO_3)_4Cl{\cdot}3CH_3OH$ (**4.2**).

Gd-O(2)	2.2841(17)	O(2)-Ga-O(2*)†	180.00
P(1)-O(1)	1.500(2)	O(1)-P(1)-O(2)	117.45(11)
P(1)-O(2)	1.5104(16)	O(1)-P(1)-C(1)	112.67(11)
P(1)-C(1)	1.797(3)	O(1)-P(1)-C(7)	108.17(10)
P(1)-C(7)	1.845(3)	O(2)-P(1)-C(1)	107.45(11)
Gd-O(2)-P(1)	143.85(10)	O(2)-P(1)-C(7)	107.94(10)
O(2)-Ga-O(2*)†	87.52(6)	C(1)-P(1)-C(7)	101.97(12)
O(2)-Ga-O(2*)†	92.48(6)		

† The O atoms are related to each other by symmetry.

The switch from $[M(H_4ppba)_2]^{5+}$ ($M=La^{3+}$-Tb^{3+}) to $[M'(H_3ppba)_2]^{3+}$ ($M'=Al^{3+}$, Ga^{3+}, In^{3+}, Ho^{3+}-Lu^{3+}) is an interesting phenomenon that we did not witness in the H_3ppma system. It is possible that the size of the metal ion and the nature of the H-bonding network in the uncoordinated upper part of the tripodal ligand have some role in this behavior. It is a well-known fact that early lanthanide trivalent metal ions are larger than late lanthanide trivalent metal ions. The 90° angles between the phosphinate O donors in **4.1** have two unique angles of 88.88(6)° and 91.12(6)°, whereas the unique angles in the **4.2** are 87.52(6)° and 92.48(6)°. It is possible that the larger Ln^{3+} ions can tolerate this compression of the bond angles better than the smaller Ln^{3+} and group 13 metal ions. As a result of the compression at the bottom of the tripod, the upper tripod can open up and a rearrangement of the H-bonding network can occur (including the apical N proton) to produce the observed +5 complex. This explanation is also supported by the dramatic change in the P=O and P-O stretching frequencies in the IR spectra of the complexes.

4.3.3. 1:1 Complexes of H_3ppba with the Lanthanides

In order to investigate further the strange behavior of the 2:1 La^{3+}-Sm^{3+} complexes, including the possibility of 1:1 complex formation, a study of the system in 1:1 ratios was initiated. Under similar conditions to those which produced the 2:1 complexes, 1:1 ratios of $M(NO)_3$ ($M=La^{3+}$-Lu^{3+}) and H_3ppba were reacted in methanol. These reactions afforded complexes of the type $[M(H_4ppba)]^{4+}$ in 14-34% yield. Upon mixing of the starting materials, a finely-divided precipitate immediately formed for most of the lanthanides. Towards the end of the series (Tm^{3+}-Lu^{3+}), no precipitate formed and prismatic crystals appeared corresponding to the $[M(H_3ppba)_2]^{3+}$ complexes over a

period of 48 hours. This was verified crystallographically for the Yb^{3+} complex (the full solution of the structure was not completed once this was discovered).

Unlike those of the 2:1 complexes, the +LSIMS mass spectra of the 1:1 complexes show no substantial evidence of 2:1 peaks (Table 4.8). In some of the complexes, 2:1 peaks were observed at trace levels (20x gain). The possibility exists that a small excess of ligand may have been present in these cases. Lanthanide nitrate salts are very hygroscopic and the excess water would not have been accounted for if it were present.

Table 4.8 +LSIMS data for all 1:1 H_3ppba complexes.

Complex	$[M(Hppba)]^+$ *m/z*
$[La(ppba)](NO_3)_3Cl{\cdot}3H_2O$	1015
$[Ce(ppba)](NO_3)_3Cl{\cdot}5H_2O$	1016
$[Pr(ppba)](NO_3)_3Cl{\cdot}4H_2O$	1017
$[Nd(ppba)](NO_3)_3Cl{\cdot}4H_2O$	1020
$[Sm(ppba)](NO_3)_3Cl{\cdot}3H_2O$	1028
$[Eu(ppba)](NO_3)_3Cl{\cdot}3H_2O$	1029
$[Gd(ppba)](NO_3)_3Cl{\cdot}3H_2O$	1034
$[Tb(ppba)](NO_3)_3Cl{\cdot}3H_2O$	1035
$[Dy(ppba)](NO_3)_3Cl{\cdot}3H_2O$	1040
$[Ho(ppba)](NO_3)_3Cl{\cdot}3H_2O$	1041
$[Er(ppba)](NO_3)_3Cl{\cdot}3H_2O$	1044

The IR spectra of the 1:1 complexes La^{3+}-Er^{3+} are remarkably similar (Figure 4.6). The $\nu(NO_3)$ peak is at 1384 cm^{-1}, which is the same frequency as that seen in the 2:1 complexes. With the exception of complexes of La^{3+} Sm^{3+}, and Er^{3+} which have an additional peak at 1238 cm^{-1}, all the other complexes share similar features in the $\nu(PO)$ region of the spectrum (1303, 1181, 1134, 1054 cm^{-1}). The IR spectrum of the Ho^{3+} complex has a peak at 1238 cm^{-1} which is seen as a small shoulder on the broad peak at 1181 cm^{-1}. The fact that this same peak is seen the 2:1 Nd^{3+} and Eu^{3+} IR spectra (Figure 4.4) supports the possibility that a 1:1 complex may be present depending on the exact conditions of preparation of the early lanthanide 2:1 complexes. The IR spectra of the late lanthanide 2:1 complexes (Figure 4.3) demonstrate that these metals have no propensity to form 1:1 complexes under these conditions.

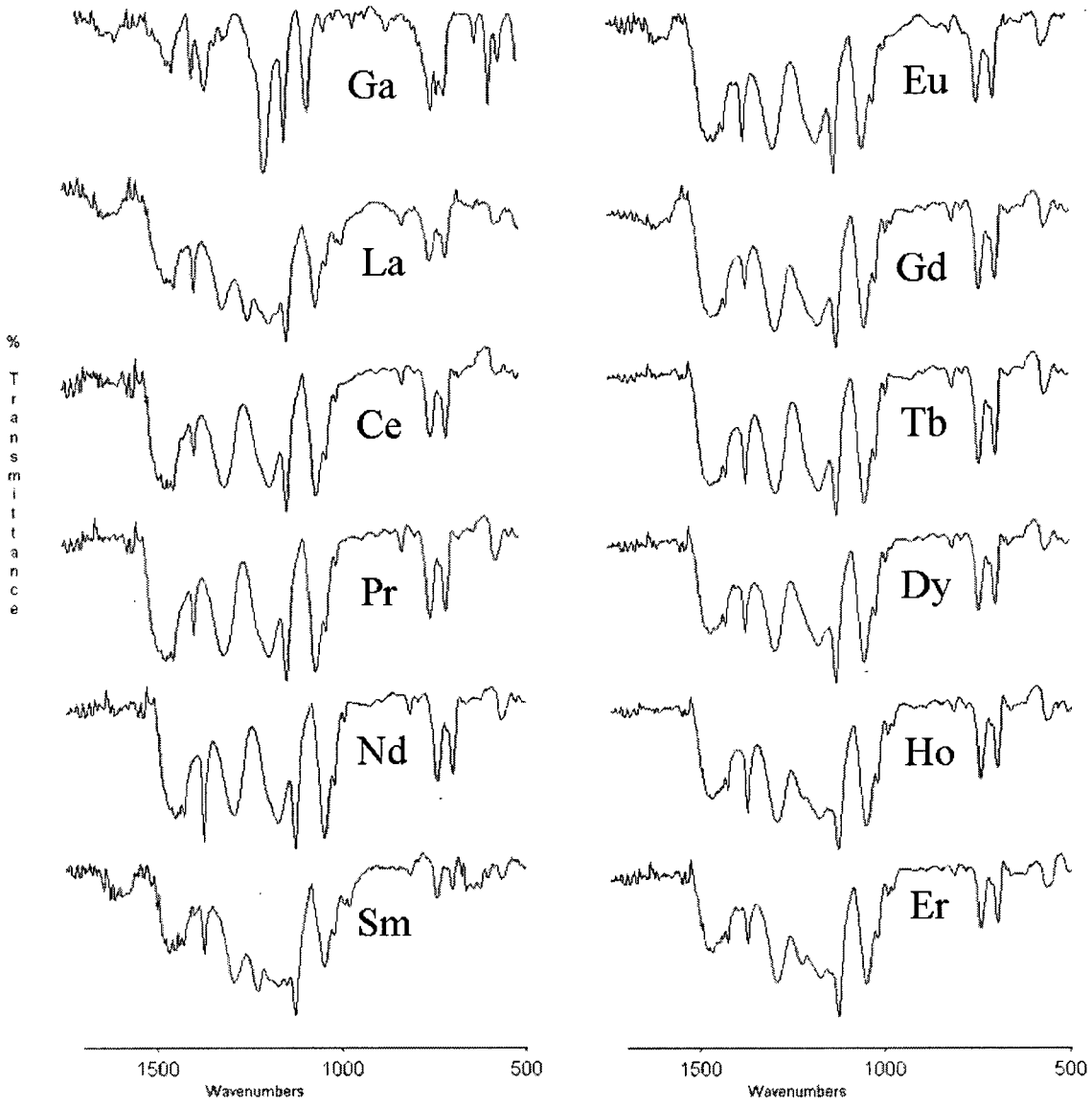

Figure 4.6. IR spectra of $[Ln(H_4ppba)](NO_3)_3Cl$, Ln as indicated. The IR spectrum of **4.1** (M=Ga) is included for comparison.

With a small variation in hydration, the elemental analyses for the 1:1 complexes are very consistent (Table 4.9). All the complexes appear to have the formulation $[M(H_4ppba)](NO_3)_3Cl{\cdot}xH_2O$. As expected, the carbon content is much lower than in any of the 2:1 complexes (Table 4.7), and the nitrogen content is much higher, owing to the

lack of a second carbon-rich ligand. The analyses of the Ho^{3+} and Er^{3+} complexes appear to have slightly higher levels of carbon, perhaps because of the preference of the late Ln^{3+} to form 2:1 complexes in this system.

Table 4.9. Elemental analyses for all 1:1 H_3ppba complexes.

Complex	C	H	N
	Calcd. (found)	Calcd. (found)	Calcd. (found)
$[La(ppba)](NO_3)_3Cl{\cdot}3H_2O$	44.54 (44.83)	4.98 (4.89)	7.57 (7.20)
$[Ce(ppba)](NO_3)_3Cl{\cdot}5H_2O$	43.30 (43.20)	5.15 (4.90)	7.36 (7.15)
$[Pr(ppba)](NO_3)_3Cl{\cdot}4H_2O$	43.86 (44.12)	5.06 (4.94)	7.46 (7.04)
$[Nd(ppba)](NO_3)_3Cl{\cdot}4H_2O$	43.75 (44.04)	5.05 (4.89)	7.44 (7.02)
$[Sm(ppba)](NO_3)_3Cl{\cdot}3H_2O$	44.15 (43.94)	4.94 (4.68)	7.51 (7.25)
$[Eu(ppba)](NO_3)_3Cl{\cdot}3H_2O$	44.10 (44.58)	4.93 (4.76)	7.50 (7.21)
$[Gd(ppba)](NO_3)_3Cl{\cdot}3H_2O$	43.92 (43.92)	4.91 (4.76)	7.47 (7.31)
$[Tb(ppba)](NO_3)_3Cl{\cdot}3H_2O$	43.86 (44.19)	4.91 (4.75)	7.46 (7.13)
$[Dy(ppba)](NO_3)_3Cl{\cdot}3H_2O$	43.74 (43.98)	4.89 (4.72)	7.44 (7.05)
$[Ho(ppba)](NO_3)_3Cl{\cdot}3H_2O$	43.66 (44.98)*	4.89 (4.69)	7.43 (6.98)
$[Er(ppba)](NO_3)_3Cl{\cdot}3H_2O$	43.59 (44.90)*	4.88 (4.82)	7.41 (6.91)

* The high carbon content of these complexes is explained in the text.

Because all the 1:1 complexes precipitate as highly insoluble powders, no crystals suitable for an X-ray structural analysis could be obtained. The complexes only have limited solubility, even in solvents such as DMSO; after dissolution they are

unrecoverable. The question remains as to what type of 1:1 complex they form (Scheme 4.1). Given that the elemental analysis supports the formulation $[M(H_4ppba)]^{4+}$, wherein all four N atoms are protonated, it seems highly unlikely that an encapsulated complex is formed. The $\nu(NO_3)$ in the IR spectra is identical to that of the two structurally characterized 2:1 complexes, therefore, it is unlikely that the NO_3^- ligands are coordinated to Ln^{3+} in the 1:1 complexes. Given this combined evidence, the most reasonable assumption is that the complexes are monocapped, with 3-5 H_2O molecules completing the coordination sphere.

4.3.4. 1:1 Complex of Ga^{3+} and H_3ppa

Reaction of tris(4-(phenylphosphinato)-3-azabutyl)amine ($H_3ppa \cdot HCl \cdot H_2O$) with $Ga(NO_3)_3 \cdot 6H_2O$ in methanol at a 1:1 molar ratio results in the formation of a finely-divided white precipitate after standing for 48 h. Elemental analysis of this precipitate gives the composition $[Ga(ppa)] \cdot 3H_2O$ (**4.4**). Clearly, this is a very interesting result because it is possible that an encapsulated 1:1 complex has formed. The lack of counterions strongly suggests that the pendant N donors are not protonated NH_2^+, but rather the neutral NH. Unlike the $[M(H_4ppba)]^{4+}$ complexes described previously, the formation of an encapsulated 1:1 complex is a distinct possibility. The +LSIMS data support the formulation as 1:1; a large peak at *m/z* 675 corresponding to $[Ga(Hppa)]^+$ is seen. Only a trace peak is seen at *m/z* 1285 corresponding to the 2:1 complex $[GaH_4(ppa)_2]^+$.

The IR spectra of the H_3ppa ligand and **4.4** have several notable features (Figure 4.7). One of the $\nu(PO)$ bands shifts from 1188 to 1181 cm^{-1} upon complex formation. The band at 954 cm^{-1} in the free ligand disappears completely. There is no indication of a

free nitrate at *ca.* 1385 cm^{-1}. The broad ν(NH) peak shifts from 3414 cm^{-1} in the free uncomplexed ligand to 3421 cm^{-1} in the complex, which may indicate that the N donors are involved in complex formation. The seemingly unusual strengthening of the N-H bond upon coordination may occur because the N atom is first deprotonated from NH_2^+ to NH, then is subsequently coordinated to Ga^{3+}. Since this is a two step process, it is difficult to state with absolute certainty that the N donors are coordinated to Ga^{3+} on the basis of IR spectroscopy alone.

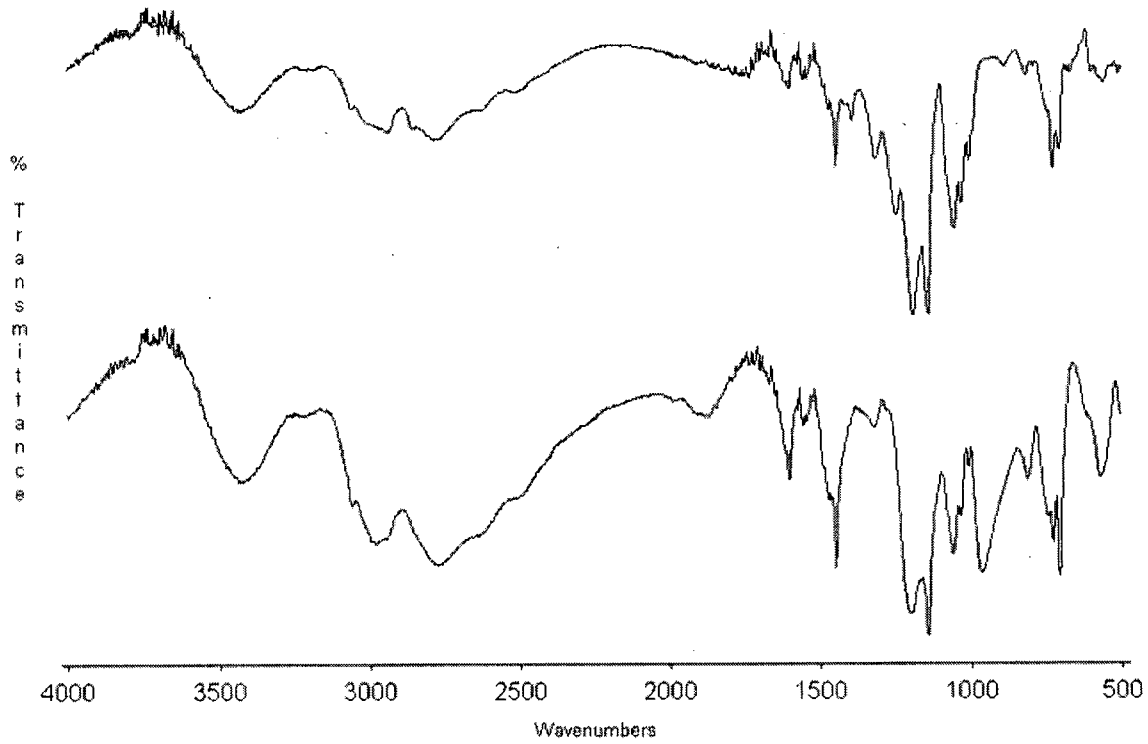

Figure 4.7. IR spectra of $[Ga(ppa)]\cdot 3H_2O$ (**4.4**) (top) and $H_3ppa\cdot HCl\cdot H_2O$ (bottom).

The ^{31}P NMR spectrum of the complex in methanol is complicated and contains at least seven resonances between 23.7-24.9 ppm, shifted downfield from the ligand in which it is seen as a singlet at 21.1 ppm. The ^{1}H NMR spectra of the complex and the free ligand demonstrate significant shifts of the CH_2 groups compared to the free ligand

(Figure 4.8). Although the speciation in solution is complicated, the shifts of the pendant CH_2 arms are strongly indicative of pendant N atom coordination to the metal. It is plausible to regard the complex as encapsulated, but in the absence of X-ray structural data, it cannot be stated for certain.

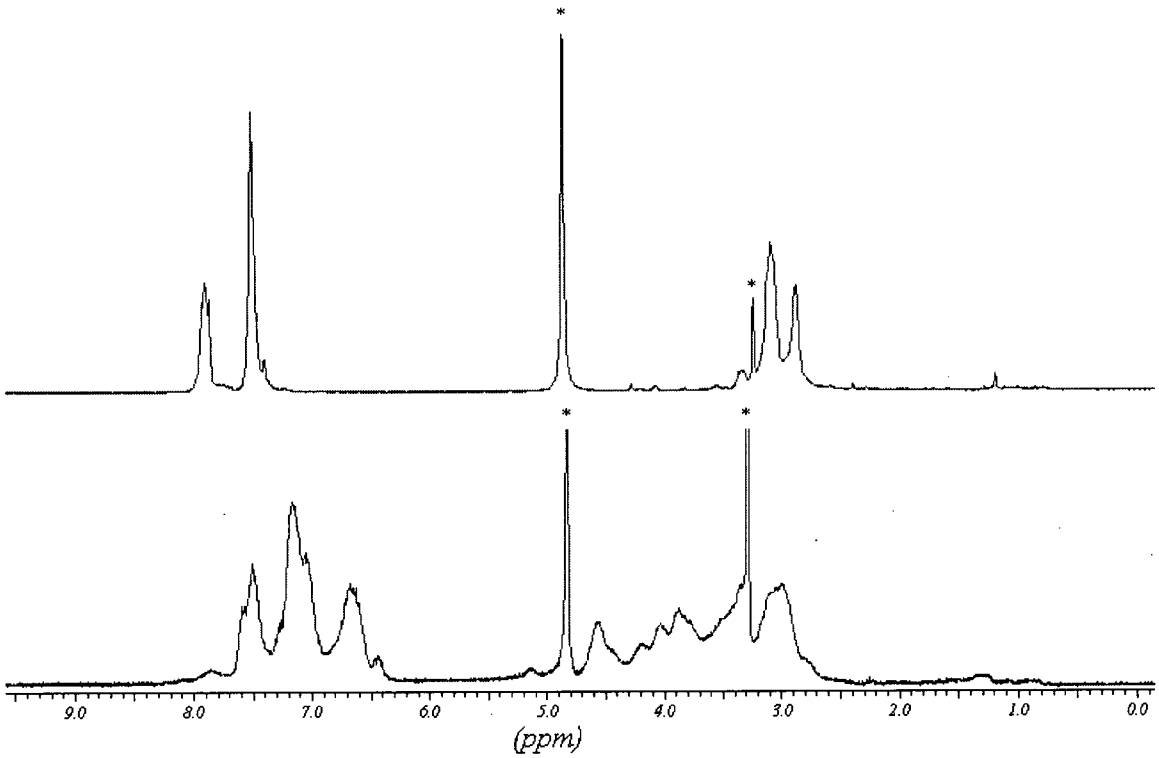

Figure 4.8. ^1H NMR spectra (300 MHz) of $[Ga(ppa)]\cdot 3H_2O$ (**4.4**) (top) and $H_3ppa\cdot HCl\cdot H_2O$ (bottom) in d_4-methanol; (* = H_2O and CH_3OH impurities).

4.4. Conclusions

In order to obtain 1:1 complexes of the group 13 metals Al^{3+}, Ga^{3+}, In^{3+} and the lanthanides, two new amine-phosphinate tripod ligands were synthesized. H_3ppba was synthesized by the Moedritzer-Irani reaction of tris(2-benzylaminoethyl)amine and phenylphosphinic acid to afford tris(4-(phenylphosphinato)-3-benzyl-3-azabutyl)amine (H_3ppba·2HCl·H_2O) in good yield. The reaction of H_3ppba·2HCl·H_2O with H_2 at 70 bar with a 10% Pd on C catalyst yielded tris(4-(phenylphosphinato)-3-azabutyl)amine (H_3ppa), a water soluble tripodal amine phosphinate ligand containing three secondary amine functional groups. H_3ppba·2HCl·H_2O was reacted with Al^{3+}, Ga^{3+}, In^{3+} and Ln^{3+} in 2:1 ratios and was found to form bicapped complexes of the type $[M(H_3ppma)_2]^{3+}$ ($M=Al^{3+}$, Ga^{3+}, In^{3+}, Ho^{3+}-Lu^{3+}) or $[M(H_4ppma)_2]^{5+}$ ($M=La^{3+}$-Tb^{3+}). Crystal structures were obtained for $[Ga(H_3ppba)_2]^{3+}$ and $[Gd(H_4ppba)_2]^{5+}$, and a combination of IR spectroscopic, mass spectrometric and elemental analytical data were used to infer the structures of the remaining metal complexes. The bicapped geometry is formed by a pair of ligands coordinating to the metal centre through its phosphinate O atoms only. Either 3 or 4 of the nitrogen atoms on each ppba unit are protonated, and an H-bonded network is formed in the empty space of the tripod. 1:1 complexes of the type $[M(H_4ppba)_2]^{4+}$ ($M=La^{3+}$-Er^{3+}) were obtained by the reaction of H_3ppba·2HCl·H_2O and the appropriate metal salts at 1:1 molar ratios. Although an X-ray structure was not obtained, the combination of IR spectroscopic, mass spectrometric and elemental analysis data strongly support the formation of a monocapped complex wherein the nitrate counterions are not coordinated to the metal centre. 1:1 molar ratios of H_3ppa·HCl·H_2O and $Ga(NO_3)_3$·$6H_2O$ in methanol afford the 1:1 complex [Ga(ppa)]·$3H_2O$. Although ^1H and ^{31}P NMR

spectroscopies, IR spectroscopy, +LSIMS and elemental analysis support the formation of a 1:1 encapsulated complex, the exact nature of the complex cannot be ascertained without an X-ray structural analysis.

4.5. References

1) Anderson, C. J.; Welch, M. J. *Chem. Rev.* **1999**, *99*, 2219.

2) Caravan, P.; Ellison, J. J.; McMurry, T. J.; Lauffer, R. B. *Chem. Rev.* **1999**, *99*, 2293.

3) Liu, S.; Rettig, S. J.; Orvig, C. *Inorg. Chem.* **1992**, *31*, 5400.

4) Liu, S.; Wong, E.; Karunaratne, V.; Rettig, S. J.; Orvig, C. *Inorg. Chem.* **1993**, *32*, 1756.

5) Liu, S.; Wong, E.; Rettig, S. J.; Orvig, C. *Inorg. Chem.* **1993**, *32*, 4268.

6) Wong, E.; Liu, S.; Lügger, T.; Hahn, F. E.; Orvig, C. *Inorg. Chem.* **1995**, *34*, 93.

7) Wong, E.; Caravan, P.; Liu, S.; Rettig, S.; Orvig, C. *Inorg. Chem.* **1996**, *35*, 715.

8) Lowe, M. P.; Rettig, S. J.; Orvig, C. *J. Am. Chem. Soc.* **1996**, *118*, 10446.

9) Lowe, M. P.; Caravan, P.; Rettig, S. J.; Orvig, C. *Inorg. Chem.* **1998**, *37*, 1637.

10) Setyawati, I. A.; Liu, S.; Rettig, S. J.; Orvig, C. *Inorg. Chem.* **2000**, *39*, 496.

11) Broan, C. J.; Cole, E.; Jankowski, K. J.; Parker, D.; Pulukkody, K.; Boyce, B. A.; Nigel, R. A. B.; Millar, K.; Millican, A. T. *Synthesis* **1992**, 63.

12) Cole, E.; Copley, R. C. B.; Howard, J. A. K.; Parker, D.; Ferguson, G.; Gallagher, J. F.; Kaitner, B.; Harrison, A.; Royle, L. *J. Chem. Soc., Dalton Trans.* **1994**, 1619.

13) Aime, S.; Botta, M.; Parker, D.; Williams, J. A. G. *J. Chem. Soc., Dalton Trans.* **1996**, 17.

14) Huskowska, E.; Maupin, C. L.; Parker, D.; Williams, J. A. G.; Riehl, J. P. *Enantiomer* **1997**, *2*, 381.

15) Aime, S.; Batsanov, A. S.; Botta, M.; Dickins, R. S.; Faulkner, S.; Foster, C. E.; Harrison, A.; Howard, J. A. K.; Moloney, J. M.; Norman, T. J.; Parker, D.; Royle, L.; Williams, J. A. G. *J. Chem. Soc., Dalton Trans.* **1997**, 3623.

16) Aime, S.; Botta, M.; Dickins, R. S.; Maupin, C. L.; Parker, D.; Riehl, J. P.; Williams, J. A. G. *J. Chem. Soc., Dalton Trans.* **1998**, 881.

17) Pulukkody, J. P.; Norman, T. J.; Parker, D.; Royle, L.; Broan, C. J. *J. Chem. Soc., Perkin Trans. 2* **1993**, 605.

18) Aime, S.; Batsanov, A. S.; Botta, M.; Howard, J. A. K.; Parker, D.; Senanayake, K.; Williams, J. A. G. *Inorg. Chem.* **1994**, *33*, 4696.

19) Sherry, A. D. *J. Alloys Compd.* **1997**, *249*, 153.

20) Kim, W. D.; Kiefer, G. E.; Huskens, J.; Sherry, A. D. *Inorg. Chem.* **1997**, *36*, 4128.

21) Liu, S.; Edwards, D. S. *Bioconjugate Chem.* **2001**, *12*, 7.

22) Caravan, P.; Lowe, M. P.; Read, P. W.; Rettig, S. J.; Yang, L. W.; Orvig, C. *J. Alloys Compd.* **1997**, *249*, 49.

23) Perrin, D. D.; Armarego, W. L. F.; Perrin, D. R. *Purification of Laboratory Chemicals*; 2nd ed.; Pergamon Press: Toronto, **1980**.

24) Naiini, A.; Menge, W. M. P. B.; Verkade, J. G. *Inorg. Chem.* **1991**, *30*, 5009.

25) Moedritzer, K.; Irani, R. R. *J. Org. Chem.* **1966**, *31*, 1603.

26) March, J. *Advanced Organic Chemistry*; 3rd ed.; John Wiley & Sons, Inc.: New York, **1985**.

27) Mollier, H.; Vincens, M.; Vidal, M.; Pasqualini, R.; Duet, M. *Bull. Soc. Chim. Fr.* **1991**, *128*, 787.

28) Greene, T. W.; Wuts, P. G. M. *Protective Groups in Organic Synthesis*; 3rd ed.; John Wiley & Sons, Inc.: New York, **1999**.

Chapter Five

Conclusions and Further Thoughts

5.1. General Conclusions

The metal complexes discussed in this thesis have the potential to be used as diagnostic or therapeutic agents in nuclear medicine, or to act as models for new potential agents. Complexes containing the $[Re{=}O]^{3+}$ core and phosphine-phenolate ligands (H_xPO_x) were prepared and structurally characterized. The possibility of forming ternary complexes with various hydrazines was explored to evaluate the potential of H_xPO_x to act as coligands in the HYNIC bifunctional chelate system. A series of complexes were prepared by reaction of H_xPO_x with preformed rhenium-hydrazine cores, such as $[Re(Hhypy)(hypy)]^{3+}$ and $[Re(N_2PhMe)_2]^{3+}$. The new tripodal amine-phosphinate ligands H_3ppba and H_3ppa were synthesized and metal complexes containing Al^{3+}, Ga^{3+}, In^{3+} and Ln^{3+} ion were prepared. The complexes were prepared to investigate their possible use in nuclear medicine, and to explore their fundamental coordination chemistry.

In Chapter 2, $[Re{=}O]^{3+}$ complexes containing the ligands H(MePO) and $H_2(Me_2PO_2)$ were prepared. $[ReOCl(MePO)_2]$ (**2.1**) was prepared by reaction of H(MePO) with *mer*-$[ReOCl_3(PPh_3)_2]$ in ethanol and was structurally characterized. During the course of these studies, an interesting reduction route was discovered and was used to prepare **2.1** from $[NH_4][ReO_4]$. Reduction was found to occur only in acidic solution. Therefore, a two step approach was devised whereby the reduction occurred at low pH in ethanol, and subsequent metal complex formation proceeded upon raising the pH. The same acid/base reduction approach was extended to synthesize

$[ReO(Me_2PO_2)(H(Me_2PO_2)]$ (**2.2**) from $[NH_4][ReO_4]$ and the complex was structurally characterized. **2.1** and **2.2** had *cis*-(P,P) geometries in the solid state and in solution. Attempts to form ternary complexes containing various hydrazines with **2.1** and **2.2** were unsuccessful.

The successful synthesis of rhenium-hydrazine-PO_x ternary complexes was accomplished in Chapter 3. Employing the reverse of the synthetic strategy attempted in Chapter 2, $[ReCl_3(Hhypy)(hypyH)]$ was reacted with excess HPO to afford a mixture of [Re(Hhypy)(hypy)(PO)(HPO)]Cl (**3.1**) and [ReCl(Hhypy)(hypy)(PO)] (**3.2**). The mixture was subsequently separated by silica gel chromatography. An X-ray structure of **3.1** was obtained; the cationic complex was shown to have octahedral geometry and an N_3OP_2 coordination sphere. One PO ligand was bidentate, the second was monodentate and protonated; they were coordinated *trans* to one other. The two hypy ligands were coordinated *cis* to each other in a monodentate diazenido / bidentate diazene fashion. The neutral complex **3.2** was also structurally characterized; the complex had octahedral geometry and an N_3OP_2Cl coordination sphere, wherein the Cl^- ligand replaced the monodentate HPO ligand seen in **3.1**. Reaction of $[ReCl_3(Hhypy)(hypyH)]$ with H_2PO_2 and $H_2(Me_2PO_2)$ afforded $[Re(Hhypy)(hypy)(HPO_2)(H_2PO_2)]Cl$ (**3.3**) and $[Re(Hhypy)(hypy)(H(Me_2PO_2))(H_2(Me_2PO_2))]Cl$ (**3.4**), respectively. Spectroscopic evidence strongly indicated that **3.3** and **3.4** were isostructural with the structurally-characterized cation **3.1**. The reaction of H(MePO) with $[ReCl_2(N_2PhMe)_2(PPh_3)][BPh_4]$ in methanol afforded $[Re(N_2PhMe)_2(MePO)_2][BPh_4]$ (**3.5**). Elemental analysis data and spectroscopic evidence demonstrated that **3.5** is most likely an octahedral cation, with two N_2PhMe ligands coordinated *cis* to one other, and the P atoms of the two MePO ligands coordinated *trans* to one other. The H_xPO_x ligands were shown to be capable of

forming ternary complexes of rhenium containing hydrazines, provided that the hydrazine ligands were coordinated to the Re first.

In Chapter 4, the tripodal amine-phosphinate ligands H_3ppba and H_3ppa were synthesized. The N-debenzylation of H_3ppba by hydrogenation afforded the novel secondary amine tripod H_3ppa. H_3ppba was reacted with Al^{3+}, Ga^{3+}, In^{3+} and Ln^{3+} nitrates in ligand : metal ratios of 2:1. Two distinct types of complex were isolated. The group 13 metals and Ho^{3+}-Lu^{3+} afforded $[M(H_3ppba)_2]^{3+}$, and La^{3+}-Tb^{3+} afforded $[M(H_4ppba)_2]^{5+}$. Examples of both types of complex were structurally characterized; $[Ga(H_3ppba)_2](NO_3)_2Cl{\cdot}3CH_3OH$ (**4.1**) and $[Gd(H_4ppba)_2](NO_3)_4Cl{\cdot}3CH_3OH$ (**4.2**) are both bicapped complexes wherein only the phosphinate groups coordinated to the metal ion. The complexes differ in the level of protonation in the unoccupied upper portions of the tripods. The structures of the remaining complexes were shown to be identical to **4.1** or **4.2** by a combination of IR spectroscopy, mass spectrometry and elemental analysis data. At 1:1 ligand : metal ratios, H_3ppba reacted with nitrates of La^{3+}-Er^{3+} to form $[M(H_4ppba)]^{4+}$. Although a structural analysis could not be performed on any of the complexes, experimental evidence supported the formation of a 1:1 monocapped complex, wherein the nitrate counterions were not coordinated to the metal center. The empty coordination sites were likely occupied by water. Reaction of the secondary amine-phosphinate ligand H_3ppa with $Ga(NO_3)_3$ at 1:1 ratios forms $[Ga(ppa)]{\cdot}3H_2O$. Experimental evidence supported the formation of an encapsulated 1:1 complex; however, the lack of a structural analysis prevented verification of encapsulated complex formation.

5.2. Suggestions for Future Work

The HPO,[1] H_2PO_2,[1] H(MePO) and $H_2(Me_2PO_2)$ ligands have been shown to form $[Re{=}O]^{3+}$ complexes and complexes with two different rhenium-hydrazine cores. The analogous *tert*-butyl ligands, (5-*tert*-butyl-2-hydroxyphenyl)diphenylphosphine (H(*t*-BuPO)) and bis(5-*tert*-butyl-2-hydroxyphenyl)phenylphosphine ($H_2(t\text{-}Bu_2PO_2)$) have also been prepared.[2] The *tert*-butyl ligands could introduce a significant amount of steric bulk into the $[Re{=}O]^{3+}$ complexes, all of which had *cis*-(P,P) stereochemistry in solution and the solid state.

A slight excess of H(*t*-BuPO) was reacted with $[ReOCl_3(PPh_3)_2]$ in ethanol, in a manner identical to the preparation of **2.1**. The +LSIMS data for the resulting complex shows peaks corresponding to $[ReO(t\text{-}BuPO)_2(t\text{-}BuPO_2)]$ (**5.2**) + H^+ at *m/z* = 1217 and $[ReO(t\text{-}BuPO)_2]^+$ at *m/z* = 869. The latter type of peak was observed in **2.1** but the former peak has not been seen before in complexes of this type. Elemental analyses of C and H support the formation of the neutral $[ReOCl(t\text{-}BuPO)_2]$ (**5.1**). The ν(Re=O) at 960 cm^{-1} in the IR spectrum supports the formation of a $[Re{=}O]^{3+}$ complex. Preliminary ^{31}P NMR studies show a total of five resonances; two are coupled to each other with $^2J_{(P,P)}$ = 6 Hz, the remaining three are singlets that are shifted significantly downfield from the doublets. Two of the three singlets are large and it is possible that one is due to contamination of the complex with oxidized H(*t*-BuPO). It is also possible that one of the large ^{31}P NMR signals is due to a *trans* complex with identical composition to the *cis* complexes. If a *trans*-(P,P) complex were to form, and both *t*-BuPO ligands were bound

in the equatorial plane, no *trans*-(P,P) coupling would be observed since the P nuclei would be equivalent. Further investigation is warranted.

The large number of H_3ppba complexes prepared in Chapter 4 were of fundamental interest, but the lack of water solubility precluded the use of any of these complexes as diagnostic therapeutic agents. The formation of bicapped and monocapped complexes was also not favourable for this application. ^{31}P NMR studies could be used to determine the stability constant of the complexes, but the study would have to be done in methanol solution. The results of such a study would not be comparable to studies done in aqueous solution and would be of limited utility.

H_3ppa was shown by various techniques to form a 1:1 encapsulated complex with Ga^{3+} in methanol, and was highly water soluble. This is a significant result that merits further investigation. Complexes of Al^{3+}, In^{3+} and Ln^{3+} should be synthesized and characterized in solution, and if possible, in the solid state. The water solubility of these complexes will likely make them amenable to study by a number of techniques that are not useful in methanol. Potentiometric studies have been of great value in characterizing the behavior of Ln^{3+} and group 13 complexes in aqueous solution, and such studies should be undertaken in this system. Unlike the H_3ppma system, in which the complexes were all bicapped,[3-5] potentiometric titrations should be able to monitor the loss of the amine protons, and allow the formation of 1:1 encapsulated complexes to be verified. It is also of interest to know whether any water molecules are bound to the metal ion. The ^{17}O NMR spectral shifts of natural abundance H_2O in Dy^{3+} complexes have been used as a method to determine the number of bound water molecules.[5]

5.3. References

1) Luo, H.; Setyawati, I.; Rettig, S. J.; Orvig, C. *Inorg. Chem.* **1995**, *34*, 2287.

2) Kovacs, M. S.; Hein, P.; Sattarzadeh, S.; Patrick, B. O.; Emge, T. J.; Orvig, C. Submitted for publication.

3) Lowe, M. P.; Rettig, S. J.; Orvig, C. *J. Am. Chem. Soc.* **1996**, *118*, 10446.

4) Caravan, P.; Lowe, M. P.; Read, P. W.; Rettig, S. J.; Yang, L. W.; Orvig, C. *J. Alloys Compd.* **1997**, *249*, 49.

5) Lowe, M. P.; Caravan, P.; Rettig, S. J.; Orvig, C. *Inorg. Chem.* **1998**, *37*, 1637.

Appendix

X-ray crystallographic analyses of $[ReOCl(MePO)_2]$ (2.1) and $[ReO(Me_2PO_2)(H(Me_2PO_2))]$ (2.2). Data for **2.1** and **2.2** were collected on a Rigaku/ADSC CCD diffractometer at UBC at -100(1)°C. All data were processed and corrected for Lorentz and polarization effects, and absorption (semi-empirical, based on symmetry analysis of redundant data). Structure **2.1** was solved using heavy-atom Patterson methods,[1] while the structure of **2.2** was solved by direct methods.[2] Both structures were expanded using Fourier techniques.[3] Final refinements for **2.1** and **2.2** were carried out using SHELXL-97.[4] Selected crystallographic data for the complexes appears in Table A1. Complete lists of bond lengths and bond angles appear in Tables A2, A3, A4 and A5.

Final unit cell parameters for **2.1** (**2.2**) were obtained by least-squares on the setting angles for 18480 (20525) reflections with $2\theta = 5.8 - 55.8°$ (6.0 – 55.9°). **2.1** was found to crystallize in space group *C*2/*c* with two molecules of *n*-pentane in the asymmetric unit. All non-hydrogen atoms other than the *n*-pentane carbons were refined anisotropically. All hydrogens were included in fixed positions. Additionally, one phenyl ring [C(27) – C(32)] was disordered and modeled as a rigid group in two separate orientations, with relative populations of 0.72 and 0.28 for the major and minor orientations, respectively. **2.2** crystallizes in space group $P2_12_12_1$ with two molecules of acetonitrile in the asymmetric unit. All non-hydrogen atoms were refined anisotropically. The lone hydroxyl hydrogen was refined isotropically, while all others were included in

fixed positions. The enantiomer reported here was chosen based on a refinement of the Flack parameter and by the results of a parallel refinement of both enantiomers.

X-ray crystallographic analyses of [Re(Hhypy)(hypy)(PO)(HPO)][Cl] (3.1). Data for **3.1** were collected on a Rigaku/ADSC CCD diffractometer at UBC at -100(1)°C. All data were processed and corrected for Lorentz and polarization effects, and absorption (semi-empirical, based on symmetry analysis of redundant data). The structure of **3.1** was solved using heavy-atom Patterson methods[1] and was expanded using Fourier techniques.[3] Final refinements for **3.1** were carried out using SHELXL-97[4] and selected crystallographic data for the complex appears in Table A1. Complete lists of bond lengths and bond angles appear in Tables A6 and A7.

Final unit cell parameters for **3.1** were obtained by least-squares on the setting angles for 18480 reflections with $2\theta = 6.2 - 55.8°$. **3.1** crystallizes in space group $P\bar{1}$, with two chloride counterions in the asymmetric unit. All non-hydrogen atoms were refined anisotropically, while all hydrogens were included in fixed positions with the exception of H95, which was included in the refinement.. While it was evident that the large void spaces in the lattice allowed for the inclusion of disordered CH_3OH solvent, the solvent molecules were indeed extremely disordered and impossible to model properly. As a consequence, PLATON[5] was used to correct the data. The corrected data set improved the R1 value from 0.052 to 0.042.

X-ray crystallographic analysis of [ReCl(Hhypy)(hypy)(PO)] (3.2). Data for **3.2** were collected on a Nonius CAD4 diffractometer at Rutgers with graphite monochromatized Cu Kα radiation (λ = 1.5418 Å) at –120°C. The three check reflections measured every hour showed less than 1 % intensity variation. The data were

corrected for Lorentz effects and polarization, and absorption, the latter by a numerical SHELX-76[6] method. The structures were solved by direct methods using SHELXS-86.[7] All atoms were refined using SHELXL-97[4] based upon F_{obs}^2. The Uiso parameters of H4, H8, H16 and H18 were fixed to 1.2 times the equivalent isotropic U of N4, C8, C16 and C18, respectively. Scattering factors (f_o, f', f'') are as described in SHELXL-97.[4] Complete lists of bond lengths and bond angles appear in Tables A8 and A9.

X-ray crystallographic analysis of $[Ga(H_3ppba)_2][(NO_3)_2Cl]\cdot 3CH_3OH$ (4.1). Data were collected on a Rigaku/ADSC CCD diffractometer at UBC at -100(1)°C. The structure was solved by direct methods[8] and was expanded using Fourier techniques.[3] All hydrogen atoms other than those involved in hydrogen-bonding were included in calculated positions but were not refined. The unit cell contains several void spaces where solvents and counterions reside. While there are areas with significant electron density, no satisfactory models for Cl^-, NO_3^- or CH_3OH were possible. As a result, the data were corrected for the electron density in these void spaces using PLATON.[5] The corrected data greatly improved the residuals (R1 = 0.12 to 0.048). No inferences should be made as to the nature of the counterions or the amount of solvent molecules in the asymmetric unit. Readers should refer to elemental analysis results for the elucidation of the exact chemical composition of this material. Complete lists of bond lengths and bond angles appear in Tables A10 and A11.

X-ray crystallographic analysis of $[Gd(H_4ppba)_2][(NO_3)_4Cl]\cdot 3CH_3OH$ (4.2). Data were collected on a Rigaku/ADSC CCD diffractometer at UBC at -100(1)°C. The structure was solved by direct methods[8]and was expanded using Fourier techniques.[3] The material resides on a 3-fold inversion axis, with the Gd atom having a population of

1/6. Both N(1) and N(2) appear to be protonated, with the protons found and refined from a difference map. The anions appear to be a disordered mixture of Cl^- and NO_3^-. Restraints were used to fix the geometries of the two disordered NO_3^- fragments, and relative populations of 0.5 and 0.166667 were given to the major and minor fragments, respectively. A population of 0.166667 was also given to Cl(1). Unresolvable disordered solvent molecules reside in the large voids between the cationic Gd-complexes in the unit cell. The data were therefore corrected using PLATON/SQUEEZE.[5] R1 was found to drop from 0.079 to 0.034. Complete lists of bond lengths and bond angles appear in Tables A12 and A13.

References

1) Beurskens, P. T.; Admiraal, G.; Beurskens, W. P.; Garcia-Granda, S.; Gould, R. O.; Smits, J. M. M.; Smykalla, C. *The DIRDIF program system*; Technical Report of the Crystallography Laboratory: University of Nijmegen, The Netherlands, 1992.

2) Altomare, A.; Burla, M. C.; Cammalli, G.; Cascarano, M.; Giacovazzo, C.; Guagliardi, A.; Moliterni, A. G. G.; Polidori, G.; Spagna, A. *J. Appl. Cryst.* **1999**, *32*, 115.

3) Beurskens, P. T.; Admiraal, G.; Beurskens, G.; Bosman, W. P.; de Gelder, R.; Israel, R.; Smits, J. M. M. *The DIRDIF-94 program system*; Technical Report of the Crystallography Laboratory: University of Nijmegen, The Netherlands, 1994.

4) Sheldrick, G. M. *SHELXL-97, Program for Crystal Structure Refinement*; University of Göttingen: Germany, 1997.

5) Spek, A. L. *Acta Crystallogr.* **1990**, *A46*, 34.

6) Sheldrik, G. M. *SHELX76, Program for Crystal Structure Determination*; University of Cambridge: England, 1976.

7) Sheldrik, G. M. *SHELXS86, Program for the Solution of Crystal Structures*; University of Göttingen: Germany, 1986.

8) Altomare, A.; Cascarano, M.; Giacovazzo, C.; Guagliardi, A. *J. Appl. Cryst.* **1994**, *26*, 343.

Table A1. Selected Crystallographic Data for All Metal Complexes.

	2.1	**2.2**	**3.1**	**3.2**	**4.1**	**4.2**
chemical formula	$C_{48}H_{56}ClO_3P_2Re$	$C_{44}H_{41}N_2O_5P_2Re$	$C_{46}H_{41}ClN_6O_2P_2Re$	$C_{28}H_{23}ClN_6OPRe$	$C_{96}H_{114}GaN_8O_{12}P_6$	$C_{96}H_{118}ClGdN_{12}O_{24}P_6$
formula weight	964.58	925.97	993.48	712.14	1827.57	2202.60
crystal syst.	monoclinic	orthorhombic	triclinic	orthorhombic	monoclinic	trigonal
space group	*C*2/*c*	$P2_12_12_1$	$P\bar{1}$	$P2_12_12_1$	*C*1/*c*	*R*3
a (Å)	29.371(1)	9.5519(3)	14.9440(8)	12.294(2)	25.7563(7)	14.9142(4)
b (Å)	16.9227(5)	18.9971(6)	16.1173(7)	14.500(4)	23.9807(5)	
c (Å)	17.6075(9)	21.824(1)	19.003(1)	14.999(5)	17.5901(8)	44.202(2)
α(°)	90.0	90.0	81.996(2)	90.0	90.0	
β(°)	105.453(2)	90.0	77.802(2)	90.0	95.576(2)	
γ(°)	90.0	90.0	78.955(2)	90.0	90.0	
V (Å^3)	8435.3(5)	3960.2(2)	2118.4(1)	2673.8(12)	10813.2(5)	8514.8(4)
Z	8	4	4	4	4	3
density (g cm^{-3})	1.519	1.553	1.511	1.769	1.123	1.289
wavelength (Å)	0.71069	0.71069	0.71069	1.54184	0.71069	0.71069
abs. coeff. (mm^{-1})	0.3063	0.3198	0.2962	1.0651	0.399	0.764
trans. factor range	0.7656 – 1.0000	0.7617 – 1.0000	0.6273 – 1.0000	0.4055 – 0.7796	0.7770-1.0000	0.7849-1.000
temp (K)	173(1)	173(1)	173(1)	153(5)	173(1)	173(1)
R1(F_o)[a]	0.038	0.032	0.042	0.0260	0.048	0.034
wR2(F_o^2)[a]	0.111	0.078	0.106	0.0676	0.125	0.093
S[b]	0.97	0.618	1.13	1.009	1.00	1.008

[a] $R1 = \Sigma\big|\,|F_o| - |F_c|\,\big| / \Sigma|F_o|$, $I \geq 2\sigma I$; $wR2 = \{\Sigma[w(F_o^2 - F_c^2)^2]/\Sigma[w(F_o^2)^2]\}^{1/2}$, all data

[b] $S = \{\Sigma[w(F_o^2 - F_c^2)^2] / (n - p)\}^{1/2}$

Table A2. Bond Lengths (Å) for [ReOCl(MePO)$_2$] (**2.1**).

Re1	-Cl1	2.264(4)	C14	-C15	1.380(9)
Re1	-P1	2.4457(15)	C14	-C19	1.384(8)
Re1	-P2	2.4206(17)	C15	-C16	1.391(10)
Re1	-O1	2.013(4)	C16	-C17	1.377(10)
Re1	-O2	2.044(3)	C17	-C18	1.385(10)
Re1	-O3	1.680(4)	C18	-C19	1.380(9)
P1	-C1	1.797(6)	C20	-C21	1.401(8)
P1	-C8	1.816(5)	C20	-C25	1.408(9)
P1	-C14	1.821(7)	C21	-C22	1.406(9)
P2	-C20	1.781(6)	C22	-C23	1.367(9)
P2	-C27A	1.842(7)	C23	-C24	1.394(10)
P2	-C33	1.817(6)	C24	-C25	1.376(10)
P2	-C27B	1.783(19)	C24	-C26	1.520(11)
O1	-C2	1.364(8)	C27A	-C28A	1.389(11)
O2	-C21	1.334(7)	C27A	-C32A	1.390(12)
C1	-C2	1.394(7)	C27B	-C28B	1.39(3)
C1	-C6	1.389(9)	C27B	-C32B	1.39(3)
C2	-C3	1.392(10)	C28A	-C29A	1.390(11)
C3	-C4	1.376(13)	C28B	-C29B	1.39(3)
C4	-C5	1.397(10)	C29A	-C30A	1.392(13)
C5	-C6	1.404(10)	C29B	-C30B	1.39(3)
C5	-C7	1.502(13)	C30A	-C31A	1.389(14)
C8	-C9	1.390(9)	C30B	-C31B	1.39(4)
C8	-C13	1.404(8)	C31A	-C32A	1.390(11)
C9	-C10	1.393(10)	C31B	-C32B	1.39(3)
C10	-C11	1.370(11)	C33	-C38	1.414(8)
C11	-C12	1.404(10)	C33	-C34	1.373(9)
C12	-C13	1.379(8)	C34	-C35	1.388(9)

Table A3. Bond Angles (deg) for [ReOCl(MePO)$_2$] (**2.1**).

Cl1	-Re1	-P1	162.66(10)	C27A	-P2	-C33	105.7(3)
Cl1	-Re1	-P2	94.44(12)	C27B	-P2	-C33	99.8(8)
Cl1	-Re1	-O1	81.89(15)	Re1	-O1	-C2	121.7(3)
Cl1	-Re1	-O2	91.57(14)	Re1	-O2	-C21	126.3(4)
Cl1	-Re1	-O3	98.23(16)	P1	-C1	-C2	115.3(4)
P1	-Re1	-P2	100.69(5)	P1	-C1	-C6	124.6(4)
P1	-Re1	-O1	81.00(12)	C2	-C1	-C6	120.1(5)
P1	-Re1	-O2	83.41(12)	O1	-C2	-C1	121.6(5)
P1	-Re1	-O3	91.00(14)	O1	-C2	-C3	119.2(5)
P2	-Re1	-O1	160.08(10)	C1	-C2	-C3	119.2(6)
P2	-Re1	-O2	77.96(12)	C2	-C3	-C4	119.9(6)
P2	-Re1	-O3	87.18(14)	C3	-C4	-C5	122.7(7)
O1	-Re1	-O2	82.57(15)	C4	-C5	-C6	116.6(8)
O1	-Re1	-O3	112.70(16)	C4	-C5	-C7	121.6(8)
O2	-Re1	-O3	162.80(15)	C6	-C5	-C7	121.8(7)
Re1	-P1	-C1	97.33(19)	C1	-C6	-C5	121.6(6)
Re1	-P1	-C8	111.92(19)	P1	-C8	-C9	121.8(4)
Re1	-P1	-C14	126.4(2)	P1	-C8	-C13	118.9(4)
C1	-P1	-C8	107.5(3)	C9	-C8	-C13	119.2(5)
C1	-P1	-C14	106.1(3)	C8	-C9	-C10	119.8(6)
C8	-P1	-C14	105.8(2)	C9	-C10	-C11	120.9(7)
Re1	-P2	-C20	101.9(2)	C10	-C11	-C12	119.9(6)
Re1	-P2	-C27A	114.6(3)	C11	-C12	-C13	119.6(6)
Re1	-P2	-C33	115.6(2)	C8	-C13	-C12	120.6(5)
Re1	-P2	-C27B	122.8(8)	P1	-C14	-C15	122.4(5)
C20	-P2	-C27A	110.6(3)	P1	-C14	-C19	117.9(4)
C20	-P2	-C33	108.2(3)	C15	-C14	-C19	119.6(6)
C20	-P2	-C27B	107.8(8)	C14	-C15	-C16	120.3(6)
C15	-C16	-C17	120.1(6)	C30A	-C31A	-C32A	120.1(8)
C16	-C17	-C18	119.3(6)	C30B	-C31B	-C32B	120(2)
C17	-C18	-C19	120.8(6)	C27A	-C32A	-C31A	119.9(8)
C14	-C19	-C18	119.8(5)	C27B	-C32B	-C31B	120(2)
P2	-C20	-C21	113.1(5)	P2	-C33	-C38	117.7(5)
P2	-C20	-C25	127.4(5)	C34	-C33	-C38	119.4(5)
C21	-C20	-C25	119.5(5)	P2	-C33	-C34	122.8(4)
O2	-C21	-C20	120.6(5)	C33	-C34	-C35	120.2(6)
O2	-C21	-C22	120.7(5)	C34	-C35	-C36	120.3(7)
C20	-C21	-C22	118.7(6)	C35	-C36	-C37	119.6(7)
C21	-C22	-C23	120.1(6)	C36	-C37	-C38	120.9(7)
C22	-C23	-C24	122.3(6)	C33	-C38	-C37	119.5(6)
C23	-C24	-C25	117.9(6)	C2	-C3	-H3	120.14
C23	-C24	-C26	120.7(6)	C4	-C3	-H3	119.96
C25	-C24	-C26	121.4(7)	C3	-C4	-H4	118.69
C20	-C25	-C24	121.5(6)	C5	-C4	-H4	118.65
P2	-C27A	-C28A	118.6(5)	C1	-C6	-H6	119.03
P2	-C27A	-C32A	121.1(6)	C5	-C6	-H6	119.37
C28A	-C27A	-C32A	120.1(7)	C5	-C7	-H7A	109.45
C28B	-C27B	-C32B	120.1(19)	C5	-C7	-H7B	109.46
P2	-C27B	-C32B	124.5(18)	C5	-C7	-H7C	109.46
P2	-C27B	-C28B	115.4(17)	H7A	-C7	-H7B	109.39
C27A	-C28A	-C29A	120.0(7)	H7A	-C7	-H7C	109.55
C27B	-C28B	-C29B	120(2)	H7B	-C7	-H7C	109.51
C28A	-C29A	-C30A	120.0(8)	C8	-C9	-H9	120.19
C28B	-C29B	-C30B	120(2)	C10	-C9	-H9	119.99
C29A	-C30A	-C31A	119.9(7)	C9	-C10	-H10	119.68
C29B	-C30B	-C31B	120(2)	C11	-C10	-H10	119.47

Table A3. (cont.)

C10	-C11	-H11	119.97	C27A	-C28A	-H28A	120.01
C12	-C11	-H11	120.10	C29A	-C28A	-H28A	120.00
C11	-C12	-H12	120.27	C27B	-C28B	-H28B	120.08
C13	-C12	-H12	120.18	C29B	-C28B	-H28B	120.02
C8	-C13	-H13	119.68	C28A	-C29A	-H29A	120.07
C12	-C13	-H13	119.76	C30A	-C29A	-H29A	119.96
C14	-C15	-H15	119.91	C28B	-C29B	-H29B	119.89
C16	-C15	-H15	119.76	C30B	-C29B	-H29B	120.10
C15	-C16	-H16	120.03	C29A	-C30A	-H30A	119.94
C17	-C16	-H16	119.90	C31A	-C30A	-H30A	120.13
C16	-C17	-H17	120.33	C29B	-C30B	-H30B	120.01
C18	-C17	-H17	120.36	C31B	-C30B	-H30B	120.00
C17	-C18	-H18	119.65	C30A	-C31A	-H31A	119.89
C19	-C18	-H18	119.54	C32A	-C31A	-H31A	120.00
C14	-C19	-H19	120.07	C30B	-C31B	-H31B	119.98
C18	-C19	-H19	120.08	C32B	-C31B	-H31B	119.99
C21	-C22	-H22	119.91	C27A	-C32A	-H32A	120.05
C23	-C22	-H22	119.98	C31A	-C32A	-H32A	120.07
C22	-C23	-H23	118.99	C31B	-C32B	-H32B	120.10
C24	-C23	-H23	118.71	C27B	-C32B	-H32B	119.97
C20	-C25	-H25	119.21	C35	-C34	-H34	119.94
C24	-C25	-H25	119.29	C33	-C34	-H34	119.85
C24	-C26	-H26A	109.43	C36	-C35	-H35	119.93
C24	-C26	-H26B	109.41	C34	-C35	-H35	119.75
C24	-C26	-H26C	109.38	C35	-C36	-H36	120.18
H26A	-C26	-H26B	109.54	C37	-C36	-H36	120.19
H26A	-C26	-H26C	109.51	C36	-C37	-H37	119.48
H26B	-C26	-H26C	109.55	C38	-C37	-H37	119.58
C33	-C38	-H38	120.18	C42	-C43	-H43C	109.78
C37	-C38	-H38	120.35	H43A	-C43	-H43B	109.21
C39	-C40	-C41	126(4)	H43A	-C43	-H43C	109.02
C40	-C41	-C42	100(4)	H43B	-C43	-H43C	109.46
C41	-C42	-C43	91(4)	C45	-C46	-C47	134(3)
C40	-C39	-H39A	109.48	C46	-C47	-C48	156(3)
C40	-C39	-H39B	109.34	C46	-C45	-H45A	105.54
C40	-C39	-H39C	109.71	C46	-C45	-H45B	105.42
H39A	-C39	-H39B	109.33	H45A	-C45	-H45B	106.03
H39A	-C39	-H39C	109.49	C45	-C46	-H46A	103.75
H39B	-C39	-H39C	109.47	C45	-C46	-H46B	103.70
C39	-C40	-H40A	106.35	C47	-C46	-H46A	103.42
C39	-C40	-H40B	105.85	C47	-C46	-H46B	103.62
C41	-C40	-H40A	106.12	H46A	-C46	-H46B	105.22
C41	-C40	-H40B	105.26	C46	-C47	-H47A	97.68
H40A	-C40	-H40B	106.08	C46	-C47	-H47B	97.95
C40	-C41	-H41A	111.14	C48	-C47	-H47A	96.61
C40	-C41	-H41B	111.51	C48	-C47	-H47B	96.86
C42	-C41	-H41A	112.21	H47A	-C47	-H47B	103.29
C42	-C41	-H41B	112.55	C47	-C48	-H48A	109.38
H41A	-C41	-H41B	109.38	C47	-C48	-H48B	108.92
C41	-C42	-H42A	113.15	C47	-C48	-H48C	109.30
C41	-C42	-H42B	113.40	H48A	-C48	-H48B	109.49
C43	-C42	-H42A	113.58	H48A	-C48	-H48C	109.85
C43	-C42	-H42B	113.57	H48B	-C48	-H48C	109.88
H42A	-C42	-H42B	111.03	H44A	-C44	-H44B	109.26
C42	-C43	-H43A	109.48	H44A	-C44	-H44C	109.81
C42	-C43	-H43B	109.88	H44B	-C44	-H44C	109.54

Table A4. Bond Lengths (Å) for [$ReO(Me_2PO_2)(H(Me_2PO_2))$] (**2.2**).

Re1	-P1	2.4103(15)	C9	-C10	1.403(9)
Re1	-P2	2.4576(15)	C10	-C11	1.390(9)
Re1	-O1	2.036(4)	C11	-C14	1.509(10)
Re1	-O2	2.019(4)	C11	-C12	1.393(9)
Re1	-O3	2.003(4)	C12	-C13	1.378(9)
Re1	-O5	1.665(4)	C15	-C16	1.393(9)
P1	-C2	1.787(6)	C15	-C20	1.398(8)
P1	-C9	1.803(7)	C16	-C17	1.395(10)
P1	-C15	1.805(6)	C17	-C18	1.371(11)
P2	-C22	1.795(6)	C18	-C19	1.402(10)
P2	-C29	1.823(7)	C19	-C20	1.382(8)
P2	-C35	1.821(7)	C21	-C26	1.409(8)
O1	-C1	1.347(6)	C21	-C22	1.403(9)
O2	-C8	1.354(7)	C22	-C23	1.396(9)
O3	-C21	1.351(7)	C23	-C24	1.397(8)
O4	-C28	1.377(7)	C24	-C25	1.396(9)
O4	-H35	1.17(13)	C24	-C27	1.501(10)
N1	-C41	1.139(13)	C25	-C26	1.380(9)
N2	-C43	1.135(13)	C28	-C33	1.394(8)
C1	-C6	1.407(8)	C28	-C29	1.384(8)
C1	-C2	1.392(8)	C29	-C30	1.403(8)
C2	-C3	1.392(8)	C30	-C31	1.408(9)
C3	-C4	1.403(8)	C31	-C34	1.509(12)
C4	-C5	1.413(9)	C31	-C32	1.390(10)
C4	-C7	1.497(9)	C32	-C33	1.367(10)
C5	-C6	1.373(9)	C35	-C40	1.403(9)
C8	-C13	1.399(9)	C35	-C36	1.378(9)
C8	-C9	1.388(8)	C36	-C37	1.385(9)
C37	-C38	1.399(9)	C27	-H27C	0.9591
C38	-C39	1.382(9)	C27	-H27B	0.9601
C39	-C40	1.383(9)	C27	-H27A	0.9602
C3	-H3	0.9286	C30	-H30	0.9297
C5	-H5	0.9297	C32	-H32	0.9305
C6	-H6	0.9305	C33	-H33	0.9309
C7	-H7B	0.9609	C34	-H34C	0.9600
C7	-H7A	0.9600	C34	-H34A	0.9597
C7	-H7C	0.9604	C34	-H34B	0.9598
C10	-H10	0.9298	C36	-H36	0.9303
C12	-H12	0.9294	C37	-H37	0.9301
C13	-H13	0.9308	C38	-H38	0.9293
C14	-H14B	0.9610	C39	-H39	0.9296
C14	-H14C	0.9603	C40	-H40	0.9306
C14	-H14A	0.9603	C41	-C42	1.449(14)
C16	-H16	0.9304	C42	-H42B	0.9597
C17	-H17	0.9317	C42	-H42C	0.9591
C18	-H18	0.9300	C42	-H42A	0.9594
C19	-H19	0.9300	C43	-C44	1.416(13)
C20	-H20	0.9294	C44	-H44A	0.9607
C23	-H23	0.9315	C44	-H44B	0.9603
C25	-H25	0.9287	C44	-H44C	0.9611
C26	-H26	0.9299			

Table A5. Bond Angles (deg) for [ReO(Me_2PO_2)(H(Me_2PO_2))] (**2.2**).

P1	-Re1	-P2	108.22(5)	Re1	-O2	-C8	121.6(4)
P1	-Re1	-O1	75.00(11)	Re1	-O3	-C21	122.1(4)
P1	-Re1	-O2	82.41(11)	C28	-O4	-H35	113(5)
P1	-Re1	-O3	154.95(12)	O1	-C1	-C2	119.2(5)
P1	-Re1	-O5	92.99(14)	C2	-C1	-C6	119.3(5)
P2	-Re1	-O1	79.70(12)	O1	-C1	-C6	121.5(5)
P2	-Re1	-O2	160.89(11)	P1	-C2	-C3	128.2(4)
P2	-Re1	-O3	82.29(12)	C1	-C2	-C3	121.1(5)
P2	-Re1	-O5	93.96(15)	P1	-C2	-C1	110.6(4)
O1	-Re1	-O2	88.17(15)	C2	-C3	-C4	120.4(5)
O1	-Re1	-O3	85.01(15)	C3	-C4	-C5	117.4(5)
O1	-Re1	-O5	163.63(17)	C5	-C4	-C7	120.9(5)
O2	-Re1	-O3	82.00(16)	C3	-C4	-C7	121.8(5)
O2	-Re1	-O5	101.44(18)	C4	-C5	-C6	122.6(6)
O3	-Re1	-O5	109.25(17)	C1	-C6	-C5	119.2(5)
Re1	-P1	-C2	102.9(2)	O2	-C8	-C13	119.1(5)
Re1	-P1	-C9	97.93(19)	C9	-C8	-C13	118.5(6)
Re1	-P1	-C15	128.3(2)	O2	-C8	-C9	122.5(6)
C2	-P1	-C9	107.2(3)	P1	-C9	-C10	124.5(4)
C2	-P1	-C15	110.7(3)	C8	-C9	-C10	119.9(6)
C9	-P1	-C15	107.8(3)	P1	-C9	-C8	115.6(5)
Re1	-P2	-C22	96.9(2)	C9	-C10	-C11	121.6(5)
Re1	-P2	-C29	119.4(2)	C10	-C11	-C14	121.3(6)
Re1	-P2	-C35	122.7(2)	C12	-C11	-C14	121.2(6)
C22	-P2	-C29	105.2(3)	C10	-C11	-C12	117.5(6)
C22	-P2	-C35	104.3(3)	C11	-C12	-C13	121.5(6)
C29	-P2	-C35	105.3(3)	C8	-C13	-C12	120.9(6)
Re1	-O1	-C1	126.8(3)	P1	-C15	-C16	119.2(5)
P1	-C15	-C20	121.3(5)	C30	-C31	-C32	117.3(6)
C16	-C15	-C20	119.4(6)	C31	-C32	-C33	122.7(6)
C15	-C16	-C17	119.8(6)	C28	-C33	-C32	119.4(6)
C16	-C17	-C18	120.6(6)	P2	-C35	-C36	120.2(5)
C17	-C18	-C19	120.0(7)	C36	-C35	-C40	118.6(6)
C18	-C19	-C20	119.8(6)	P2	-C35	-C40	121.1(5)
C15	-C20	-C19	120.3(6)	C35	-C36	-C37	121.5(6)
O3	-C21	-C22	122.6(5)	C36	-C37	-C38	119.5(6)
C22	-C21	-C26	119.3(6)	C37	-C38	-C39	119.5(6)
O3	-C21	-C26	118.1(6)	C38	-C39	-C40	120.5(6)
P2	-C22	-C23	124.5(5)	C35	-C40	-C39	120.4(6)
C21	-C22	-C23	119.6(5)	C2	-C3	-H3	119.80
P2	-C22	-C21	115.9(4)	C4	-C3	-H3	119.82
C22	-C23	-C24	121.8(6)	C4	-C5	-H5	118.67
C23	-C24	-C27	121.0(6)	C6	-C5	-H5	118.68
C25	-C24	-C27	121.7(6)	C1	-C6	-H6	120.40
C23	-C24	-C25	117.3(6)	C5	-C6	-H6	120.42
C24	-C25	-C26	122.5(5)	C4	-C7	-H7A	109.50
C21	-C26	-C25	119.5(6)	C4	-C7	-H7B	109.41
O4	-C28	-C29	117.8(5)	C4	-C7	-H7C	109.48
O4	-C28	-C33	121.9(6)	H7A	-C7	-H7B	109.42
C29	-C28	-C33	120.3(6)	H7A	-C7	-H7C	109.56
P2	-C29	-C28	120.0(5)	H7B	-C7	-H7C	109.46
P2	-C29	-C30	120.5(5)	C9	-C10	-H10	119.29
C28	-C29	-C30	119.5(6)	C11	-C10	-H10	119.06
C29	-C30	-C31	120.7(6)	C11	-C12	-H12	119.24
C30	-C31	-C34	120.1(6)	C13	-C12	-H12	119.26

Table A5. (cont.)

C32	-C31	-C34	122.5(6)	C8	-C13	-H13	119.55
C12	-C13	-H13	119.54	H27B	-C27	-H27C	109.53
C11	-C14	-H14A	109.53	C29	-C30	-H30	119.66
C11	-C14	-H14B	109.46	C31	-C30	-H30	119.61
C11	-C14	-H14C	109.51	C31	-C32	-H32	118.74
H14A	-C14	-H14B	109.48	C33	-C32	-H32	118.52
H14A	-C14	-H14C	109.49	C28	-C33	-H33	120.28
H14B	-C14	-H14C	109.36	C32	-C33	-H33	120.32
C15	-C16	-H16	120.13	C31	-C34	-H34A	109.42
C17	-C16	-H16	120.04	C31	-C34	-H34B	109.4
C16	-C17	-H17	119.78	C31	-C34	-H34C	109.43
C18	-C17	-H17	119.64	H34A	-C34	-H34B	109.55
C17	-C18	-H18	120.05	H34A	-C34	-H34C	109.46
C19	-C18	-H18	119.99	H34B	-C34	-H34C	109.50
C18	-C19	-H19	120.13	C35	-C36	-H36	119.30
C20	-C19	-H19	120.07	C37	-C36	-H36	119.22
C15	-C20	-H20	119.88	C36	-C37	-H37	120.32
C19	-C20	-H20	119.78	C38	-C37	-H37	120.13
C22	-C23	-H23	119.09	C37	-C38	-H38	120.21
C24	-C23	-H23	119.09	C39	-C38	-H38	120.32
C24	-C25	-H25	118.76	C38	-C39	-H39	119.72
C26	-C25	-H25	118.70	C40	-C39	-H39	119.74
C21	-C26	-H26	120.30	C35	-C40	-H40	119.77
C25	-C26	-H26	120.25	C39	-C40	-H40	119.84
C24	-C27	-H27A	109.49	N1	-C41	-C42	177.2(10)
C24	-C27	-H27B	109.49	C41	-C42	-H42A	109.46
C24	-C27	-H27C	109.40	C41	-C42	-H42B	109.40
H27A	-C27	-H27B	109.48	C41	-C42	-H42C	109.48
H27A	-C27	-H27C	109.44	H42A	-C42	-H42B	109.47
H42A	-C42	-H42C	109.56	C43	-C44	-H44C	109.53
H42B	-C42	-H42C	109.46	H44A	-C44	-H44B	109.45
N2	-C43	-C44	179.7(10)	H44A	-C44	-H44C	109.37
C43	-C44	-H44A	109.52	H44B	-C44	-H44C	109.38
C43	-C44	-H44B	109.57				

Table A6. Bond Lengths (Å) for [Re(Hhypy)(hypy)(PO)(HPO)]Cl (**3.1**).

Re1	-P1	2.4137(14)	O3	-C47	1.349(7)
Re1	-P2	2.4666(14)	O4	-C76	1.326(8)
Re1	-O1	2.032(3)	O4	-H94	0.8401
Re1	-N1	1.980(4)	N1	-N2	1.299(7)
Re1	-N3	2.158(5)	N2	-C19	1.357(8)
Re1	-N4	1.780(5)	N3	-C23	1.357(7)
Re1	-H95	2.28(7)	N3	-C19	1.368(7)
Re2	-N7	1.982(4)	N4	-N5	1.240(7)
Re2	-N9	2.149(5)	N5	-C24	1.407(7)
Re2	-N10	1.793(5)	N6	-C24	1.347(9)
Re2	-O3	2.027(3)	N6	-C28	1.343(9)
Re2	-P3	2.4101(14)	N1	-H95	1.32(8)
Re2	-P4	2.4544(14)	N7	-N8	1.302(7)
P1	-C7	1.826(6)	N8	-C65	1.375(7)
P1	-C13	1.813(5)	N9	-C65	1.381(7)
P1	-C6	1.792(6)	N9	-C69	1.346(7)
P2	-C35	1.822(5)	N10	-N11	1.228(7)
P2	-C29	1.824(6)	N11	-C70	1.406(7)
P2	-C41	1.832(6)	N12	-C74	1.335(7)
P3	-C59	1.817(5)	N12	-C70	1.350(7)
P3	-C52	1.792(6)	N7	-H96	0.8789
P3	-C53	1.813(6)	C1	-C6	1.396(9)
P4	-C87	1.830(5)	C1	-C2	1.409(8)
P4	-C81	1.817(6)	C2	-C3	1.372(10)
P4	-C75	1.819(6)	C3	-C4	1.383(11)
O1	-C1	1.362(7)	C4	-C5	1.375(8
O2	-C30	1.347(8)	C5	-C6	1.412(9)
O2	-H93	0.8392	C7	-C12	1.386(8)
C7	-C8	1.385(8)	C37	-C38	1.366(10)
C8	-C9	1.405(9)	C38	-C39	1.379(9)
C9	-C10	1.376(10)	C39	-C40	1.383(9)
C10	-C11	1.370(10)	C41	-C42	1.393(10)
C11	-C12	1.391(9)	C41	-C46	1.398(9)
C13	-C14	1.399(8)	C42	-C43	1.376(9)
C13	-C18	1.391(8)	C43	-C44	1.358(10)
C14	-C15	1.387(9)	C44	-C45	1.404(10)
C15	-C16	1.382(9)	C45	-C46	1.384(9)
C16	-C17	1.359(10)	C2	-H2	0.9506
C17	-C18	1.381(9)	C3	-H3	0.9485
C19	-C20	1.400(9)	C4	-H4	0.9506
C20	-C21	1.368(10)	C5	-H5	0.9499
C21	-C22	1.394(10)	C8	-H8	0.9487
C22	-C23	1.377(9)	C9	-H9	0.9502
C24	-C25	1.371(10)	C10	-H10	0.9489
C25	-C26	1.386(11)	C11	-H11	0.9503
C26	-C27	1.386(12)	C12	-H12	0.9497
C27	-C28	1.377(14)	C14	-H14	0.9500
C29	-C30	1.431(8)	C15	-H15	0.9505
C29	-C34	1.383(9)	C16	-H16	0.9487
C30	-C31	1.378(8)	C17	-H17	0.9503
C31	-C32	1.387(10)	C18	-H18	0.9507
C32	-C33	1.384(9)	C20	-H20	0.9501
C33	-C34	1.376(8)	C21	-H21	0.9511
C35	-C36	1.390(8)	C22	-H22	0.9492
C35	-C40	1.398(8)	C23	-H23	0.9491

Table A6. (cont.)

C36	-C37	1.395(9)	C25	-H25	0.9500
C26	-H26	0.9496	C57	-C58	1.386(9)
C27	-H27	0.9487	C59	-C60	1.380(8)
C28	-H28	0.9500	C59	-C64	1.389(8)
C31	-H31	0.9506	C60	-C61	1.403(9)
C32	-H32	0.9483	C61	-C62	1.382(9)
C33	-H33	0.9493	C62	-C63	1.385(11)
C34	-H34	0.9485	C63	-C64	1.385(9)
C36	-H36	0.9503	C65	-C66	1.385(9)
C37	-H37	0.9502	C66	-C67	1.372(10)
C38	-H38	0.9497	C67	-C68	1.411(10)
C39	-H39	0.9500	C68	-C69	1.384(9)
C40	-H40	0.9488	C70	-C71	1.388(8)
C42	-H42	0.9496	C71	-C72	1.377(9)
C43	-H43	0.9487	C72	-C73	1.368(10)
C44	-H44	0.9510	C73	-C74	1.405(10)
C45	-H45	0.9497	C75	-C76	1.443(8)
C46	-H46	0.9501	C75	-C80	1.391(9)
C47	-C52	1.413(9)	C76	-C77	1.380(8)
C47	-C48	1.378(8)	C77	-C78	1.377(11)
C48	-C49	1.375(11)	C78	-C79	1.372(10)
C49	-C50	1.393(13)	C79	-C80	1.384(8)
C50	-C51	1.361(10)	C81	-C86	1.387(8)
C51	-C52	1.403(9)	C81	-C82	1.399(9)
C53	-C58	1.390(8)	C82	-C83	1.398(11)
C53	-C54	1.387(8)	C83	-C84	1.362(12)
C54	-C55	1.385(9)	C84	-C85	1.374(10)
C55	-C56	1.369(10)	C85	-C86	1.383(9)
C56	-C57	1.394(9)	C87	-C92	1.380(8)
C87	-C88	1.391(8)	C68	-H68	0.9493
C88	-C89	1.387(9)	C69	-H69	0.9507
C89	-C90	1.366(10)	C71	-H71	0.9494
C90	-C91	1.376(10)	C72	-H72	0.9496
C91	-C92	1.398(9)	C73	-H73	0.9500
C48	-H48	0.9506	C74	-H74	0.9494
C49	-H49	0.9501	C77	-H77	0.9515
C50	-H50	0.9498	C78	-H78	0.9487
C51	-H51	0.9494	C79	-H79	0.9504
C54	-H54	0.9492	C80	-H80	0.9512
C55	-H55	0.9494	C82	-H82	0.9495
C56	-H56	0.9494	C83	-H83	0.9514
C57	-H57	0.9505	C84	-H84	0.9507
C58	-H58	0.9508	C85	-H85	0.9510
C60	-H60	0.9513	C86	-H86	0.9510
C61	-H61	0.9506	C88	-H88	0.9496
C62	-H62	0.9511	C89	-H89	0.9501
C63	-H63	0.9502	C90	-H90	0.9510
C64	-H64	0.9510	C91	-H91	0.9509
C66	-H66	0.9498	C92	-H92	0.9491
C67	-H67	0.9499			

Table A7. Bond Angles (deg) for [Re(Hhypy)(hypy)(PO)(HPO)]Cl (**3.1**).

P1	-Re1	-P2	166.82(4)	O3	-Re2	-N10	108.88(15)
P1	-Re1	-O1	80.98(9)	N7	-Re2	-N9	72.31(17)
P1	-Re1	-N1	94.91(14)	P3	-Re2	-N10	93.90(15)
P1	-Re1	-N3	86.03(13)	P3	-Re2	-O3	80.89(9)
P1	-Re1	-N4	94.83(15)	P3	-Re2	-N7	95.61(14)
P2	-Re1	-O1	86.18(9)	P3	-Re2	-P4	166.85(4)
P2	-Re1	-N1	98.19(14)	N9	-Re2	-N10	163.64(16)
P2	-Re1	-N3	96.52(13)	P3	-Re2	-N9	87.16(13)
P2	-Re1	-N4	86.66(15)	Re1	-P1	-C7	115.73(18)
O1	-Re1	-N1	160.03(16)	Re1	-P1	-C6	99.9(2)
O1	-Re1	-N3	87.92(13)	Re1	-P1	-C13	115.5(2)
O1	-Re1	-N4	109.65(15)	C7	-P1	-C13	106.9(3)
N1	-Re1	-N3	72.26(17)	C6	-P1	-C7	109.9(3)
N1	-Re1	-N4	90.11(18)	C6	-P1	-C13	108.5(3)
N3	-Re1	-N4	162.35(16)	Re1	-P2	-C41	114.0(2)
N4	-Re1	-H95	55(2)	Re1	-P2	-C29	110.2(2)
O1	-Re1	-H95	163(2)	Re1	-P2	-C35	19.69(16)
P1	-Re1	-H95	92(2)	C29	-P2	-C35	08.6(3)
P2	-Re1	-H95	99(2)	C29	-P2	-C41	01.8(3)
N1	-Re1	-H95	35(2)	C35	-P2	-C41	00.8(3)
N3	-Re1	-H95	107(2)	C53	-P3	-C59	06.4(2)
P4	-Re2	-N7	97.54(14)	C52	-P3	-C59	09.7(3)
P4	-Re2	-O3	86.87(9)	Re2	-P3	-C59	14.40(17)
N7	-Re2	-N10	91.34(18)	C52	-P3	-C53	10.8(3)
P4	-Re2	-N9	97.10(13)	Re2	-P3	-C52	9.9(2)
P4	-Re2	-N10	85.52(15)	Re2	-P3	-C53	15.58(18)
O3	-Re2	-N7	159.61(16)	Re2	-P4	-C81	20.7(2)
O3	-Re2	-N9	87.42(13)	Re2	-P4	-C75	107.1(2)
C75	-P4	-C81	108.9(3)	O1	-C1	-C6	122.5(5)
Re2	-P4	-C87	111.8(2)	C2	-C1	-C6	118.6(6)
C81	-P4	-C87	102.2(3)	O1	-C1	-C2	118.8(5)
C75	-P4	-C87	105.2(3)	C1	-C2	-C3	119.8(6)
Re1	-O1	-C1	122.1(3)	C2	-C3	-C4	121.5(5)
C30	-O2	-H93	109.54	C3	-C4	-C5	120.2(6)
Re2	-O3	-C47	123.3(3)	C4	-C5	-C6	119.3(7)
C76	-O4	-H94	109.44	C1	-C6	-C5	120.6(5)
Re1	-N1	-N2	126.3(4)	P1	-C6	-C5	125.1(5)
N1	-N2	-C19	110.7(5)	P1	-C6	-C1	114.1(4)
C19	-N3	-C23	118.5(5)	P1	-C7	-C8	122.3(4)
Re1	-N3	-C19	113.0(4)	C8	-C7	-C12	119.7(5)
Re1	-N3	-C23	128.2(4)	P1	-C7	-C12	118.0(4)
Re1	-N4	-N5	177.0(3)	C7	-C8	-C9	119.2(5)
N4	-N5	-C24	118.5(5)	C8	-C9	-C10	120.6(6)
C24	-N6	-C28	116.5(7)	C9	-C10	-C11	119.9(6)
Re1	-N1	-H95	85(3)	C10	-C11	-C12	120.3(6)
N2	-N1	-H95	146(3)	C7	-C12	-C11	120.3(6)
Re2	-N7	-N8	127.1(3)	P1	-C13	-C18	121.0(5)
N7	-N8	-C65	110.1(4)	P1	-C13	-C14	119.2(4)
C65	-N9	-C69	118.1(5)	C14	-C13	-C18	119.5(5)
Re2	-N9	-C69	127.8(4)	C13	-C14	-C15	120.3(5)
Re2	-N9	-C65	113.7(4)	C14	-C15	-C16	119.3(6)
Re2	-N10	-N11	176.2(4)	C15	-C16	-C17	120.3(6)
N10	-N11	-C70	117.6(4)	C16	-C17	-C18	121.7(6)
C70	-N12	-C74	116.1(5)	C13	-C18	-C17	118.9(6)
Re2	-N7	-H96	116.40	N3	-C19	-C20	121.3(6)

Table A7. (cont.)

N8	-N7	-H96	116.47	N2	-C19	-N3	117.3(5)
N2	-C19	-C20	121.4(6)	C38	-C39	-C40	119.7(6)
C19	-C20	-C21	119.1(6)	C35	-C40	-C39	120.2(6)
C20	-C21	-C22	119.9(6)	C42	-C41	-C46	118.7(6)
C21	-C22	-C23	119.0(6)	P2	-C41	-C42	120.3(5)
N3	-C23	-C22	122.2(6)	P2	-C41	-C46	121.0(5)
N5	-C24	-C25	117.5(6)	C41	-C42	-C43	121.0(7)
N5	-C24	-N6	118.4(5)	C42	-C43	-C44	120.3(7)
N6	-C24	-C25	124.0(6)	C43	-C44	-C45	120.3(6)
C24	-C25	-C26	118.7(7)	C44	-C45	-C46	119.7(6)
C25	-C26	-C27	118.3(8)	C41	-C46	-C45	120.0(6)
C26	-C27	-C28	119.2(7)	C1	-C2	-H2	120.13
N6	-C28	-C27	123.3(8)	C3	-C2	-H2	120.03
P2	-C29	-C34	121.0(4)	C4	-C3	-H3	119.33
P2	-C29	-C30	118.8(5)	C2	-C3	-H3	119.20
C30	-C29	-C34	119.8(5)	C5	-C4	-H4	119.97
C29	-C30	-C31	118.8(6)	C3	-C4	-H4	119.88
O2	-C30	-C31	124.0(5)	C6	-C5	-H5	120.42
O2	-C30	-C29	117.2(5)	C4	-C5	-H5	120.32
C30	-C31	-C32	120.2(5)	C7	-C8	-H8	120.35
C31	-C32	-C33	120.8(5)	C9	-C8	-H8	120.40
C32	-C33	-C34	120.0(6)	C10	-C9	-H9	119.74
C29	-C34	-C33	120.3(5)	C8	-C9	-H9	119.69
C36	-C35	-C40	119.8(5)	C9	-C10	-H10	120.06
P2	-C35	-C36	123.3(4)	C11	-C10	-H10	120.02
P2	-C35	-C40	116.7(4)	C10	-C11	-H11	119.88
C35	-C36	-C37	118.8(5)	C12	-C11	-H11	119.85
C36	-C37	-C38	121.1(6)	C11	-C12	-H12	119.87
C37	-C38	-C39	120.4(6)	C7	-C12	-H12	119.82
C15	-C14	-H14	119.82	C31	-C32	-H32	1119.5
C13	-C14	-H14	119.90	C33	-C32	-H32	119.63
C16	-C15	-H15	120.40	C32	-C33	-H33	119.93
C14	-C15	-H15	120.30	C34	-C33	-H33	120.10
C15	-C16	-H16	119.89	C29	-C34	-H34	119.82
C17	-C16	-H16	119.83	C33	-C34	-H34	119.84
C16	-C17	-H17	119.12	C35	-C36	-H36	120.58
C18	-C17	-H17	119.14	C37	-C36	-H36	120.62
C17	-C18	-H18	120.58	C38	-C37	-H37	119.46
C13	-C18	-H18	120.53	C36	-C37	-H37	119.48
C19	-C20	-H20	120.35	C37	-C38	-H38	119.87
C21	-C20	-H20	120.56	C39	-C38	-H38	119.70
C20	-C21	-H21	120.07	C40	-C39	-H39	120.14
C22	-C21	-H21	120.01	C38	-C39	-H39	120.16
C23	-C22	-H22	120.48	C39	-C40	-H40	119.93
C21	-C22	-H22	120.54	C35	-C40	-H40	119.85
C22	-C23	-H23	118.86	C43	-C42	-H42	119.50
N3	-C23	-H23	118.96	C41	-C42	-H42	119.51
C26	-C25	-H25	120.70	C42	-C43	-H43	119.88
C24	-C25	-H25	120.65	C44	-C43	-H43	119.83
C25	-C26	-H26	120.90	C45	-C44	-H44	119.82
C27	-C26	-H26	120.81	C43	-C44	-H44	119.88
C28	-C27	-H27	120.44	C46	-C45	-H45	120.17
C26	-C27	-H27	120.36	C44	-C45	-H45	120.17
N6	-C28	-H28	118.35	C45	-C46	-H46	120.02
C27	-C28	-H28	118.38	C41	-C46	-H46	119.97

Table A7. (cont.)

C30	-C31	-H31	119.95	O3	-C47	-C48	118.9(6)
C32	-C31	-H31	119.84	O3	-C47	-C52	121.6(5)
C48	-C47	-C52	119.3(6)	C66	-C67	-C68	119.7(6)
C47	-C48	-C49	120.5(7)	C67	-C68	-C69	118.7(6)
C48	-C49	-C50	120.3(7)	N9	-C69	-C68	122.3(5)
C49	-C50	-C51	120.4(8)	N11	-C70	-N12	118.5(5)
C50	-C51	-C52	120.0(7)	N11	-C70	-C71	117.3(5)
C47	-C52	-C51	119.3(5)	N12	-C70	-C71	124.2(5)
P3	-C52	-C51	126.5(5)	C70	-C71	-C72	117.9(6)
P3	-C52	-C47	114.1(4)	C71	-C72	-C73	119.8(6)
P3	-C53	-C54	123.0(4)	C72	-C73	-C74	118.3(6)
P3	-C53	-C58	118.2(4)	N12	-C74	-C73	123.7(5)
C54	-C53	-C58	118.8(5)	P4	-C75	-C76	118.5(5)
C53	-C54	-C55	120.2(6)	P4	-C75	-C80	121.0(4)
C54	-C55	-C56	120.3(6)	C76	-C75	-C80	119.3(5)
C55	-C56	-C57	120.8(6)	O4	-C76	-C75	117.3(5)
C56	-C57	-C58	118.4(5)	O4	-C76	-C77	125.2(6)
C53	-C58	-C57	121.4(5)	C75	-C76	-C77	117.4(6)
P3	-C59	-C60	118.1(4)	C76	-C77	-C78	122.3(6)
P3	-C59	-C64	121.6(4)	C77	-C78	-C79	120.2(6)
C60	-C59	-C64	119.8(5)	C78	-C79	-C80	120.1(7)
C59	-C60	-C61	120.6(6)	C75	-C80	-C79	120.7(6)
C60	-C61	-C62	119.1(6)	P4	-C81	-C82	122.0(5)
C61	-C62	-C63	120.2(6)	C82	-C81	-C86	120.2(6)
C62	-C63	-C64	120.6(6)	P4	-C81	-C86	117.7(5)
C59	-C64	-C63	119.7(5)	C81	-C82	-C83	117.9(7)
N8	-C65	-N9	116.6(5)	C82	-C83	-C84	121.9(8)
N8	-C65	-C66	121.1(5)	C83	-C84	-C85	119.4(7)
N9	-C65	-C66	122.3(6)	C84	-C85	-C86	120.9(7)
C65	-C66	-C67	118.7(6)	C81	-C86	-C85	119.6(6)
P4	-C87	-C88	119.1(4)	C60	-C61	-H61	120.35
P4	-C87	-C92	122.2(4)	C62	-C61	-H61	120.52
C88	-C87	-C92	118.7(5)	C61	-C62	-H62	119.94
C87	-C88	-C89	119.9(6)	C63	-C62	-H62	119.90
C88	-C89	-C90	121.1(6)	C62	-C63	-H63	119.60
C89	-C90	-C91	119.6(6)	C64	-C63	-H63	119.79
C90	-C91	-C92	119.8(6)	C59	-C64	-H64	120.07
C87	-C92	-C91	120.7(6)	C63	-C64	-H64	120.22
C47	-C48	-H48	119.72	C65	-C66	-H66	120.66
C49	-C48	-H48	119.80	C67	-C66	-H66	120.63
C48	-C49	-H49	119.94	C66	-C67	-H67	120.18
C50	-C49	-H49	119.79	C68	-C67	-H67	120.07
C49	-C50	-H50	119.88	C67	-C68	-H68	120.68
C51	-C50	-H50	119.68	C69	-C68	-H68	120.58
C50	-C51	-H51	119.95	N9	-C69	-H69	118.93
C52	-C51	-H51	120.01	C68	-C69	-H69	118.76
C53	-C54	-H54	119.92	C70	-C71	-H71	120.95
C55	-C54	-H54	119.83	C72	-C71	-H71	121.11
C54	-C55	-H55	119.85	C71	-C72	-H72	120.14
C56	-C55	-H55	119.87	C73	-C72	-H72	120.06
C55	-C56	-H56	119.66	C72	-C73	-H73	120.81
C57	-C56	-H56	119.54	C74	-C73	-H73	120.90
C56	-C57	-H57	120.75	N12	-C74	-H74	118.22
C58	-C57	-H57	120.81	C73	-C74	-H74	118.13
C53	-C58	-H58	119.22	C76	-C77	-H77	118.90

Table A7. (cont.)

C57	-C58	-H58	119.41	C78	-C77	-H77	118.83
C59	-C60	-H60	119.66	C77	-C78	-H78	119.92
C61	-C60	-H60	119.75	C79	-C78	-H78	119.92
C78	-C79	-H79	119.84	C81	-C86	-H86	120.19
C80	-C79	-H79	120.01	C85	-C86	-H86	120.18
C75	-C80	-H80	119.65	C87	-C88	-H88	120.06
C79	-C80	-H80	119.68	C89	-C88	-H88	119.99
C81	-C82	-H82	120.97	C88	-C89	-H89	119.36
C83	-C82	-H82	121.13	C90	-C89	-H89	119.52
C82	-C83	-H83	119.00	C89	-C90	-H90	120.18
C84	-C83	-H83	119.08	C91	-C90	-H90	120.20
C83	-C84	-H84	120.25	C90	-C91	-H91	120.11
C85	-C84	-H84	120.36	C92	-C91	-H91	120.04
C84	-C85	-H85	119.58	C87	-C92	-H92	119.68
C86	-C85	-H85	119.51	C91	-C92	-H92	119.61

Table A8. Bond Lengths (Å) for [ReCl(Hhypy)(hypy)(PO)] (**3.2**).

Re1	-Cl1	2.4136(16)	C11	-C12	1.394(8)
Re1	-P1	2.4000(16)	C12	-C13	1.399(8)
Re1	-O1	2.035(4)	C13	-C14	1.380(9)
Re1	-N1	1.779(5)	C14	-C15	1.378(9)
Re1	-N4	1.942(4)	C15	-C16	1.377(8)
Re1	-N6	2.136(5)	C17	-C18	1.408(8)
P1	-C11	1.811(5)	C17	-C22	1.395(8)
P1	-C17	1.798(5)	C18	-C19	1.374(8)
P1	-C23	1.802(6)	C19	-C20	1.383(9)
O1	-C28	1.337(7)	C20	-C21	1.388(9)
N1	-N2	1.237(7)	C21	-C22	1.373(9)
N2	-C1	1.431(8)	C23	-C28	1.399(8)
N3	-C1	1.339(8)	C23	-C24	1.393(8)
N3	-C5	1.340(8)	C24	-C25	1.393(8)
N4	-N5	1.312(7)	C25	-C26	1.393(9)
N5	-C6	1.381(7)	C26	-C27	1.380(8)
N6	-C6	1.358(7)	C27	-C28	1.399(8)
N6	-C10	1.363(8)	C2	-H2	0.72(7)
N4	-H4N	0.80(7)	C3	-H3	0.98(7)
C1	-C2	1.386(9)	C4	-H4	0.95(7)
C2	-C3	1.371(10)	C5	-H5	0.84(7)
C3	-C4	1.377(11)	C7	-H7	0.87(7)
C4	-C5	1.378(9)	C8	-H8	0.85(8)
C6	-C7	1.389(8)	C9	-H9	0.90(6)
C7	-C8	1.376(9)	C10	-H10	0.86(8)
C8	-C9	1.379(8)	C12	-H12	1.02(7)
C9	-C10	1.361(8)	C13	-H13	0.90(7)
C11	-C16	1.400(8)	C14	-H14	1.03(7)
C15	-H15	0.83(7)	C22	-H22	1.09(9)
C16	-H16	0.98(7)	C24	-H24	0.84(7)
C18	-H18	1.06(6)	C25	-H25	0.98(6)
C19	-H19	0.85(8)	C26	-H26	0.91(9)
C20	-H20	0.78(8)	C27	-H27	0.86(8)
C21	-H21	0.80(7)			

Table A9. Bond Angles (deg) for [ReCl(Hhypy)(hypy)(PO)] (**3.2**).

Cl1	-Re1	-P1	161.77(5)	Re1	-N6	-C10	127.5(4)
Cl1	-Re1	-O1	81.54(12)	C6	-N6	-C10	118.0(5)
Cl1	-Re1	-N1	93.43(15)	N5	-N4	-H4N	112(5)
Cl1	-Re1	-N4	99.14(14)	Re1	-N4	-H4N	120(4)
Cl1	-Re1	-N6	87.23(13)	N2	-C1	-C2	117.1(6)
P1	-Re1	-O1	80.72(12)	N2	-C1	-N3	118.9(5)
P1	-Re1	-N1	96.31(15)	N3	-C1	-C2	124.0(6)
P1	-Re1	-N4	96.13(14)	C1	-C2	-C3	118.6(7)
P1	-Re1	-N6	88.09(13)	C2	-C3	-C4	118.9(6)
O1	-Re1	-N1	109.16(18)	C3	-C4	-C5	118.4(6)
O1	-Re1	-N4	160.14(18)	N3	-C5	-C4	124.5(6)
O1	-Re1	-N6	88.31(17)	N5	-C6	-C7	121.2(5)
N1	-Re1	-N4	90.7(2)	N5	-C6	-N6	116.5(5)
N1	-Re1	-N6	162.44(19)	N6	-C6	-C7	122.4(5)
N4	-Re1	-N6	71.94(18)	C6	-C7	-C8	118.3(5)
Re1	-P1	-C11	121.00(17)	C7	-C8	-C9	119.6(6)
Re1	-P1	-C17	112.96(19)	C8	-C9	-C10	120.1(6)
Re1	-P1	-C23	99.8(2)	N6	-C10	-C9	121.7(5)
C11	-P1	-C17	107.3(3)	P1	-C11	-C12	117.5(4)
C11	-P1	-C23	105.4(3)	P1	-C11	-C16	123.0(4)
C17	-P1	-C23	109.4(3)	C12	-C11	-C16	119.4(5)
Re1	-O1	-C28	123.4(4)	C11	-C12	-C13	120.5(5)
Re1	-N1	-N2	174.7(4)	C12	-C13	-C14	119.1(6)
N1	-N2	-C1	118.9(5)	C13	-C14	-C15	120.5(6)
C1	-N3	-C5	115.6(5)	C14	-C15	-C16	121.2(6)
Re1	-N4	-N5	128.7(4)	C11	-C16	-C15	119.4(5)
N4	-N5	-C6	108.4(4)	C18	-C17	-C22	118.7(5)
Re1	-N6	-C6	114.5(4)	P1	-C17	-C18	119.0(4)
P1	-C17	-C22	122.2(5)	C8	-C9	-H9	124(4)
C17	-C18	-C19	120.7(5)	C10	-C9	-H9	116(4)
C18	-C19	-C20	120.1(5)	N6	-C10	-H10	114(5)
C19	-C20	-C21	119.5(6)	C9	-C10	-H10	124(5)
C20	-C21	-C22	121.1(6)	C11	-C12	-H12	123(4)
C17	-C22	-C21	119.9(5)	C13	-C12	-H12	117(4)
C24	-C23	-C28	120.7(5)	C12	-C13	-H13	122(4)
P1	-C23	-C24	125.2(5)	C14	-C13	-H13	119(4)
P1	-C23	-C28	114.1(4)	C13	-C14	-H14	116(4)
C23	-C24	-C25	120.3(6)	C15	-C14	-H14	123(4)
C24	-C25	-C26	118.8(5)	C14	-C15	-H15	121(5)
C25	-C26	-C27	121.2(6)	C16	-C15	-H15	118(5)
C26	-C27	-C28	120.5(5)	C11	-C16	-H16	122(4)
C23	-C28	-C27	118.6(5)	C15	-C16	-H16	119(4)
O1	-C28	-C23	121.8(5)	C17	-C18	-H18	116(4)
O1	-C28	-C27	119.6(5)	C19	-C18	-H18	123(4)
C1	-C2	-H2	116(6)	C18	-C19	-H19	112(4)
C3	-C2	-H2	125(5)	C20	-C19	-H19	127(4)
C2	-C3	-H3	122(5)	C19	-C20	-H20	115(5)
C4	-C3	-H3	118(5)	C21	-C20	-H20	125(6)
C3	-C4	-H4	118(4)	C20	-C21	-H21	113(5)
C5	-C4	-H4	123(5)	C22	-C21	-H21	125(5)
N3	-C5	-H5	117(4)	C17	-C22	-H22	117(5)
C4	-C5	-H5	118(4)	C21	-C22	-H22	123(5)
C6	-C7	-H7	125(5)	C23	-C24	-H24	126(5)
C8	-C7	-H7	116(5)	C25	-C24	-H24	114(5)
C7	-C8	-H8	117(5)	C24	-C25	-H25	122(4)

Table A9. (cont.)

C9	-C8	-H8	122(5)	C26	-C25	-H25	119(4)
C25	-C26	-H26	117(5)	C26	-C27	-H27	124(5)
C27	-C26	-H26	121(5)	C28	-C27	-H27	115(5)

Table A10. Bond Lengths (Å) for $[Ga(H_3ppba)_2](NO_3)_2Cl{\cdot}3CH_3OH$ (**4.1**).

Ga1	-O1	1.9498(14)	N3	-H50	0.90(3)
Ga1	-O3	1.9512(15)	N4	-H51	0.95(4)
Ga1	-O5	1.9515(15)	C1	-C2	1.520(4)
P1	-O1	1.5052(15)	C4	-C5	1.380(4)
P1	-O2	1.4927(18)	C4	-C9	1.389(4)
P1	-C3	1.833(2)	C5	-C6	1.392(5)
P1	-C4	1.796(2)	C6	-C7	1.366(5)
P2	-O3	1.5047(15)	C7	-C8	1.381(5)
P2	-O4	1.4925(17)	C8	-C9	1.391(4)
P2	-C19	1.834(2)	C10	-C11	1.512(3)
P2	-C20	1.791(2)	C11	-C12	1.394(4)
P3	-O5	1.5048(16)	C11	-C16	1.391(4)
P3	-O6	1.4919(17)	C12	-C13	1.402(4)
P3	-C35	1.834(2)	C13	-C14	1.378(6)
P3	-C36	1.795(2)	C14	-C15	1.372(5)
N1	-C1	1.479(3)	C15	-C16	1.390(4)
N1	-C17	1.482(3)	C17	-C18	1.521(4)
N1	-C33	1.481(3)	C20	-C25	1.386(4)
N2	-C2	1.514(3)	C20	-C21	1.397(4)
N2	-C3	1.496(3)	C21	-C22	1.383(4)
N2	-C10	1.523(3)	C22	-C23	1.377(5)
N3	-C18	1.515(3)	C23	-C24	1.367(5)
N3	-C19	1.496(3)	C24	-C25	1.389(4)
N3	-C26	1.525(3)	C26	-C27	1.506(4)
N4	-C34	1.512(3)	C27	-C32	1.388(4)
N4	-C35	1.498(3)	C27	-C28	1.398(4)
N4	-C42	1.524(3)	C28	-C29	1.405(5)
N2	-H49	0.97(4)	C29	-C30	1.377(5)
C30	-C31	1.368(5)	C10	-H10B	0.9913
C31	-C32	1.383(4)	C12	-H12	0.9491
C33	-C34	1.521(4)	C13	-H13	0.9493
C36	-C37	1.391(4)	C14	-H14	0.9501
C36	-C41	1.388(4)	C15	-H15	0.9511
C37	-C38	1.386(4)	C16	-H16	0.9490
C38	-C39	1.386(5)	C17	-H17A	0.9895
C39	-C40	1.366(5)	C17	-H17B	0.9913
C40	-C41	1.385(4)	C18	-H18A	0.9899
C42	-C43	1.507(4)	C18	-H18B	0.9901
C43	-C48	1.392(4)	C19	-H19A	0.9892
C43	-C44	1.393(4)	C19	-H19B	0.9910
C44	-C45	1.385(4)	C21	-H21	0.9490
C45	-C46	1.366(5)	C22	-H22	0.9500
C46	-C47	1.376(5)	C23	-H23	0.9504
C47	-C48	1.404(5)	C24	-H24	0.9498
C1	-H1A	0.9897	C25	-H25	0.9500
C1	-H1B	0.9900	C26	-H26A	0.9896
C2	-H2A	0.9914	C26	-H26B	0.9899
C2	-H2B	0.9894	C28	-H28	0.9512
C3	-H3A	0.9906	C29	-H29	0.9515
C3	-H3B	0.9900	C30	-H30	0.9485
C5	-H5	0.9499	C31	-H31	0.9500
C6	-H6	0.9501	C32	-H32	0.9506
C7	-H7	0.9502	C33	-H33A	0.9904
C8	-H8	0.9503	C33	-H33B	0.9906
C9	-H9	0.9492	C34	-H34A	0.9905

Table A10. (cont.)

C10	-H10A	0.9899	C34	-H34B	0.9891
C35	-H35A	0.9899	C42	-H42A	0.9901
C35	-H35B	0.9893	C42	-H42B	0.9912
C37	-H37	0.9493	C44	-H44	0.9490
C38	-H38	0.9511	C45	-H45	0.9500
C39	-H39	0.9502	C46	-H46	0.9492
C40	-H40	0.9508	C47	-H47	0.9494
C41	-H41	0.9500	C48	-H48	0.9496

Table A11. Bond Angles (deg) for $[Ga(H_3ppba)_2](NO_3)_2Cl{\cdot}3CH_3OH$ (**4.1**).

O1	-Ga1	-O3	91.12(6)	O5	-P3	-C35	103.95(10)
O1	-Ga1	-O5	91.07(6)	O5	-P3	-C36	110.33(10)
O1	-Ga1	-O1_a	180.00	O6	-P3	-C35	110.87(10)
O1	-Ga1	-O3_a	88.88(6)	O6	-P3	-C36	109.82(10)
O1	-Ga1	-O5_a	88.93(6)	C35	-P3	-C36	99.47(10)
O3	-Ga1	-O5	91.10(6)	Ga1	-O1	-P1	143.84(9)
O1_a	-Ga1	-O3	88.89(6)	Ga1	-O3	-P2	143.77(9)
O3	-Ga1	-O3_a	180.00	Ga1	-O5	-P3	143.82(9)
O3	-Ga1	-O5_a	88.90(6)	C1	-N1	-C17	108.9(2)
O1_a	-Ga1	-O5	88.93(6)	C1	-N1	-C33	108.73(19)
O3_a	-Ga1	-O5	88.90(6)	C17	-N1	-C33	108.7(2)
O5	-Ga1	-O5_a	180.00	C2	-N2	-C3	111.06(18)
O1_a	-Ga1	-O3_a	91.11(6)	C2	-N2	-C10	112.11(19)
O1_a	-Ga1	-O5_a	91.07(6)	C3	-N2	-C10	111.54(19)
O3_a	-Ga1	-O5_a	91.10(6)	C18	-N3	-C19	111.13(18)
O1	-P1	-O2	120.10(9)	C18	-N3	-C26	111.97(19)
O1	-P1	-C3	104.05(9)	C19	-N3	-C26	111.53(18)
O1	-P1	-C4	110.50(10)	C34	-N4	-C35	111.31(18)
O2	-P1	-C3	110.76(10)	C34	-N4	-C42	112.35(19)
O2	-P1	-C4	109.84(10)	C35	-N4	-C42	111.35(18)
C3	-P1	-C4	99.50(10)	C10	-N2	-H49	102(2)
O3	-P2	-O4	120.25(9)	C3	-N2	-H49	106(2)
O3	-P2	-C19	104.07(9)	C2	-N2	-H49	114(2)
O3	-P2	-C20	110.40(10)	C26	-N3	-H50	103.9(19)
O4	-P2	-C19	110.75(10)	C18	-N3	-H50	114.5(19)
O4	-P2	-C20	109.74(10)	C19	-N3	-H50	103(2)
C19	-P2	-C20	99.52(10)	C34	-N4	-H51	114(2)
O5	-P3	-O6	120.27(9)	C35	-N4	-H51	104(2)
C42	-N4	-H51	103(2)	C21	-C22	-C23	120.2(3)
N1	-C1	-C2	112.3(2)	C22	-C23	-C24	120.3(3)
N2	-C2	-C1	112.0(2)	C23	-C24	-C25	120.1(3)
P1	-C3	-N2	114.25(15)	C20	-C25	-C24	120.5(3)
C5	-C4	-C9	119.2(2)	N3	-C26	-C27	114.8(2)
P1	-C4	-C5	119.9(2)	C26	-C27	-C28	119.3(2)
P1	-C4	-C9	120.73(19)	C26	-C27	-C32	121.9(2)
C4	-C5	-C6	120.6(3)	C28	-C27	-C32	118.7(3)
C5	-C6	-C7	119.7(3)	C27	-C28	-C29	119.8(3)
C6	-C7	-C8	120.8(3)	C28	-C29	-C30	119.9(3)
C7	-C8	-C9	119.4(3)	C29	-C30	-C31	120.4(3)
C4	-C9	-C8	120.3(3)	C30	-C31	-C32	120.2(3)
N2	-C10	-C11	114.45(19)	C27	-C32	-C31	121.0(3)
C10	-C11	-C16	121.6(2)	N1	-C33	-C34	112.1(2)
C10	-C11	-C12	119.6(3)	N4	-C34	-C33	112.1(2)
C12	-C11	-C16	118.7(2)	P3	-C35	-N4	114.07(16)
C11	-C12	-C13	120.2(3)	P3	-C36	-C41	119.90(19)
C12	-C13	-C14	119.7(3)	P3	-C36	-C37	120.88(18)
C13	-C14	-C15	120.7(3)	C37	-C36	-C41	119.0(2)
C14	-C15	-C16	119.8(3)	C36	-C37	-C38	120.3(3)
C11	-C16	-C15	120.9(3)	C37	-C38	-C39	119.9(3)
N1	-C17	-C18	112.2(2)	C38	-C39	-C40	120.0(3)
N3	-C18	-C17	112.0(2)	C39	-C40	-C41	120.5(3
P2	-C19	-N3	114.17(15)	C36	-C41	-C40	120.2(3)
P2	-C20	-C25	120.08(19)	N4	-C42	-C43	114.6(2)
C21	-C20	-C25	118.8(2)	C44	-C43	-C48	118.4(3)
P2	-C20	-C21	120.90(18)	C42	-C43	-C48	119.8(2)

Table A11. (cont.)

C20	-C21	-C22	120.1(3)	C42	-C43	-C44	121.8(3)
C43	-C44	-C45	120.9(3)	C4	-C9	-H9	119.81
C44	-C45	-C46	120.2(3)	C8	-C9	-H9	119.90
C45	-C46	-C47	120.5(3)	N2	-C10	-H10A	108.71
C46	-C47	-C48	119.8(3)	N2	-C10	-H10B	108.67
C43	-C48	-C47	120.2(3)	C11	-C10	-H10A	108.63
N1	-C1	-H1A	109.11	C11	-C10	-H10B	108.61
N1	-C1	-H1B	109.08	H10A	-C10	-H10B	107.57
C2	-C1	-H1A	109.12	C11	-C12	-H12	119.90
C2	-C1	-H1B	109.17	C13	-C12	-H12	119.86
H1A	-C1	-H1B	107.97	C12	-C13	-H13	120.17
N2	-C2	-H2A	109.22	C14	-C13	-H13	120.14
N2	-C2	-H2B	109.14	C13	-C14	-H14	119.67
C1	-C2	-H2A	109.18	C15	-C14	-H14	119.63
C1	-C2	-H2B	109.25	C14	-C15	-H15	120.09
H2A	-C2	-H2B	107.95	C16	-C15	-H15	120.10
P1	-C3	-H3A	108.72	C11	-C16	-H16	119.52
P1	-C3	-H3B	108.71	C15	-C16	-H16	119.58
N2	-C3	-H3A	108.65	N1	-C17	-H17A	109.20
N2	-C3	-H3B	108.64	N1	-C17	-H17B	109.22
H3A	-C3	-H3B	107.68	C18	-C17	-H17A	109.17
C4	-C5	-H5	119.69	C18	-C17	-H17B	109.11
C6	-C5	-H5	119.73	H17A	-C17	-H17B	107.83
C5	-C6	-H6	120.07	N3	-C18	-H18A	109.16
C7	-C6	-H6	120.24	N3	-C18	-H18B	109.25
C6	-C7	-H7	119.55	C17	-C18	-H18A	109.21
C8	-C7	-H7	119.63	C17	-C18	-H18B	109.14
C7	-C8	-H8	120.22	H18A	-C18	-H18B	107.96
C9	-C8	-H8	120.35	P2	-C19	-H19A	108.77
P2	-C19	-H19B	108.76	C31	-C32	-H32	119.57
N3	-C19	-H19A	108.72	N1	-C33	-H33A	109.16
N3	-C19	-H19B	108.67	N1	-C33	-H33B	109.21
H19A	-C19	-H19B	107.55	C34	-C33	-H33A	109.11
C20	-C21	-H21	119.96	C34	-C33	-H33B	109.19
C22	-C21	-H21	119.98	H33A	-C33	-H33B	107.93
C21	-C22	-H22	119.86	N4	-C34	-H34A	109.26
C23	-C22	-H22	119.91	N4	-C34	-H34B	109.23
C22	-C23	-H23	119.89	C33	-C34	-H34A	109.14
C24	-C23	-H23	119.77	C33	-C34	-H34B	109.13
C23	-C24	-H24	119.96	H34A	-C34	-H34B	107.88
C25	-C24	-H24	119.96	P3	-C35	-H35A	108.79
C20	-C25	-H25	119.80	P3	-C35	-H35B	108.81
C24	-C25	-H25	119.75	N4	-C35	-H35A	108.73
N3	-C26	-H26A	108.59	N4	-C35	-H35B	108.74
N3	-C26	-H26B	108.63	H35A	-C35	-H35B	107.50
C27	-C26	-H26A	108.61	C36	-C37	-H37	119.84
C27	-C26	-H26B	108.54	C38	-C37	-H37	119.87
H26A	-C26	-H26B	107.47	C37	-C38	-H38	120.02
C27	-C28	-H28	120.13	C39	-C38	-H38	120.08
C29	-C28	-H28	120.06	C38	-C39	-H39	119.98
C28	-C29	-H29	119.98	C40	-C39	-H39	120.00
C30	-C29	-H29	120.13	C39	-C40	-H40	119.79
C29	-C30	-H30	119.81	C41	-C40	-H40	119.66
C31	-C30	-H30	119.76	C36	-C41	-H41	119.85
C30	-C31	-H31	119.98	C40	-C41	-H41	119.92

Table A11. (cont.)

C32	-C31	-H31	119.78	N4	-C42	-H42A	108.64
C27	-C32	-H32	119.46	N4	-C42	-H42B	108.5
C43	-C42	-H42A	108.63	C45	-C46	-H46	119.79
C43	-C42	-H42B	108.64	C47	-C46	-H46	119.72
H42A	-C42	-H42B	107.52	C46	-C47	-H47	120.12
C43	-C44	-H44	119.51	C48	-C47	-H47	120.10
C45	-C44	-H44	119.56	C43	-C48	-H48	119.87
C44	-C45	-H45	119.88	C47	-C48	-H48	119.92
C46	-C45	-H45	119.92				

Table A12. Bond Lengths (Å) for $[Gd(H_4ppba)_2](NO_3)_4Cl{\cdot}3CH_3OH$ (**4.2**).

Gd1	-O2	2.2841(17)	C10	-C11	1.379(5)
P1	-O1	1.500(2)	C11	-C12	1.392(7)
P1	-O2	1.5104(16)	C12	-C13	1.365(6)
P1	-C1	1.797(3)	C13	-C14	1.397(5)
P1	-C7	1.845(3)	C15	-C16	1.517(4)
O3A	-N3A	1.214(17)	C2	-H2	0.9514
O3B	-N3B	1.07(3)	C3	-H3	0.9511
O5A	-N3A	1.113(14)	C4	-H4	0.9502
O5B	-N3B	1.22(3)	C5	-H5	0.9497
N1	-C7	1.498(3)	C6	-H6	0.9512
N1	-C8	1.524(3)	C7	-H7B	0.9889
N1	-C15	1.522(3)	C7	-H7A	0.9893
N2	-C16	1.514(3)	C8	-H8B	0.9906
N1	-H1A	0.98(5)	C8	-H8A	0.9889
N2	-H2A	0.89(7)	C10	-H10	0.9496
C1	-C2	1.388(4)	C11	-H11	0.9497
C1	-C6	1.393(4)	C12	-H12	0.9500
C2	-C3	1.387(4)	C13	-H13	0.9502
C3	-C4	1.378(5)	C14	-H14	0.9508
C4	-C5	1.377(6)	C15	-H15B	0.9907
C5	-C6	1.396(5)	C15	-H15A	0.9902
C8	-C9	1.502(4)	C16	-H16A	0.9891
C9	-C10	1.384(4)	C16	-H16B	0.9907
C9	-C14	1.393(5)			

Table A13. Bond Angles (deg) for $[Gd(H_4ppba)_2](NO_3)_4Cl{\cdot}3CH_3OH$ (**4.2**).

O2	-Gd1	-O2_a	87.52(6)	C15	-N1	-H1A	104.1(19)
O2	-Gd1	-O2_b	87.52(7)	C7	-N1	-H1A	112.4(18)
O2	-Gd1	-O2_c	180.00	C8	-N1	-H1A	109.2(16)
O2	-Gd1	-O2_d	92.48(6)	C16	-N2	-H2A	109.92(15)
O2	-Gd1	-O2_e	92.48(7)	C16_a	-N2	-H2A	109.92(16)
O2_a	-Gd1	-O2_b	87.52(6)	C16_b	-N2	-H2A	109.92(15)
O2_a	-Gd1	-O2_c	92.48(6)	O3A	-N3A	-O5A	122.2(14)
O2_a	-Gd1	-O2_d	180.00	O3B	-N3B	-O5B	118(3)
O2_a	-Gd1	-O2_e	92.48(6)	P1	-C1	-C6	121.1(2)
O2_b	-Gd1	-O2_c	92.48(7)	C2	-C1	-C6	119.3(3)
O2_b	-Gd1	-O2_d	92.48(6)	P1	-C1	-C2	119.7(2)
O2_b	-Gd1	-O2_e	180.00	C1	-C2	-C3	120.7(3)
O2_c	-Gd1	-O2_d	87.52(6)	C2	-C3	-C4	119.5(3)
O2_c	-Gd1	-O2_e	87.52(7)	C3	-C4	-C5	120.8(3)
O2_d	-Gd1	-O2_e	87.52(6)	C4	-C5	-C6	119.9(3)
O1	-P1	-O2	117.45(11)	C1	-C6	-C5	119.8(3)
O1	-P1	-C1	112.67(11)	P1	-C7	-N1	113.9(2)
O1	-P1	-C7	108.17(10)	N1	-C8	-C9	115.7(2)
O2	-P1	-C1	107.45(11)	C8	-C9	-C14	119.1(3)
O2	-P1	-C7	107.94(10)	C10	-C9	-C14	118.7(3)
C1	-P1	-C7	101.97(12)	C8	-C9	-C10	121.9(3)
Gd1	-O2	-P1	143.85(10)	C9	-C10	-C11	121.0(3)
C7	-N1	-C8	112.1(2)	C10	-C11	-C12	119.9(4)
C7	-N1	-C15	111.03(19)	C11	-C12	-C13	119.8(3)
C8	-N1	-C15	107.59(18)	C12	-C13	-C14	120.4(3)
C16	-N2	-C16_a	109.0(2)	C9	-C14	-C13	120.1(3)
C16	-N2	-C16_b	109.0(2)	N1	-C15	-C16	113.4(2)
C16_a	-N2	-C16_b	109.0(2)	N2	-C16	-C15	114.7(2)
C3	-C2	-H2	119.61	C11	-C10	-H10	119.54
C1	-C2	-H2	119.64	C9	-C10	-H10	119.46
C4	-C3	-H3	120.30	C10	-C11	-H11	120.05
C2	-C3	-H3	120.19	C12	-C11	-H11	120.03
C5	-C4	-H4	119.71	C11	-C12	-H12	120.07
C3	-C4	-H4	119.53	C13	-C12	-H12	120.10
C4	-C5	-H5	120.05	C12	-C13	-H13	119.81
C6	-C5	-H5	120.08	C14	-C13	-H13	119.79
C1	-C6	-H6	120.13	C13	-C14	-H14	120.02
C5	-C6	-H6	120.04	C9	-C14	-H14	119.87
N1	-C7	-H7A	108.84	C16	-C15	-H15A	108.81
N1	-C7	-H7B	108.77	N1	-C15	-H15A	108.97
H7A	-C7	-H7B	107.55	N1	-C15	-H15B	108.94
P1	-C7	-H7B	108.79	H15A	-C15	-H15B	107.61
P1	-C7	-H7A	108.77	C16	-C15	-H15B	108.92
C9	-C8	-H8A	108.43	N2	-C16	-H16B	108.56
N1	-C8	-H8A	108.32	N2	-C16	-H16A	108.64
N1	-C8	-H8B	108.34	H16A	-C16	-H16B	107.47
H8A	-C8	-H8B	107.47	C15	-C16	-H16A	108.61
C9	-C8	-H8B	108.32	C15	-C16	-H16B	108.66